POLITECNICO DI MILANO

DEPARTMENT OF MECHANICAL ENGINEERING

DOCTORAL PROGRAMME IN MECHANICAL ENGINEERING

Diffusion Coatings for High-Temperature Applications on Ni-base Superalloys

Supervisor:

Prof. Elisabetta Gariboldi

Prof. Maurizio Vedani

Tutor:

Prof. Alfredo Cigada

The Chair of the Doctoral Program:

Prof. Giampiero Mastinu

Doctoral Dissertation of:

Xinghua Han

Matricola: **738807**

2011-Cycle XXIV

Acknowledgments

That is more than words can express,

To my supervisors, Prof. Maurizio Vedani and Elisabetta Gariboldi,

To my tutor, Prof. Alfredo Cigada,

To my Coordinator, Prof. Giampiero Mastinu,

To Politecnico di Milano,

To AvioFix company,

To Prof. Qiang Feng in China,

To my colleagues in the Department of Mechanical Engineering at Politecnico,

To my love family,

To Alessandro and his family,

To all my friends, specially to Qiang Ge, Geng Liu, Jing Zhang, Zhingying Wang, Shuying Tang, Wenjia Cui, Ilka Wunderlich,

To those all who have helped and encouraged me.

I thank a lot for your great supports and helps during my PhD study!

I express my best wishes that all have beautiful today and tomorrow!

I will train myself hard, soon my day will come!

Abstract

The trend in modern turbo-engines is toward a continuous increase in turbine inlet temperatures. Increasing the inlet temperature of a gas turbine from 900°C to 1250°C can result in a 30% increase in the energy output of the turbine, with fuel consumption remaining equal. Hot components of gas turbines made by Ni-base superalloys operating in aggressive environments are subjected to a number of different attacks, such as, oxidation, hot corrosion, erosion, sulphidising, chlorination. The use of protective coatings has been a way to remedy these problems for alloys in harsh environments.

The coatings nowadays for high temperature applications include mainly diffusion coatings, overlay coatings and thermal barrier coatings (TBC). The protective character of diffusion coatings attributes to the protective nature of the Al_2O_3, Cr_2O_3 and SiO_2 scale formed respectively on the aluminide, chrominide or silicides at elevated temperatures. Diffusion coatings have first been developed and still are the most used coatings. Aluminide diffusion coatings are proved to be the cost-effective solution for high temperature oxidation, which are used widely for protecting turbine blades and vanes. The properties of the aluminide coating depend on the process methodologies used to deposit the coating, the substrate composition and the subsequent treatment. The coating deposition rate and morphology depend on the process temperature and time. Processing temperature influences the rate of

diffusion, at which alloy elements may diffuse and the metallurgy of the surface compound may form, thus, it is a critical parameter in the processing and manufacturing of diffusion coatings. The coating time at temperature defines the thickness of the coating formed during the diffusion step. The thickness of the coating is also a main factor of protecting property of the coatings. Two basic mechanisms typify the diffusion coatings, depending on whether the main diffusing species is aluminum diffusing from the coating to substrate or the base metal of the substrate alloy diffusing outward to the coating layer. These coatings are usually produced by pack cementation, out-of-pack cementation and chemical vapor deposition (CVD), which involve the diffusion of a predominant element such as, for example, aluminum to form 'diffusion coatings' layers.

In this thesis, we mainly studied the aluminide diffusion coatings on high-temperature Ni-base superalloy CMSX4. The coating procedure and its resulted coating layer features are mainly illustrated. During the process, the aluminium made available by the carrier vapor phase, moves inward into the component by solid state diffusion to form β-NiAl with the outward diffused Ni. In pure Ni (Ni201), aluminizing results in the formation of a set of single-phase layers. The diffusion coating formed on the pure Ni served as a comparison for coatings on CMSX4.

In chapter 1, the evolution of the Ni-base superalloys and its strengthening mechanisms and applications are first given. Then the corrosion and oxidation degradation processes have been discussed. The Ni-base superalloys are designed to have lower Al and more other refractory elements in order to increase the creep mechanical properties. The lower concentration of Al and the loss of surface protection can result in very high rates of attack to the substrate, leading to the catastrophic component failure. Hence, this is the main reason for applying a surface coating to ensure the operating efficiency of the components made by Ni-base superalloy. In the following sections, the processes of different diffusion coatings are discussed in detail. The diffusion coatings are also used as bond-coat in TBC. The interdiffusion degradation of the coating and the formation of α-Al_2O_3 during service are also introduced. At last, the cyclic oxidation test on the quality of the coatings is described, for that the cyclic oxidation is a critical factor for examining the adherence of the protective coating layer.

In chapter 2, the experimental materials CMSX4 and Ni201 are analyzed and prepared for vapor-phase aluminizing. The aluminizing process plan and the resulted metallographic surface analyses are given. These analyses are based on the SEM, EDS, EBSD and GDOES techniques. The techniques of EBSD and GDOES are special introduced.

In chapter 3, the SEM microstructure features of the coating layers on the substrate at different temperatures and times are obtained. The chemical composition profiles of the coating layers based on the EDS and GDOES techniques are illustrated. The layered structures and orientation relationship between coating layer and substrate are also shown in EBSD analyses.

In Chapter 4, the chemical profiles on the surface of the diffusion coatings are discussed. The diffusion mechanisms, orientation relationship between coating and substrate, the interdiffusion of alloy elements, the effects of anisotropy of the substrate to the coatings features are elucidated based on results and analyses in Chapter 3.

In the end, Chapter 5 concludes the results of this thesis work and gives suggestions for future work to be carried out.

Contents

CHAPTER 1

Ni-base Superalloy and Coatings

1.1 Introduction to Ni-base Superalloys and Coatings

Ni-base superalloys have very high performance which usually combine high melting point, high strength (tensile strength, creep strength, fatigue strength), ductility, toughness and corrosion resistance at higher temperatures. An important application of Ni-base superalloys is for the production of blades and vanes in gas turbines (Fig. 1-1). Turbine blades are critical components in both aeronautical and stationary gas turbines. The engine performance is closely related to the capability of materials to withstand higher and higher temperatures. Stimulated by the demand of military aircraft and civil air transport after 1955, the cast superalloys have replaced the initial wrought superalloys. The Ni-base superalloys have a matrix γ phase, with a face-

centered cubic (FCC) structure, containing a dispersion of ordered intermetallic precipitate particles of the type γ'-Ni_3Al [1, 2].

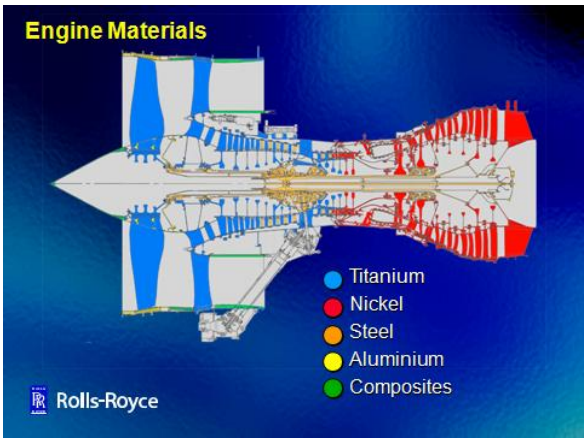

Figure 1-1: *In a jet engine, the turbine part is made by Ni-base superalloys (red parts) [3].*

The evolution of the high temperature capacity of the Ni-base superalloy over about 60 years' period is shown in Fig. 1-2 [4]. The engine performance is closely related to the capability of materials to withstand higher and higher temperatures. After the year of 1955, cast tubine blades and vanes with equiaxed structure were produced by using higher γ' volume fractions in order to increase the operating temperatures. Common equaxied superalloys are In713, In100, and René80. The grain boundaries of this equaixed structure were strengthened by carbon, boron and zirconium, hafnium. It was found that the grain boundaries represented weak points. In 1960s, the creep strength and ductility were significantly improved by elimination of transversal grain boundaries, by means of directionally solidified (DS) blades where columnar grains were aligned to the blade axis, the DS blade and its microstructures are shown in Fig. 1-3b. The creep strength was thus increased so that a 58°C temperature advantage at high temperature and low stresses could be achieved. Typical DS superalloys are Mar-M200 and their series. After this development occurred, about thirty year's ago, the 1st single crystal (SC) alloys were produced by removing the grain boundaries completely, since the grain boundaries represent weak points in the microstructure and stress tends to concentrate there [5]. This allowed, in turn, the removal of grain-boundaries strengthening elements such as carbon, boron and zirconium and hafnium. Further, since creep failure is almost always a grain

boundary initiated phenomenon due to either grain boundary sliding or vacancy condensation on boundaries perpendicular to the applied tensile stress, the development of SC turbine components has resulted in further creep property improvements since SC components contain no grain boundaries.

The cast turbine blades made by these three techniques are illustrated in Fig. 1-3.

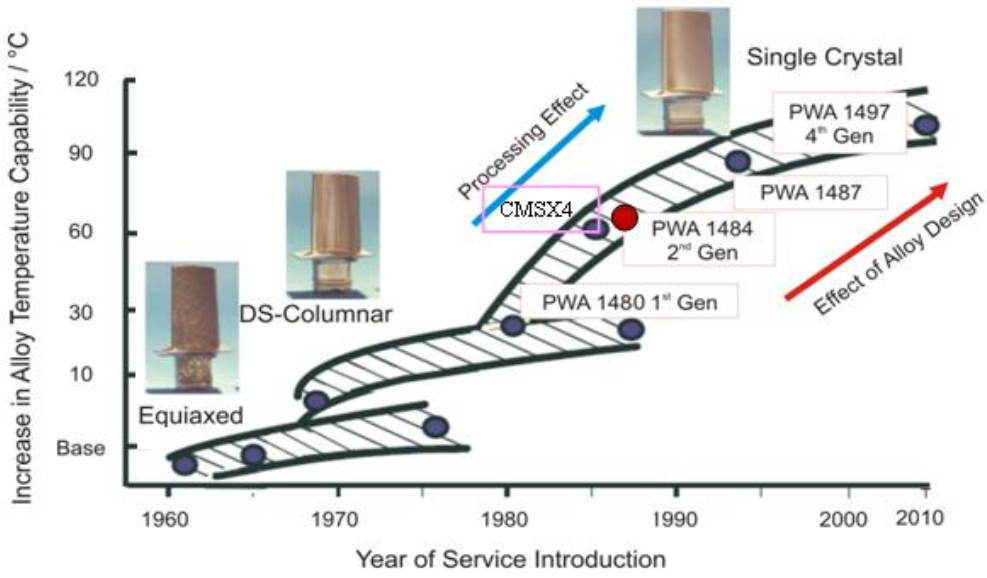

Figure 1-2: *Evolution of the Ni-base superalloy over about 60 years' period.*

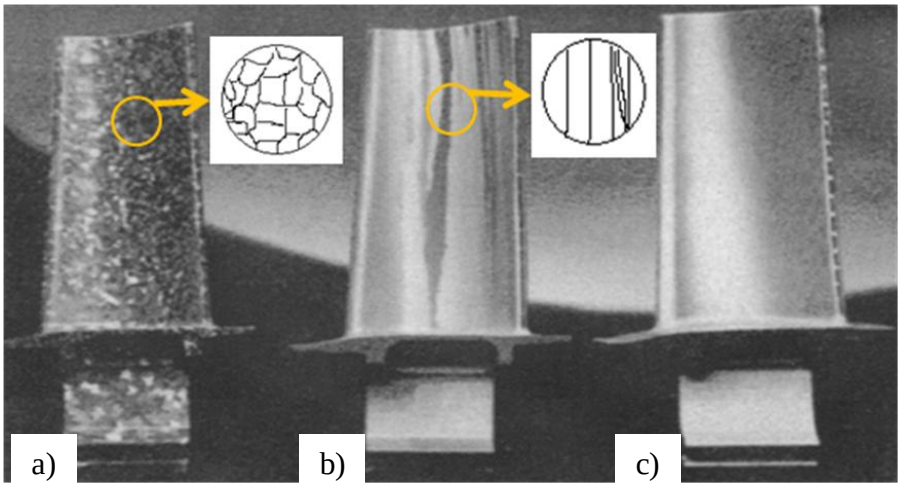

Figure 1-3: *Cast turbine blades: a) Equiaxed, b) Directionally solidified (DS), c) Single crystal (SC).*

The 1st generation of SC superalloys have derived from conventional DS casting alloys. Pratt and Whitney's PWA-1480 was the first industrial SC alloy and has been used in civilian engines followed by CMSX2, RenèN4, AM1. Alloy designers continued to seek to improve the creep strength. For this purpose, new generation alloys have been developed between the years of 1980 and 2000. The 2nd generation SC alloys have increased the creep strength by the addition of Re (3wt%). The 3rd generation with higher Re (up to 6wt%) [6]. Recently, new Ni-base alloys for higher performances have been developed worldwide. For example, the new 4th generation alloys SC MC-NG has been designed by Snecma and Turbomeca in France [7]. The 4th generation alloy LDSX has been developed in UK [8]. The chemical composition of superalloy has progressively begun more complex, such as the microstructure stability problems. The 4th generation of superalloys reflects this complexity.

Ni-base superalloy contain mainly Ni and many refractory elements, which has increased the properties of superalloy, but Ni is an expensive material, some alloying elements are also expensive, such as Re. Further, the alloying elements and heat treatment also make superalloy difficult to machine and to weld, increasing fabrication costs, part rejection rates and rework. Therefore, light density and low costs materials for high temperature became the trend. New ceramic systems (silicon nitrides, eutectic composites) and refractory intermetallics are investigated as potential solutions for the 2020 aero turboengines.

1.2 Strengthening Mechanisms in Ni-base Superalloy

Pure metals are soft and generally do not have adequate environmental resistance. This is true also for nickel. Therefore, they are seldom used without strengthening by various mechanisms. Precipitation hardening and solid-solution strengthening methods are effective at high temperatures, the former being the most important.

In precipitation strengthening, the solute atoms participate in creating a fine and uniformly dispersed second phase. Trandionally, two heat treatment are used for Ni-base superalloys. First is the solution heat treatment to homogenize the microstructure and reduce the effects of elemental segredation. The second is aging treatments to develop the γ' precipitates. In Ni-base superalloys, precipitates of γ'-[$Ni_3(Al,Ti)$], provide the first and important mechanism for strengthening Ni base

superalloys. γ'-[Ni_3(Al,Ti)] precipitate phases acting as a coherent barrier to dislocation motion have increased greatly the creep resistance. The creep resistance is dependent on slowing the speed of dislocations within the crystal structure. Chemical additions such as Al and Ti promotes the creation of the γ' phase. The γ' phase size can be precisely controlled by careful precipitation hardening heat treatments. Many superalloys have a two-step heat treatment which creates a dispersion of square γ' particles with a fine dispersion between γ matrix. The γ' phase has an ordered face centered lattice type LI_2. The γ' crystal is shown in Fig. 1-4b, Al locates at the corners of the cells while Ni located at the face center of the cube [9]. The crystal structures of γ-Ni and the β-NiAl phase are also shown in Fig. 1-4a and 1-4c. The body-center cubic (BCC) crystal is formed with Ni located in the corner and Al located in the center of the cube. The β-NiAl is the main phase formed during the diffusion aluminide coating which will be discussed in a following part of this thesis.

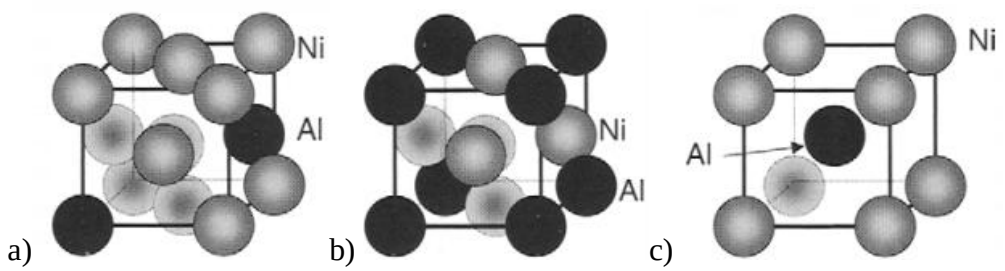

Figure 1-4: *Cubic phases in the Ni-base superalloys. a) γ-Ni matrix, b) γ'-Ni_3Al, c) β-NiAl.*

The γ'-[Ni_3(Al,Ti)] phase is not strictly stoichiometric. There may exist an excess of vacancies in one of the sublattices, which leads to deviations from stoichiometry. Sublattice of Al and Ni of the γ' phase can solute a considerable proportion of other elements. For example, the Ni sites may also contain Co, Cr and Mo, while the Al sites may contain Ti and Nb. The γ' phase hardens the alloy by the dissociating dislocations, which leads to the anti-phase boundary (APB). It turns out that at elevated temperatrure, the free energy associated with the APB is considerably reduced if it lies on a particular plane, which by coincidence is not a permitted slip plane. One set of partial dislocations bounding the APB cross-slips, so that the APB lies on the low-energy plane, which is coincidently the plane coherent with γ matrix.

Thus the dislocations are effectively locked. By this mechanism, the yield strength of γ' phase increases with temperature up to 1000°C. The size, coherency and volume fraction of the precipitates control the strength achieved by this process [1, 9]. The precipitate of γ' has also greatly increased the creep performance. Across a wide range of temperatures and levels of applied stress, creep deformation on the microscale is restricted to the low-energy plane, where γ channels lie between the γ' phases, therefore, creep dislocations can not penetrate the γ' precipitates. A rough estimation of the alloy strength can be estimated by the Orowan stress, Gb/l, G is the shear modulus, b is the Burgers vector and l is the width of the γ' channels. For example, if G=50 GPa, b=0.25 nm, l=100 nm, the strength would yields 125 MPa. For uniaxial loading along [001], the Schmid factor assuming {111}<1-10> slip is 1/√6, then 125*√6 yields 306 MPa. Thus at elevated temperatures, Ni-base superalloys can behave good performance [1].

In solid-solution strengthening, the solute atoms (like Al) randomly substitute for the solvent atoms (like Ni) without altering the cystal structure (Fig. 1-5a).

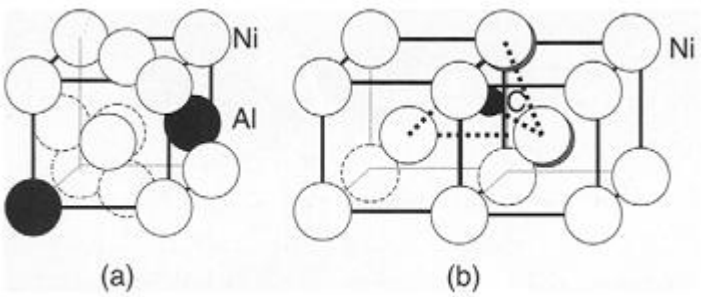

Figure 1-5: *Schematic of solid solution: a) Substitutional (Al dissolved in Ni), b) Interstitial (C dissolved in Fe).*

The γ phase with a face-center crystal (FCC) lattice constitutes the matrix of the Ni-base alloys. γ-phase is strengthened by solid-solution with different species of atoms randomly distributed. Several metallic elements (Co, Cr, Mo, Fe, Ta, W, Re etc.) dissolve in the γ matrix, randomly replacing the Ni atom. Because of their size difference relative to the Ni matrix, the substituting solute atoms create local stress fields that impede dislocation motion by interacting with the stress fields of dislocations. In addition, the solute atoms may also enter the solvent in the interstitial

sites (Fig. 1-5b). For example, carbon, being a small atom, forms an interstitial solid solution with Ni. The carbides in the matrix of Ni-base superalloy, are made up with some of the alloying elements (MC type carbide with Ti, Ta, W, Mo, Hf, Nb and $M_{23}C_6$ type carbide with Cr, W, and Mo in Ni base alloy) at the grain boundaries. They pin the grain boundaries and improve the resistance to sliding and migration that would occur during creep diffusion. However, if they precipitate as a continuous grain boundary film, the fracture toughness, ductility and rupture strength of the alloy may be reduced.

1.3 Chemistry of the Ni-base SC Superalloy and the Manufacturing of CMSX4

1.3.1 Role of Different Alloying Elements

The most advanced SC superalloy turbine blades are now operating at a temperature greater than 85% of their absolute melting temperature [2]. As introduced above, Ni-base superalloys achieve their high strengths at elevated temperatures through strengthening by a relatively high volume fraction of γ'-Ni_3Al precipitates in the γ-Ni matrix. These alloys are also strengthened by constituents in solid solution (i.e. W, Ta, Mo, Re) and carbides. The effects of the various alloying elements commonly used in Ni-base superalloys are summarized in Tab. 1-1 and Fig. 1-6. The principal γ'-forming elements are Ti and Ta, and a less degree of Nb by substituting Al in γ'-Ni_3Al. Cr, Co and Mo prefer to partition into the γ matrix, where they act mainly as solid solution strengthening elements to increase the creep properties. Al plays a fundamental role in promoting the formation of a stable Al_2O_3 alumina surface scale which promotes the oxidation resistance. Cr and Al also strengthen the matrix to a certain extent. From the chemistry point of view, a modern SC superalloy would have about 6wt% Al. Heavy refractory elements Mo, W, Re, Ta can increase the creep properties by solid solution strengthening. Especially, Re has the effect of retarding the coarsening of γ' phase. The Re addition benefits creep and mechanical fatigue properties, but also shows oxidation, hot corrosion and coating performance. Excessive amounts of Ta, Re, Mo and W promote the formation of the so-called topologically close-packed (TCP) phases, such as σ, μ, P etc., which often occur with

a highly brittle complicated morphology. These TCPs may induce deleterious effects on the mechanical properties, such as loss of ductility, decrease of creep strength.

TCPs are believed to be negative formation within the microstructure. This is due to the needle-like or acicular shape TCPs, they can deleterious effect on the surrounding matrix. These phases are thought to be act as stress concentrations within a material because of their structure. If the strengtheners like W and Re are within the TCPs and not the matrix, then the materials' strength degrades. Because of these negative effects, TCPs need to be avoided or minimized. The presence and their negative effects have been found and studied by many authors in the real and experimental fields [7, 9, 10]. These phases are also occurred during the diffusion aluminide coating in later part of this work. So the benefits effects of the refractory elements should be balanced among each other, because of the potential consequence could be disastrous.

Table 1-1: *Effects of the major alloying elements in Ni-base superalloy [2]*

Element	Matrix-γ strengthening	Increase in γ' volume fraction	Grain boundary precipitates	Other effects
Cr	moderate	moderate	$M_{23}C_6$ M_7C_3	Improve corrosion resistance; Promotes TCP phases
Mo	high	moderate	M_6C MC	Increase density
W	high	moderate		Promote TCP phases σ, μ (Mo, W)
Ta	high	large		
Nb	high	large	NbC	Promote γ' and δ phases
Ti	moderate	very large	TiC	
Al	moderate	very large		Al improves oxidation resistance
Fe		γ'→β, η, γ'' or δ		Decrease oxidation resistance; promotes TCP phases σ, laves
Co	slight	moderate in some alloys		Raises solidus; may raise or lower solves
Re	moderate			Retards coarsening; increase misfit
C	moderate		carbides	
B.Zr	moderate			Inhibit carbide coarsening; improve grain boundary strength; improve creep strength and ductility

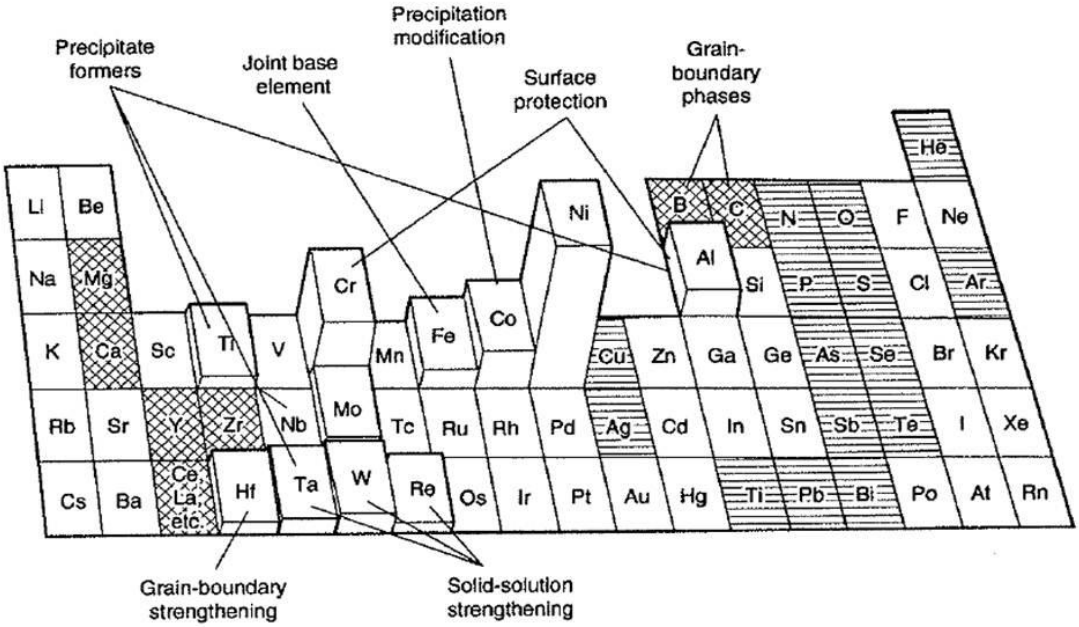

Figure 1-6: *Alloying elements used in Ni-base superalloys. Beneficial minor elements are marked with cross-hatch, while detrimental elements are marked with horizontal line hatch [11].*

1.3.2 Chemical Composition of Ni-base SC Superalloys

Since the first SC superalloy emergerd in 1980s, the chemical compositions of the Ni-based SC superalloys have evolved significantly. Many alloy producers and engine manufacturers are still engaged in increasing the properties of the Ni-base superalloys. The chemcical composition of 1st, 2nd, 3rd and 4th generation SC superalloys is given in Tab. 1-2.

Table 1-2: *Chemical compositions (wt%) of Ni-base superalloys in different generations (based on data taken from [1-2, 5-6, 12-13]).*

		Desity g/cm^3	Ni	Al	Cr	Co	W	**Ti**	Mo	Ta	**Re**	Hf	**Ru**
1st (SC)	PWA-1480	8.7	62.5	5	10	5	4	**1.5**	0	12	**0**	0	**0**
	RenéN4	8.56	62.6	3.7	9	8	6	**4.2**	2	4	**0**	0	**0**
2nd (SC)	CMSX4	8.7	61.8	5.6	6.5	9	6	**1**	0.6	6.5	**3**	0.1	**0**
	PWA1484	8.95	59.6	5.6	5	10	6	**0**	2	8.7	**3**	0.1	**0**
	TMS82+	8.93	62.4	5.3	4.9	7.8	8.7	**0.5**	1.9	6	**2.4**	0.1	**0**
3rd (SC)	CMEX10	9.05	69.6	5.7	2	3	5	**0.2**	0.4	8	**6**	0.03	**0**
	RenéN6	8.97	57.4	5.75	4.2	12.5	6	**0**	1.4	7.2	**5.4**	0.15	**0**
	TMS75	8.89	59.9	6	3	12	6	**0**	2	6	**5**	0.1	**0**
4th SC	MC-NG	8.75	70.5	5.2	4	<0.2	5	**1.1**	1	5	**4**	0.1	**4**
	LDSX1	9.15	66.1	6	3	3	2.9	**0.25**	2.5	6.5	**6.2**	0.1	**3.5**

From Tab.1-2, some feathers of the superalloys in different generations is notewhorthy. The 1st generation of SC superalloys contain mainly Cr, Co, Mo, W, Al, Ti and Ta. Based on these alloying elements, the 2nd generation SC superalloys are added significantly large amount of expensive refratory element Re (up to 3wt%). Hf is added to improve the ductility and castability. The 3rd generation alloys are produced with much higher Re (up to 6 wt%), balanced by less Cr to avoid σ phase formation and eventually 4th generation alloys with higher Re and Ru contents (up to 4 wt%). It is worth noting the reduction of Ti and the introduction of significant additions of Re. The concentration of Ti is reduced in order to increase the solidus temperature and balance the volume fraction of γ'. The creep-strengthening effect has been increased by the addition of Re [6]. A major problem of 2nd generation Re-bearing alloys was their microstructure stability, i.e. the propensity to form undesirable topologically close-packed (TCP) brittle phases such as σ, μ or P phases during exposure at high temperature [14-19]. It is recognized that superalloys which contain high level of Mo, Re, W are prone to precipitate TCPs. The 3rd generation alloys are typical CMSX10 and ReneN6, which exhibits higher creep strength and rupture strength than 2nd generation alloys. The tendency to the precipitation of TCPs is still an important problem for 3rd generation alloys.

Considering the chemical composition of alloying elements in typical superalloys of different genetations, Fig. 1-7 shows how Ni-base alloy compositions have changed since 1960s and clearly shows that except the very recently 4th generation alloys, the Cr content has been drastically reduced from about 8wt% to about 2 wt% and that Al contents have increased to about 6 wt%.

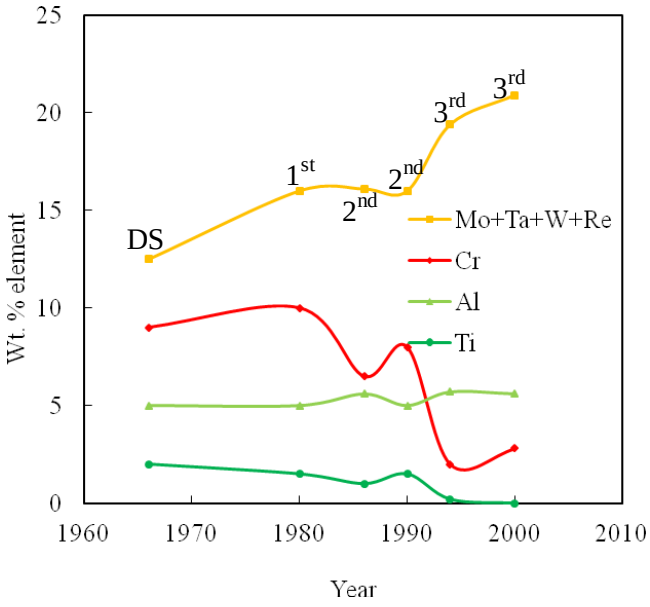

Figure 1-7: *Variations of alloying element additions to some typical Ni-based SC alloys with the year of alloy producing (based on data [1-2, 5-6, 12-13]).*

A key indication from Fig. 1-8 is the increasing in refractory element content, such that over the 30 years period between 1965 and 1995, total amount of additions of Ta+Re+W+Mo have increased from 12.5 to 20 wt%. The reasons for these changes in composition mechanisms involved in developing Ni-base alloys for optimum creep resistance at temperature up to 1100°C [6]. The more the amount of refractory element contents, the stronger the alloy creep resistance.

1.3.3 Optimisation of the Chemistry of Ni-base SC Superalloy

Fig. 1-8 shows the creep rupture lives of the SC Ni-base superalloy TMS 75 (2nd generation) and TMS82+ as a function of the amount of γ' phase. The creep rupture life is largest when the γ' fractions is about 70%. The creep performance doesn't increase monotonically as the γ' fraction is increased. So the γ'-forming elements such as Al, Ti, Ta should be high such that the γ' fractions becomes about ~70%.

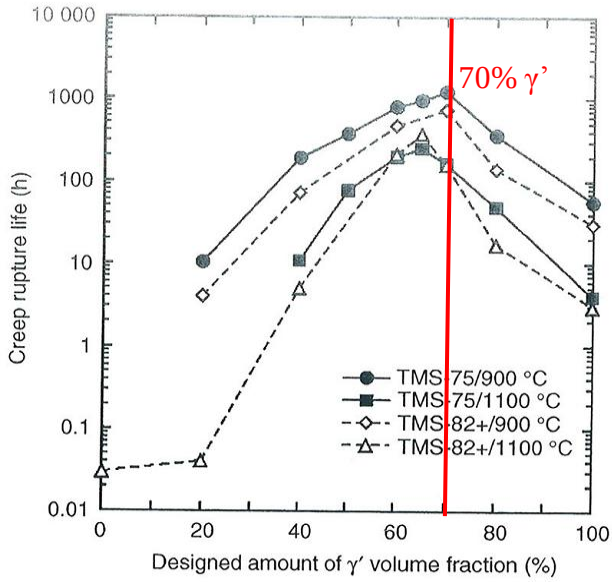

Figure 1-8: *Variation of the creep rupture lives of the SC superalloy TMS-75 and TMS-82+, as a function of the amount of γ' phase. The creep rupture life is largest when the γ' fraction is about 70% [1].*

The γ/γ' lattice misfit is also affected by the chemical composition of the alloy. The alloys of negative misfit possesses greater creep resistance than those with positive misfit. The composition of the alloy must be chosen such that the γ/γ' lattice misfit is small, which minimizes the γ/γ' interfacial energy so that γ' coarsening is restricted. The lattice misfit δ is defined according to

$$\delta = 2 \times \left[\frac{a_{\gamma'} - a_{\gamma}}{a_{\gamma'} + a_{\gamma}} \right] \qquad (1)$$

where $a_{\gamma'}$ and a_{γ} and are the lattice parameters of the γ and γ' phases, respectively. When the misfit is small, less than about 0.5%, the γ' particles are cuboids with sharp corners with elastic coherency.

The precipitates become spherical as the magnitude of the misfit increases, and coherency is lost. When designing alloys, an additional consideration is the strong temperature dependence of the lattice misfit. For example, during creep deformation especially in the low stess high temperature interfacial dislocation networds develop at the γ/γ' interface. The γ' precipitates coarsen directionally either parallel or

perpendicular to the external stress axis. When the temperature changes, a finite time is required for δ to attain its equilibrium value. A new coherent γ/γ' interface and the equilibration of coherency stresses are established by the elemental partitioning between γ and γ' phases [1].

Pyczak et al. [20] have experimentally demonstrated that addition of Ru and Re decrease the lattice misfit and thus modified the coherency stresses between γ and γ' accordingly.

Anisotropy

Anisotropy is the properties of being directionally dependent, as opposed to isotropy. It can be defined as a difference, when measured along different axes, in a material's physical or mechanical properties. It is well established that the thermal mechanical properties of Ni-base SC alloys have a strong crystal orientation dependence. For example, a change in tensile orientation drastically affects the creep life. An orientation relationship between TCP precipitates and matrix superalloys have been reported in [15]. V. Sass and co-workers [21] have also confirmed that for CMSX4 alloy, the primary creep behavior of near [001] and [011] oriented crystals is highly sensitive to even small misorientations. The aluminized Ni-base superalloys have also exhibit some orientation dependence in terms of microstrucurtre observed by the Murakami et al. [22]. They found that the preferential formation of some special zone along the {001}<110> directions.

1.3.4The Heat Treatment of CMSX4

The 2nd generation SC alloy CMSX4 which contains 10 alloying elements is made by cast. As the alloy solidifies from the melt, the first solid to form is enriched with the higher melting point elements, like W and Re. As more solid is formed, the liquid in the region of the 'mushy zone' becomes depleted in W and Re and enriched with the lower melting points elements, like Al, Ta and Ti. This gradients then causes heterogeneity of the mechanical and physical properties. The optical micrographs of dendritic structure of as-cast CMSX4 is shown in Fig. 1-9. The light colored dendritic region is enriched with W and Re, while the dark colored interdendritic region is enriched with Al, Ta, Ti. The segregated 'white' γ+γ' eutectic is shown between the dendritic arms which is formed by the compositional gradients during solidification [23, 24]. SEM reveals a relatively fine γ' distributed with the dendrite cores that become coarser near the eutectic regions.

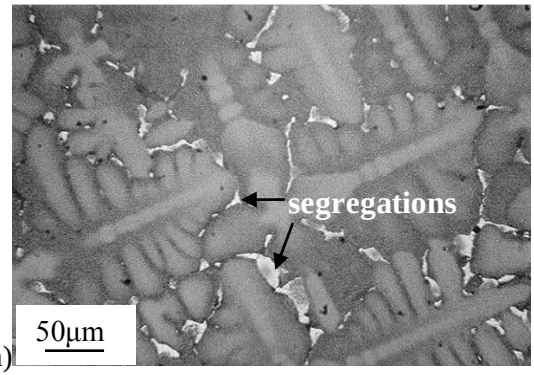

a)

Figure 1-9: *Optical micrograph of as-cast CMSX4. The segregations are locted inside the interdendrites.*

The high strength of CMSX4 depends on the alloy composition, while they also rely largely on proper heat treatment to bring out these exceptional properties. Two step of heat treatments are traditionally used. First step is the solution heat treatment, designed to homogenize the microstructure and reduce the effects of elemental segregation. The second step is aging heat treatment, designed to precipitate a second phase γ', thus to obtain a cuboidal γ/γ' microstructure.

The effect of solution treatment on SC Ni-base superalloy has been analysed in [24-26]. In the literature, the solutioning heat treatment and aging treatment are explained in detail.

Table 1-3: *Heat treatment schedules.*

Heat treatment	Procedures
Solution	1276°C(4h)→ 1287°C(2h)→1296°C(3h)→1304°C(3h) → 1315°C(1h)→ 1321°C(2h)→ 1324(2h)/gas furnace quench
Aging	1140°C(6h)/air cooled→ 871°C(20h)/air cooled

Tab.1-3 has listed the the standard solution heat treatment and the aging heat treatment schedules. Solution heat treatment is typically ended with a rapid quench to retain the microstructure that was present at the elevated temperatures. This means that much of the γ' is dissolved within the γ-matrix, however, the rapid cooling rate isn't so fast to prevent precipitation. Aging heat treatment are usually performed at a lower temperature than solution heat treatment, because they don't need this to exceed the γ' sovlus temperature. The aging treatment serves to grow the cuboidal γ'

structure and allow it become uniform [25]. In order to obtain maximum strength in the alloy, the γ' precipitate must form and grow to be optimal size.

During the heat treatment, if not fully solution heat treatment is given, a large amount of residual regregation structures are still evident, shown in Fig. 1-10a. While, if ideally solution heat treatment is carried out, the homogenized microstructure will be obtained (Fig.1-10b)

a) 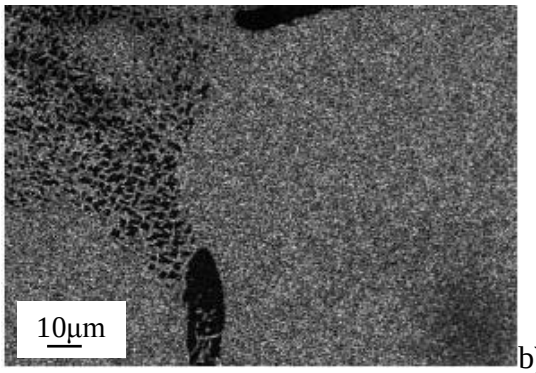

b) 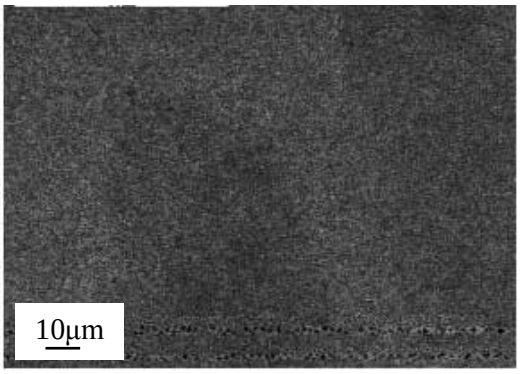

Figure 1-10: *Low magnification of CMSX4 after solution treatment, a) Not fully solutioned structure with segregations, b) Homogenized microstructure obtained by full solution heat treatment.*

The uniform microstructure of CMSX4 after full solution heat treatment at higher manigification is shown in Fig. 1-11a. The γ/γ' eutectics have been dissolved and a fine γ' (approximately 0.3 - 0.5 μm) is apparent throughout the microstructure. After aging, the γ' slightly coarsened to 0.5μm in size and formed very uniform, cuboidal structure (Fig. 1-11b). The composition of γ'-Ni_3Al and the γ matrix in CMSX4 contains the refractory alloying elements Ta, Re, W and Mo, Ta enters γ' due to its solubility in this phase.

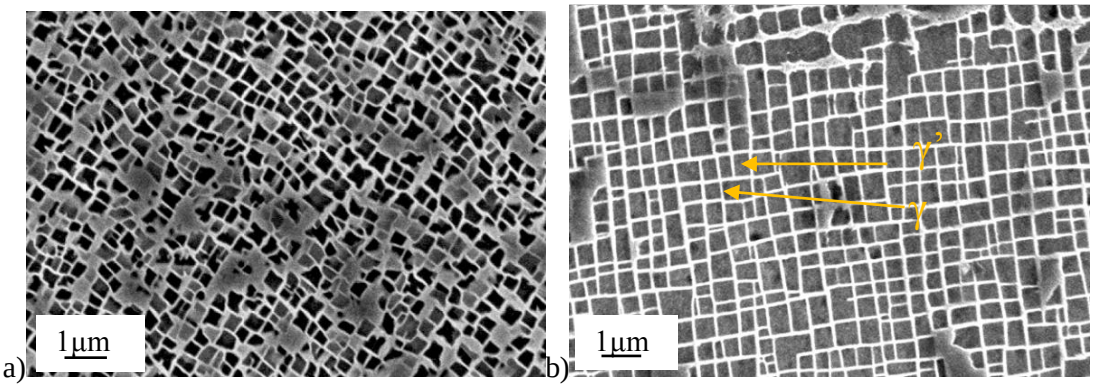

Figure 1-11: *High magnification of SEM microstructure of CMSX4, a) After the standard solution heat treatment, γ' is irregular in size and shape, b) After aging, γ' has coarsened has become more regular [81].*

The superalloys must be able to maintain strength and structure integrity for extended periods of time. At high operating temperature, diffusion can take place and can significantly affect the microstructure. Two common occurrences are the coarsening of γ' and the formation of TCPs phase. G.E. Fucks [26] has also compared the performance of modified heat treatment and the standard heat treatment. The modified heat treatment proved to be insufficient to produce an acceptable homogeneous microstructure in CMSX4, and after long-term exposure time, many TCPs occurred. While, the uniform microstructure formed by strandard heat treatment appears to be much more TCP resistant.

TCPs

The 'topologically close packed' (TCP) intermetallic phases, are embrittling secondary phases appeared during heat treatment or sevice exposure. They are mainly involved transition elements, in which the atoms are more closely spaced than in normal geometrically close packed structures [2]. The solubility of elements W, Re, Mo and Cr is much lower in β and γ' than in γ, and therefore the precipitation of these elements in TCPs is inevitable. TCPs can intrude into the substrate to a considerable distance (up to 100 μm) and destroy the γ/γ' microstructure.

σ Phase

The prototype of σ phase is the FeCr compound. It is particularly deleterious due to its brittle nature and its tendency to form long plates or needles on well-defined habit planes, facilitating the initiation, cause a catastrophic drop in ductility and propogation of cracks.

Hammerschmidt et al. [27] have calculated the σ formation in Re-W system. They found that for σ, chemical composition approximately is $Re_{0.33}W$, $Re_{0.3\text{-}0.5}W$, and $Re_{0.6\text{-}0.9}W$.

μ Phase

μ phase has been shown to have a detrimental effect on mechanical properties, due to its tendency to form embrittling intergranular precipitates. The general formula for μ phase is $(Co, Fe, Ni)_7(MoWCr)_6$. The authors C.M. F. Rae and co-workers [28] have found that for alloys CMSX4 Pt-aluminized, the TCPs precipitates have approximately the same composition, which is the μ phase enriched W and Mo.

As illustrated previously, the development of SC Ni-base superalloys for turbine blades contain relatively high percentage of refractory elements such as Ta, W, Re, Mo, which enhance the high-temperature properties. However, this is done at the expense of the Cr and Al. Given the severe environmental conditions in which the blade operates, the consume of the Al and Cr implies even greater degradation problems. To alleviate this lack of appropriate oxidation corrosion resistance, surface treatment or an external coating is applied to the blades. Its purpose of the coating is to allow for the growth of a resistant oxide layer.

In this thesis, the main alloy on which the aluminizing processed is CMSX4 alloy. It was provided by Aviofix company.

1.4 Oxidation and Corrosion Degradation Processes

The properties espected from superalloys are high temperature creep, high fatigue life, phase stability, as well as oxidation and corrosion resistance. This thesis mainly focused on the topic of oxidation and corrosion resistance.

The development of coating technology is impelled by the serious results by oxidation and corrosion and how the mechanisms by which they occur. Hot components of gas turbines operating in aggressive environments are subjected to a number of modes of attacks termed collectively high temperature corrosion, which include oxidation, sulphidising, carburizing, chlorination, erosion and hot corrosion induced by molted salts. The use of protective coatings has been an answer to remedy the lack of high temperature surface stability of metals and alloys in harsh environments [29].

In practice, the oxidation behavior of the SC superalloy is complicated by the many different elements. Consider, for example, a 3rd generation alloy such as CMSX10, which doesn't form an alumina scale. During oxidation, an external scale of NiO forms very rapidly and spallation occurs readily. The underlying metal, being depleted in Ni, forms β-NiAl, which grows into the metal by a process of internal oxidation. Degradation is further complicated by the formation of Cr, W, and Ta rich oxides beneath the NiO scale. These effects are due to the choice of alloy composition, for which the Re is high at 6 wt% to confer creep strengthening with the Cr content reduced to 2 wt% in an attempt to prevent TCP formation. The Cr content is too low to prevent either the formation of a thick external Ni scale or to resist attack by internal oxidation. For these reasons, for adequate environmental performance, it is necessary to coat CMSX10 by the process of aluminizing [1]. A recent comparative study of the cyclic oxidation performance of typical 1st, 2nd, 3rd and 4th generation SCz superalloys has confirmed that in the latest generations of superalloys in Fig. 1-12, the weight decrease by spallation of the scale in cyclic oxidation becomes larger as the generation advances. Ru and Re were found to degrade the oxidation resistance by the vaporization of their oxide, such as RuO_4 and Re_2O_7, which made the Al_2O_3 scale structure uneven, causing scale spallation and finally, large mass decreases [30]. Since less emphasis has been given to oxidation resistance, the superalloys should rely on coating technologies to improve the resistance to environmental degradation.

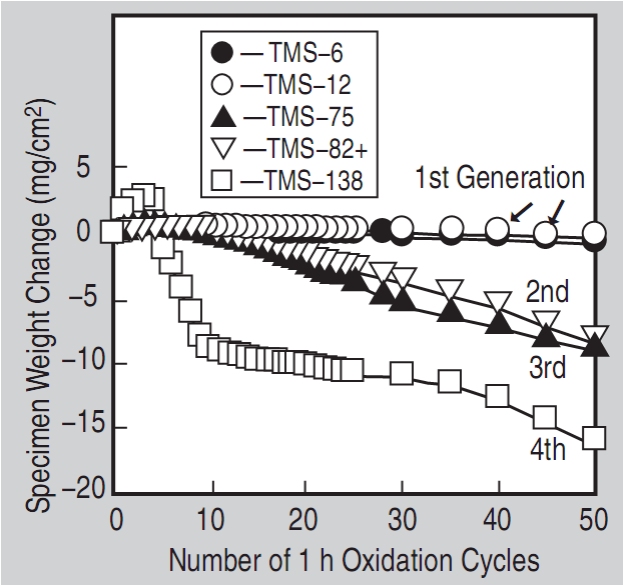

Figure 1-12: *Cyclic oxidation testing at 1100°C (1h hold at high temperature) for various generation of SC superalloys.*

In Ni-base superalloys, aluminum participates in the formation of the increased high-temperature oxidation resistance of the alloy. It is kept at a level below 6 wt% to maximize creep strength. If such bare alloys are exposed to the environment of high-temperature turbine engines, they will degrade fast by several of the processes discussed below. It is now currently accepted that protective coatings on Ni-base superalloys encounter two types of high temperature corrosion degradation. Fig. 1-13 shows the corrosion and oxidation rates in different temperature ranges. High temperature hot corrosion (HTHC), also designed as Type I HC, involves the transport of sulphur from a sulphatic deposit (generally Na_2SO_4) across a performed oxide into the metallic material with the formation of the most stable sulphides. Once stable sulphide formers (e.g. Cr) are fully reached with the sulphur moving across the scale, then base metal sulphides can form with catastrophic consequences as they are molten at the temperatures at which Type I HC is observed, typically in the 800 to 950° C range. It is caused by molted salt deposition on the coating surface. Thus, the formation of NiS_2 (molten at 645°C) can cause degradation levels which are serious enough to cause major component degradation. The most suitable materials which can resist Type I hot corrosion are diffusion coatings and overlay coatings containing up to 25 wt% Cr and 6 wt% Al. Low temperature hot corrosion (LTHC), also know as Type II HC, occurs in the 600°-800°C range. The low temperature hot corrosion

mechanism involves the formation of base metal sulphates which require a certain partial pressure of sulphur trioxide for their stabilization. These sulphates react with alkali metal sulphates to form low melting point compounds which prevents a protective oxide forming [6, 29, 31].

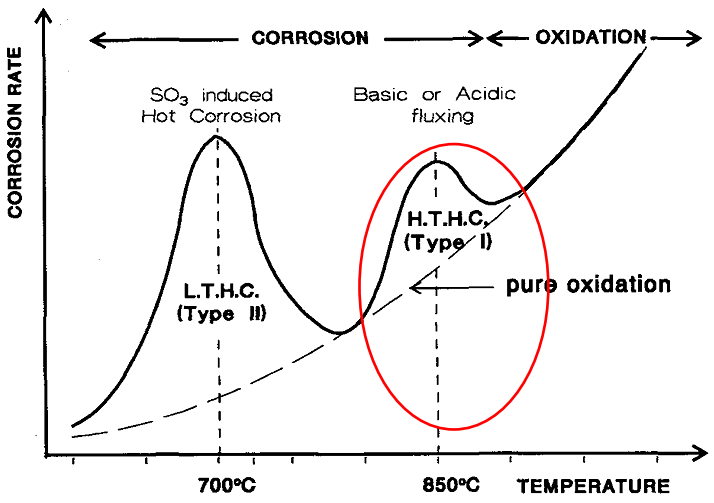

Figure 1-13: *Corrosion rate versus temperature.*

Generally speaking, gas turbine blades operate on a relatively wide range of operating temperature and environments. Thus, some beneficial protective coatings to HTHC are necessary.

The schematic diagram in Fig. 1-14 shows the effect of Cr composition on the hot corrosion and oxidation resistance of several types of aluminide diffusion coating and overlay coatings. This thesis is mainly focused on the aluminide diffusion coating. The Pt-modified aluminide coating is also discussed.

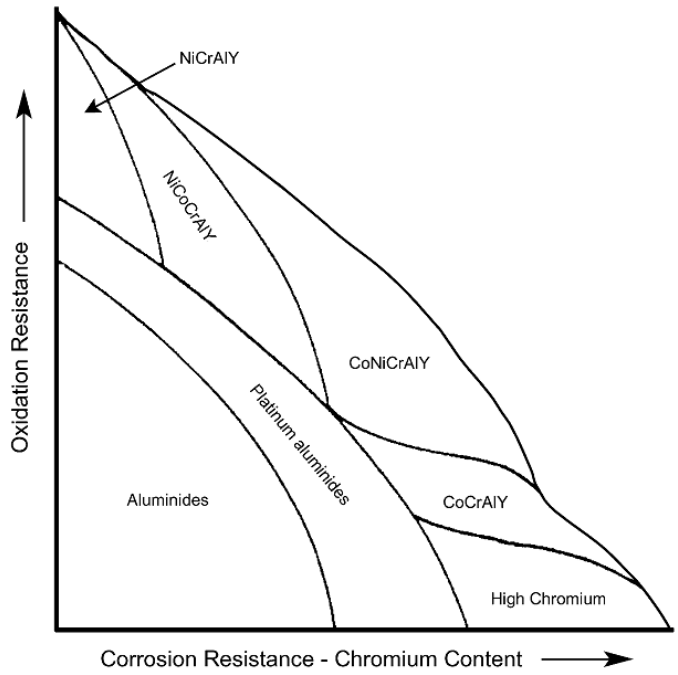

Figure 1-14: *Relative oxidation and corrosion resistance of high temperature coating systems [27].*

From the above analysis, generally speaking, the blades should satisfy the very wide range of operating temperatures. The aluminide coatings are used for Type I hot corrosion and oxidation conditions, but not used under Type II consitions. On the other hand, chromised and chrome-aluminide perform well under Type II condition. Silicon containing and/or chromium rich diffusion coatings offer improved corrosion resistance at the lower temperatures.

The aluminum and chromium contents referred to above apply to isothermal oxidation conditions. However, when thermal cycling conditions prevail, oxide scale can spall from the substrate surface due to thermally induced stresses. The oxidation resistance under such conditions can be markedly improved by the addition of so-called reactive elements (RE) (Y, Hf, Ce) to alloys and coatings. The RE segregate to grain boundaries within alumina scales causing a reduction in Al and O transport rates through the oxide and thus reduce oxidation rates. The effect of additional of RE is also discussed in Section 1.5.2.6.

1.5 Oxidation and Corrosion Resistant Coatings-types and Chemistries

As discussed in last section, the term 'oxidation/corrosion' is meant to refer to high temperature interactions between the superalloy or coated superalloy and the environment. The major active element is oxygen, however, corrosive effects can result from other elements such as sodium, sulfur. The coatings for Ni-base superalloys were developed to provide good oxidation/corrosion. The performance of the coating lies in the formation a layer of oxide scale, limiting access of oxygen and corroding salt to the base substrate.

Comprehensive reviews on high-temperature coating have appeared regularly since the early 1970s. Coatings are tailored for specific applications by controlling their elemental composition, microstructure, and by selection of manufacturing. Fig. 1-15 lists the coating processes mainly used in the industry. Roughly, it is divided into the types, one is the metallic coating, the another is ceramic coating. The main coating talked in this thesis is focused in diffusion coatings. TBC (Thermal Barrier Coating) is belong to ceramic coating which depositing a ceramic layer on the surface of the alloy. However, the expansiton coefficient between the ceramic coating and base substrate is always a critic problem which can lead to crack. Thus diffusion coating can be used as bond coat prior to the deposition of ceramic coating.Therefore, there is also close relationship between metallic coatings and ceramic coatings.

A high quality of coating must be thermodynamically stable, can maintain a uniform thickess during service. It should have slow growth rate when oxidizing, and higher adherence with substrate. The coating is also required to withstand service-related creep, fatigue and impact loading of surface without failure.

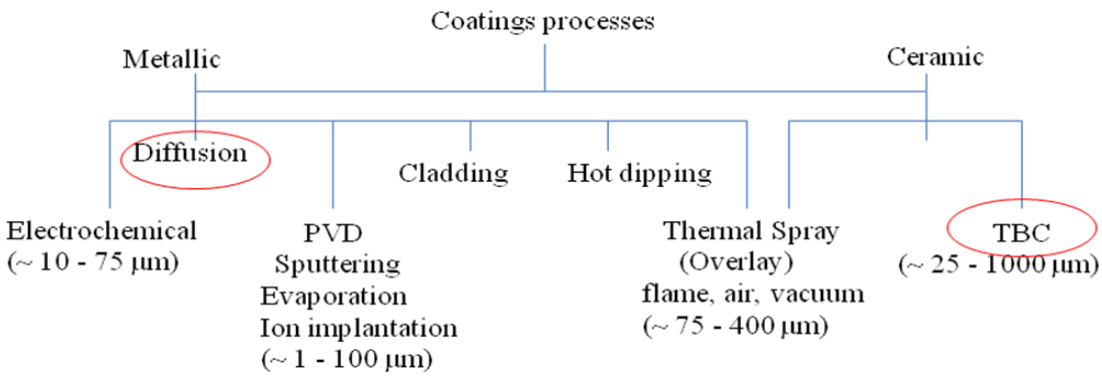

Figure 1-15: *Some common coating methods.*

In a word, a high-temperature protective coating must provide adequate environmental resistance, should be chemically and mechanically compatible. The performance of the coatings lies in the formation of thin oxide scales on the coating surface, that limit access of oxygen and corroding salts. The diffusion coatings such as aluminides (e.g. NiAl) can form Al-rich β-phase (BCC, B2) layer on the surface of the substrate alloy. This layer serves as an Al reservoir for the formation of a protective α-alumina scale which as a diffusion barrier to minimize further reactions. Alumina has been found to be the most effective protective material which regard to oxygen and is also beneficial with regard to most of the other reactive environment elements. My thesis work is focused mainly on the diffusion coating. Diffusion coating has also been used as bond coat for thermal barrier coating (TBC)previously deposited on the substrate. Thus, the metallic coating and ceramic coating are connected together.

The detail describtion of the relationship of diffusion aluminide coating and some TBC coating is given in Section 1.5.2.7.

R. Streiff [31] has made a classification of the coating respect to the status of the available coatings (shown in Fig. 1-16).

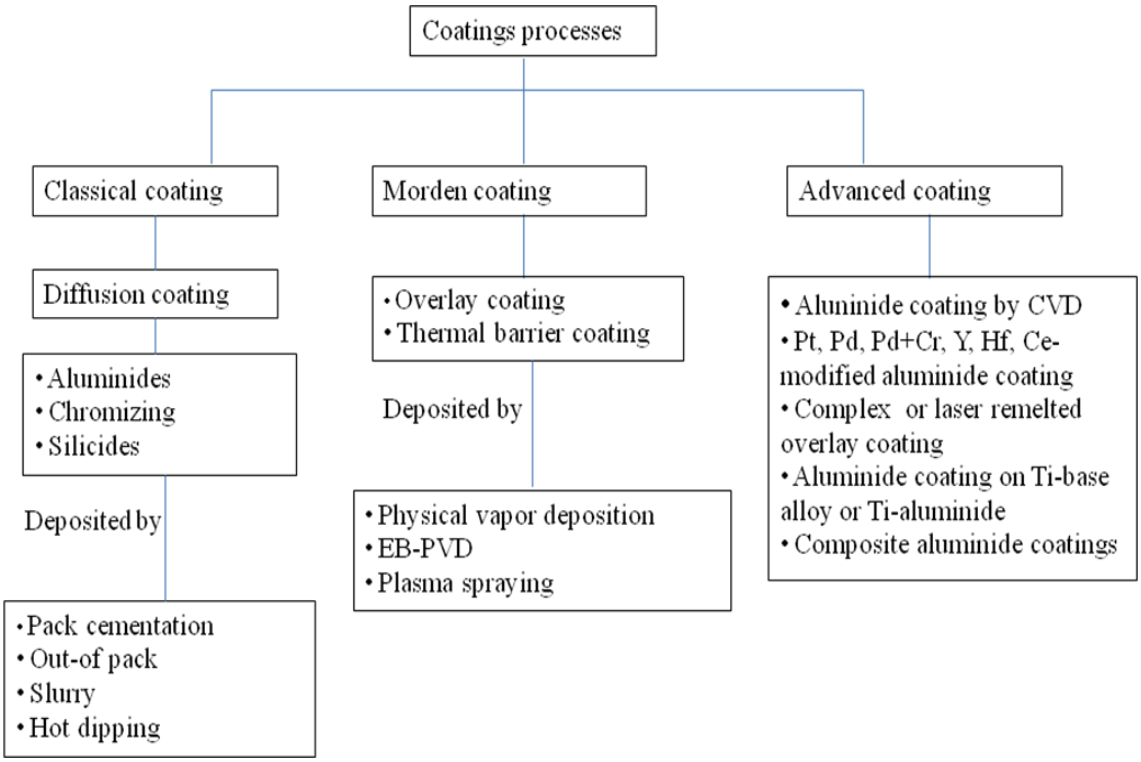

Figure 1-16: *Classification of the coating methods according to the status of the available coatings.*

As shown in Fig. 1-16, aluminide diffusion coatings belongs to the 'classic' coatings since it was fully developed in the late 1960s. Nevertheless, aluminizing is the most widely diffused coating even nowadays. The selection of the process depends on the component design and the application. For example, coatings required for protection against hot corrosion may not be optimum for oxidation protection.

1.5.1 Diffusion Coatings on Ni-base Superalloys

In the late 1960s, aluminizing was first applied to the protection of aeronautical gas turbines [31]. Aluminide diffusion coatings are now routinely used in the hot sections of gas turbines to enhance their resistance to high temperature oxidation and hot corrosion. Plain aluminides have provided cheap and cost-effective solutions to protect superalloy components within the high-pressure turbine of both aero and industrial gas turbines. Therefore, they are the most widely used coatings in service within the gas-tubrine industry. The diffusion coating processes have also been improved by enriching the surface in Al, Cr, Si etc. These aluminizing, chromizing, and siliconizing processes result in enhanced oxidation and/or corrosion resistance

through the formation of protective thermally grown oxides of Al_2O_3, Cr_2O_3 and SiO_2 as discussed later in this work. It consists of a substrate alloy surface layer enriched with the oxide scale formers Al, Cr, Si or their combination to a depth of 10 to 100 µm.There was renewed progress in siliconizing and silicon-modified aluminide diffusion coatings for high temperature service in early 1970s.

A major problem encountered with such coatings is that the coefficient of thermal expansion of the alumina layer differs from the coefficient of expansion of the base material and the coating material which are generally similar. During thermal cycling, stresses develop between the alumina layer and the coating material. The alumina layer, which is relatively brittle, tends to crack and spall off thus exposing a fresh surface to the deleterious atmosphere. This repeated formation and spallation of the oxide layer causes the reduction of the coating material in aluminum content. When the aluminum level of the coating material drops below a certain point the coating becomes ineffective as an alumina former and the protective benefits of the coating material are lost.

Diffusion coatings can be applied to hot gas components by a variety of techniques including pack-cemetation, out-of-pack, gas and vapor phase chemical vapor deposition etc. Comprehensive reviews of the methods are given by Pomeroy[6], R. Strieff [31], R. Sivakumar and B.L. Mordike [32], Goward [33], J. T. Demasi-Marcin and D.K. Cupta [34]. The diffusion coating with combined aluminum and chromium or aluminum and silicon has also been produced [35, 34]. Pt, Pd-modified aluminides have also been studied by many researchers [37-39]. Reactive elements (Y, Hf, Zr)-modified aluminide have been investigated since they were found to improve cyclic oxidation resistance [39-41]. Generally speaking, all diffusion coatings are formed as a result of two distinctly similar process steps [42]:

(i) The diffused elements (Al, Cr, Si) must be brought into contact with surface to be coated. For metallic systems, a vapor species with a high solute metal content is needed. It is most commonly achieved through the use of a halide salt, or salt mix, which may involve fluoride, chloride, or iodide species.

(ii) The diffused elements (Al, Cr, Si) diffuses into the component surface. This step is a key stage for diffusion coatings. This diffusion step leads to the formation of the surface alloy or intermetallic compounds often in a layered structure. The process temperature influences the rate of diffusion, surface

layers in terms of thickness and chemical composition. When more than one elements diffuses, it also affect the other elements diffusing and their equilibrium composition. This aspect will be explained in more detail using the 'pack-cementation' processes (see Section 1.5.2.1). The time at temperature controls the degree of interdiffusion, establishes the concentration gradients that will develop from the surface to the interior of the coating and defines the various layers that may form as dictated by thermodynamic and kinetic considerations.

1.5.1.1 Diffusion Concepts in the Alloys

Background in the fundamental concepts of thermodynamics, kinetics of reactions, diffusion, crystal structure, phase equilibrium, and phase diagrams of alloys is essential in order to understand the selection, processing, and behavior of high-temperature coatings.

Diffusion is the process of mass transport through matter. Our interest is in mass transport through solids. Generally, there are three major mechanisms for diffusion in solids. In the first, known as volume diffusion, atoms diffuse by migrating from atomic sites through vacancies. The second mechanism is a modification of the first in which atoms migrate through defect sites such as dislocations, surface, and grain boundaries where the amount of vacancies is higher. The third mechanism involves movement through interstitial atomic sites. The driving force for diffusion is the reduction in free energy. In the most practical cases this translates into the existence of a concentration gradient and diffusion occurring from higher concentration C_i to lower concentration C_f (Fig. 1-17).

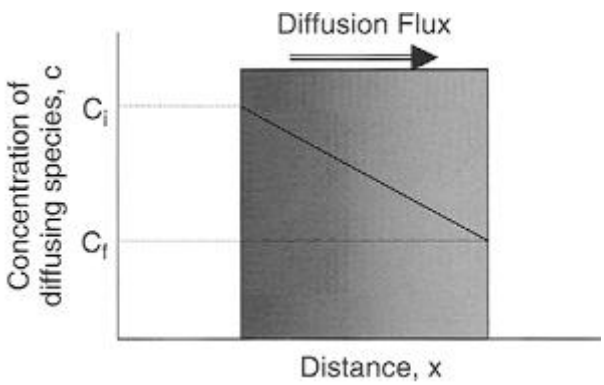

Figure 1-17: *One dimention of Diffusion.*

The rate of diffusion is governed by Fick's first and second laws, valid in the case of steady state condition and specific diffuse condition, respectively. These laws are represented by two equations.

The first law of diffusion: Under steady-state conditions, that is, when the concentration at any point does not chance with time, the flux of diffusing species is given by Fick's first law,

$$J = -D\Delta c \qquad (2)$$

With J being the flux (atom/m^{2}s), D the constant of proportionality called the diffusivity or diffusion coefficient (m^2/s), and Δ the differential operator, given by $\frac{\partial i}{\partial x} + \frac{\partial j}{\partial x} + \frac{\partial k}{\partial x}$. Here *i, j, k* are unit vectors along the orthogonal x, y, z directions, respectively. Thus Δc is the concentration gradient, c being the concentration (atomic). In one dimension, $\frac{\partial c}{\partial y} = \frac{\partial c}{\partial z} = 0$, above equations law reduces to

$$J = -D\, dc/dx \qquad (3)$$

The second law of diffusion: Under non-steady-state conditions, where the concentration at any point changes with time, the rate of change of concentration is given in three dimensions by

$$dc/dt = D(d^2c/dx^2 + d^2c/dy^2 + d^2c/dz^2) \qquad (4)$$

In one dimension this equation reduces to

$$dc/dt = D\, d^2c/dx^2 \qquad (5)$$

The diffusion coefficient D is strongly temperature dependent and can be expressed in the form of the Arrhenius equation,

$$D = D_0 \exp(-\Delta H/RT) \qquad (6)$$

D_0 is a constant which involves the expected frequency of jump of atoms, and ΔH is the activation energy of the diffusion process. Typically, the relative values of diffusion coefficient rank in the following order:

$$D_{surface} \rangle D_{grainboundry} \rangle D_{volume} \qquad (7)$$

Or in terms of activation energy,

$$\Delta H_{surface} \langle \Delta H_{grainboundry} \langle \Delta H_{volume} \qquad (8)$$

Here the subscript "surface", "grain boundary", and "volume" indicate that the diffusion paths are predominantly over surface, along grain boundaries, or within the grain, respectively. The diffusion is easy at the grain boundary and is sensitive to the effect of temperature. The comparative order of diffusion coefficient is very important in understanding the behavior of coatings. Coatings are typically fine grained with more grain boundaries compared with substrate materials. Diffusion rates in coatings are therefore expected to be faster than in substrate of similar composition [9].

1.5.1.2 Ni-Al Binary Phase Diagram

Even if we will focus on a Ni-base superalloy of complex chemical composition, the equilibrium binary phase diagram (Fig. 1-18), can give useful information of the typical phases in Al diffused coating of Ni-base superalloy.

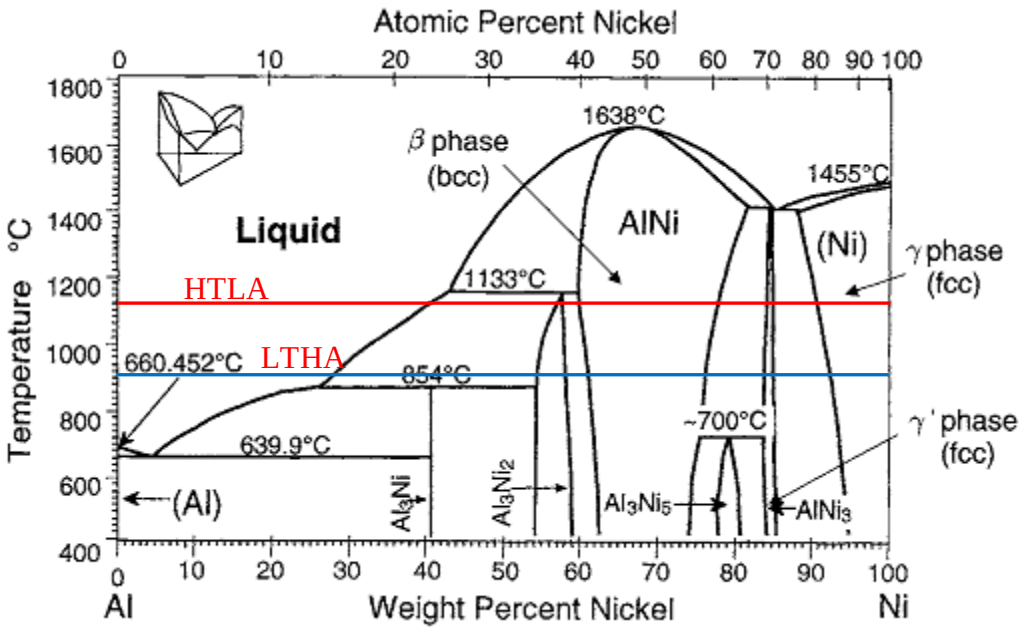

Figure 1-18: *The Ni-Al phase diagram [43].*

Additional information contained in the diagram includes the melting temperatures as a function of composition and the range of composition within which multiple phases coexist in equilibrium. The γ phase dissolves up to 4 wt% Al below 400°C. The solubility increases as the temperature is raised. The γ' phase, on the other hand, has a narrower phase field, which means that the composition does not depart

significantly from Ni_3Al. The β field is very broad, indicating that in this phase the concentration of Al can depart widely from the stoichiometric composition NiAl. Also, the melting point of the β phase is much higher than that of pure Ni. These characteristics of the β phase are very favorable in high temperature coatings. The high Al concentration helps in providing a large reservoir of Al for oxidation protection through the formation and replenishment of Al_2O_3 scale. The change in microstructure of a β-phase-containing coating on thermal exposure can also be analyzed by the use of the phase diagram.

This binary diagram serves as a referece for the phases formed during aluminizing on pure Ni which will be given in detail. Here, we just analysis several common phase in this diagram. The low activity high temperature (HTLA) coating is performed at 950°C - 1100°C. The Al concentration is in the range of 40 - 45 at%. At this range, only β-NiAl layer formed on the external surface of the alloy. While, for LTHA coating, the temperature range is 700°C - 950°C and with higher concentration of Al. Thus, Al_2O_3 phase is typically formed.

1.5.2 The Classes of Diffusion Coatings

High temperature coatings based on intermetallic compounds such as aluminides are extensively used to protect gas turbine hot section components from attack in aggressive environments. There are three major processes (Fig. 1-19) by which the aluminide can be formed. Here in the following, we focused on the aluminizing process, there are typically formed by pack cementation, out-of-pack cementation and by chemical vapor deposition (CVD) which involve the diffusion element such as aluminum (chrominum or silicon).

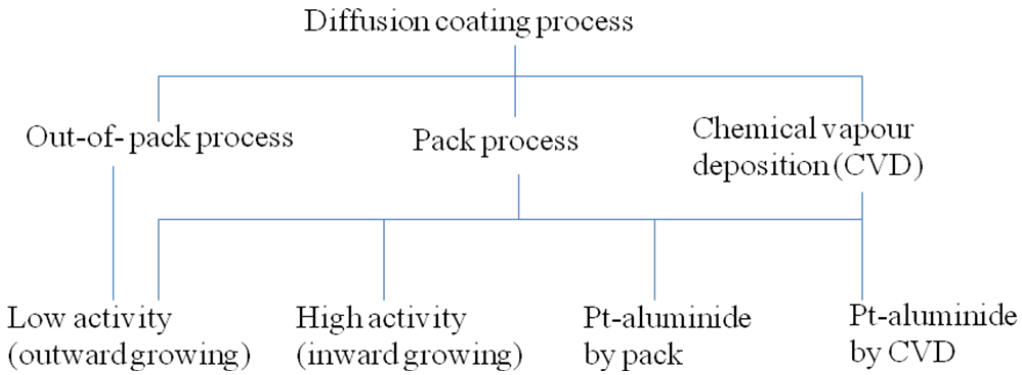

Figure 1-19: *Various diffusion coating methods.*

Since the first introduction of pack cementation to gas turbines, it is still extensively used. The pack processes include also chromizing and siliconizing. The chromized and silicized coatings are limited in use to temperature of below 950°C since both form volatile species which afford no protection against oxidation or corrosion but can, however, be used successfully at lower temperatures. Typical pack powder compositions are shown in Table 1-4.

Table 1-4: *Typical pack powder compositions.*

Diffusion coating	Pack composition(wt%)	Coating temperature range, °C
Aluminizing	1-15Al, 1-3NH_4Cl, balance Al_2O_3	750-1050
Chromizing	48Cr, 4NH_4Cl, balance Al_2O_3	750-1050
Siliconizing	5Si, 3NH_4Cl, balance Al_2O_3	750-1050

In view of the fact that turbine blades and vanes encounter temperature to 1100°C, aluminizing is the most important and widely used in the gas turbine industry. For example, the vast majority of aeroengine turbine blade areofoils are aluminized in some way to improve their resistance to high-temperature oxidation or as a bond coat prior to the deposition of the TBC. Chromising is of particular use for resistance toward Type II hot corrosion and has also been found to be of major benefit in protecting Ni-based alloys from corrosion by sulphatic deposits in chemical plant. For Siliconizing, because silica has low solubility in molten sulfates, it is expected that siliconized diffusion coatings would do well against Type II hot corrosion. The silica scales, can not resistant to Type I corrosion. The siliconzing coating is usually sued on gas turbines for marine application. Such coatings are rarely used on Ni-base alloys because of the formation of brittle or low-melting phase.

One of the steps, which is common among the three processes, is the generation of vapors containing aluminum or the other metallic constituent of the coatings. The key step is the formation of a volatile alumininum subhalide, AlXn (X=F, Cl, Br; n<3), which occurs at temperature > 800°C. This species reacts with the surface of a Ni alloy to deposit aluminium by the following reaction:

$$AlX_n + Ni \rightarrow AlNi_y + AlX_3 \qquad (9)$$

The difference between in the processes lies in the way that the AlX_n is generated and transported. The intermetallic layer created at the surface has the composition $NiAl_y$ ($3 \geq y \geq 1/3$). Whilst the aluminium is brought to the surface by a vapor phase process, its diffusion into the surface is a solid state process.

The vapors are transported to and react with the alloy constituents forming the aluminide coating. Additionally heat treatment may be required to achieve desired composition, microstructure, and properties through diffusion processes. The difference among the process in Fig. 1-19 lies in the method by which the halide vapors are created and transported to the component [44].

Two basic mechanisms differ the diffusion coatings depending on whether the main diffusing species is aluminium diffusing from the coating or is the base metal diffusing from the substrate alloy. The two mechanisms lead to two types of coatings known as inward and outward diffusion which will be described in Section 1.5.2.5.

1.5.2.1 Pack Cementation Aluminide Process and Effects of the Activitors

The pack contains a donor alloy (releases solute material at a known rate and hence determines the pack activity), a halide activator and an inert oxide diluent which prevents pack sintering.

During pack aluminizing, the component to be coated is firstly cleaned, dried and then placed in an air-tight retort containing a mixture powder of aluminium (or an aluminum alloy), a halide activator (NH_4Cl or NaCl or CrF_2) which reacts with aluminum to generate the aluminum halide vapors and an inert Al_2O_3 filler which prevents the sources form sintering on continued exposure to high temperature [1]. The inert filler powder also provides interconnected porosity for vapor transport [45]. Fig. 1-20 presents the schematic of a classical cementation box. The box is then inserted into a furnace and heated in the temperature range 800-1100°C in a protective atmosphere such as argon or H_2. The components may be buried in or placed above the powder mixture. The exact process cycle, time and temperature are dependent on the required coating, coating thickness and subsequent heat treatment. The pack cementation process is essentially an in situ chemical vapor deposition (CVD) coating process.

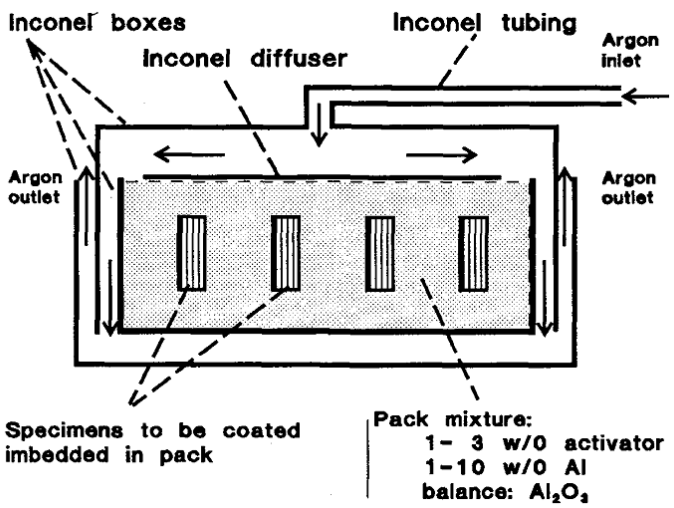

Figure 1-20: *Schematic of a classical cementation box.*

The reactions is occurred between the mixed powder and components to form β-NiAl coating. Fig. 1-21 Shows the schematically the different coating steps. The formation of aluminide coatings by pack cementation has been studied extensively. The strucuture and composition of the coatings have been found to be dependent on the substrate alloy [31, 42, 46]. This implies that the coatings are generally tailor made for a specific alloy.

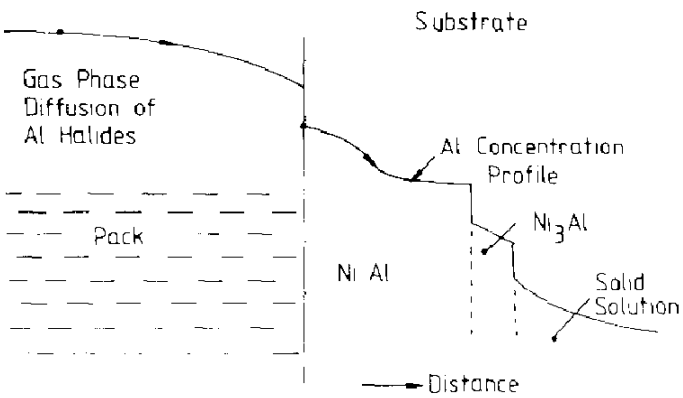

Figure 1-21: *Schematic diagram of layered features during pack aluminizing [32].*

Good coating reproducibility, low cost and ideally suited for coating small components are the main advantage of the pack process. The disadvantages are the limited flexibility of coating composition of the coating and the coating thickness.

Pack-particles may entrap in the outer layer of the coating, which hinder the continuous of the coating scale.

1.5.2.2 Out-of-pack Vapor Phase Aluminizing Process

The out-of-pack or over-pack process operates in a manner similar to pack cementation, except that the components to be coated are suspended either above the pack or below from the pack (vapor generator) retort.

The transport of aluminum species from the vapor phase to the substrate occurs by gas-phase diffusion and by solid-phase diffusion of aluminum into the substrate to form the aluminide phases. The former increases the surface concentration of aluminum in the coating while the latter decreases it. The surface composition of the coating tends to reach a steady state value in a short time after the commencement of the process. In the vapor phase aluminizing, the rate of transport of aluminum to the substrate is much faster than the solid phase diffusion of aluminum into the substrate. Thus the composition of aluminide coating is decided by the kinetics of the solid phase diffusion. The coating process is divided into a number of steps. They are:

a) Formation of the aluminum subchlorides by the reaction of the aluminum metal or alloy and the aluminum chloride vapor.

b) Transport of the subchlorides to the substrate by gas-phase diffusion.

c) Reaction leading to the deposition of aluminum at the substrate surface.

d) Diffusion of aluminum into substrate with the formation of the coating consisting of different intermetallic phases.

e) Diffusion of the reaction products from the substrate back to the reactor.

Steps (a) and (c) are very fast at the operating temperature, therefore, the thickness of the coating process is controlled by step (b) the vapor transport and (d) the solid-phase diffusion. Step (e) decides the purity of the coating.

The schematic diagram of the out-of-pack process is given in Fig. 1-22. The coating vapors are transported to the components by an inert carrier gas. Plumbing is designed that the vapors can access to both external and internal surfaces of the components. The retort is inserted into a furnace and held at the desired temperature for the selected duration.

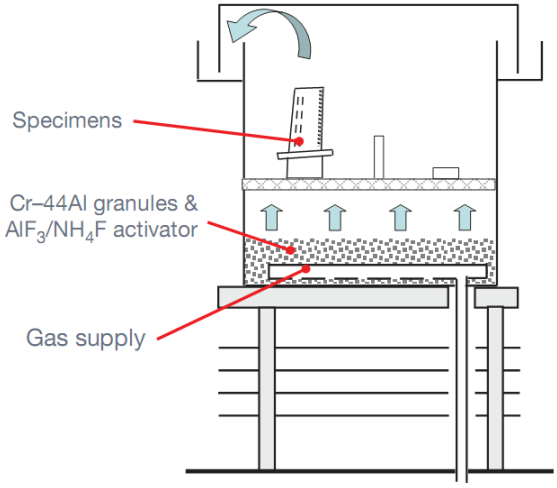

Figure 1-22: *Schematic of the out-of-pack vapor phase aluminizing process [48].*

This approach results in a much cleaner and uniform coating for very complicated geometry components, with no entrapped pack particles.

In industry, for example, components are aluminized using a proprietary SIFCO vapor phase aluminizing process. A picture of the facility is shown in Fig. 1-23a. At the beginning of the vapor phase coating process, the components, activators and fillers are loaded into a coating box, then the coating box is covered with a retort. During the vapor phase process, the coating box is heated to an elevated temperature of about 1080°C, held for 3 to 4 h, and then cooled down to room temperature. The temperature profile during the aluminizing process is shown in Fig.1-23b.

a) 
b) 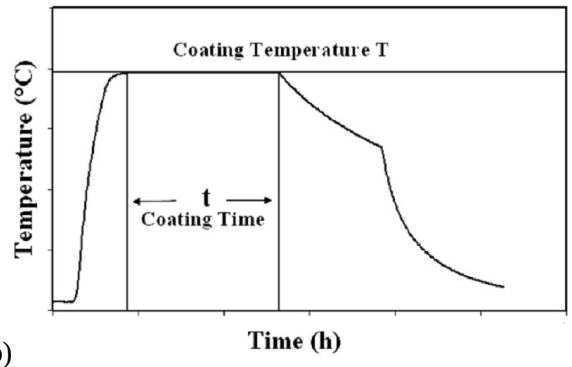

Figure 1-23: *a) SIFCO vapor phase coating process facility, b) Vapor phase coating thermal cycle process [37].*

1.5.2.3 Gas Phase Chemical Vapor Deposition (CVD) Processes

In CVD processes (shown in Fig. 1-24), the $AlCl_3$ is generated outside of the reactor prior to its introduction into the reaction vessel, which allows its flow rate and activity to be accurately controlled, so that consistent and uniform aluminide layers can be produced. A particular benefit of this system is the cleanness of the coatings yielding improved oxidation resistance and the fact that the gas can pass through, as well as over hollow components, such as turbine blades with cooling channels so that internal and external surfaces can be diffusion coated. In contrast, pack aluminizing can cause cooling holes to be blocked with diluent particles which require removal after processing. An additional benefit of the CVD process is that the chemistry can be carefully controlled enabling additional elements such as Y, Al, Si and Hf to be incorporated into coating at precise level.

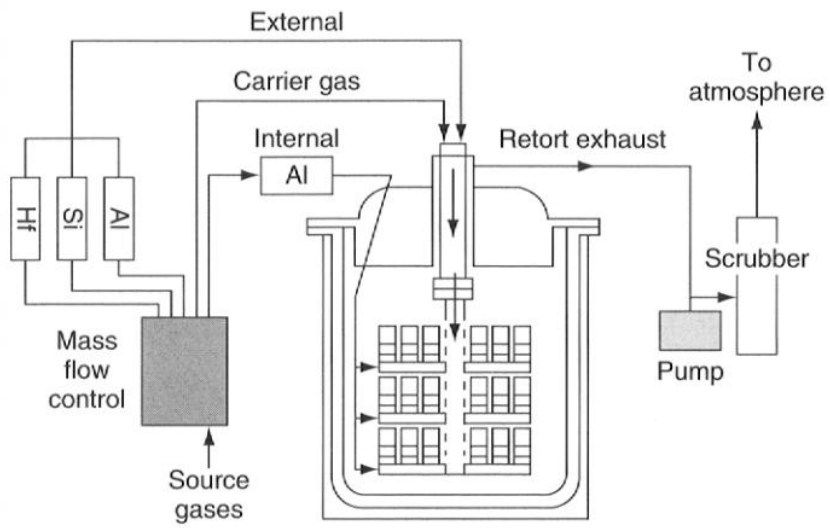

Figure 1-24: *Schematic of the low-activity codeposition of Si, Hf and Al in CVD coating [39].*

1.5.2.4 Slurry-based Diffusion Coatings

Slurry-based diffusion coatings are commercially available, offering similar chemistries to those found in conventional pack cementation aluminide coatings. In slurry cementation, the coating materials and halide activator are blended as a slurry or particle-loaded paint system, using either an organic binder or a water-based emulsion. The slurry/paint system can be applied to be part to be coated through

dipping or spraying at or near room temperature. The slurry spray is then cured onto the part through a low-temperature thermal treatment, typically around 200°C. The cured pre-diffusion coating may contain only Al, Al+Cr, Al+Si or Al+Cr+Si, depending on the final service conditions. After this, the precoted parts are heated in a furnace to allow the diffusing of Al (Si and other additions). The hold temperature of this step is in the range of 650-1100°C, depending on the substrate to be coated and its final application. The temperature is chosen such that the coating material contained in the slurry reacts and interdiffuses with the substrate to form the final intermetallic coatings [9, 48].

1.5.2.5 Diffusion Coating Mechanism

Aluminizing is achieved by two different processes which are based on the activity of aluminium in the gas phase and the aluminizing temperature. The low activity high temperature (LAHT) process is a 'one step' methods, with outward diffusion of Ni to form β-NiAl coating. On the other hand, the high activity low temperature (HALT) process concerns the inward diffusion of aluminum, typically giving rise to a δ-Ni_2Al_3 coating which requires subsequent heat treatment to convert it to β-NiAl. Because δ-Ni_2Al_3 is a brittle phase which has lower mechanical property than β-NiAl. As might be expected, the mechanisms by which the coatings grow are also different. For the LAHT process the aluminium activity is insufficient for it to be the predominant diffusing species and accordingly, coatings form by the diffusion of Ni from the alloy substrate into the region of the coating. For the HALT process, the aluminium activity in the gas phase and at the surface of the coating is high enough to facilitate the inward of Al into the alloy substrate. The growth mode is an important factor when considering coating integrity, since coatings formed by outward Ni diffusion can trap diluents particles (alumina) brought by aluminizing packs. While, in the coating β-NiAl phase layer of LTHA, much unwanted phases can precipitate dispersively, which decrease the mechanical property of the coating. Which coating process is selected depends upon a number of features, e.g. heat treatment specifications for the substrate alloy, applications, nature of packs available, integrity issues, etc. Squillace [49] has presented a comparation between the two processes of coatings. The coating layers have similar thickess, but the structure is substantially different. Both processes have achieved an aluminide layer with acceptable oxidation resistance for specific applications.

High Temperature Low Activity Coating (HTLA)

In HTLA aluminizing (low aluminum content in the pack (1.2-1.5 wt% of Al), 900°C-1150°C), the aluminum is deposited on the surface, but at a reduced rate, and nickel simultaneously diffuses outward to the surface. Then a β-NiAl surface layer forms. Fig. 1-25 is an example of the concentration profiles obtained from pure nickel specimen aluminized for 20 to 60 h at 1000°C in packs of various Al : Ni ratios [50]. The curves exhibit a pronounced inflection and steep drop in the composition range of 50 at% to 45 at% of Al. Surface concentrations decrease from 54.7 at% to 48.6 at% of Al with drcreasing pack Al:Ni ratio and it may be seen that the length of nearly horizontal portion of the curves and the total thickness of the β-NiAl layer decrease correspondingly.

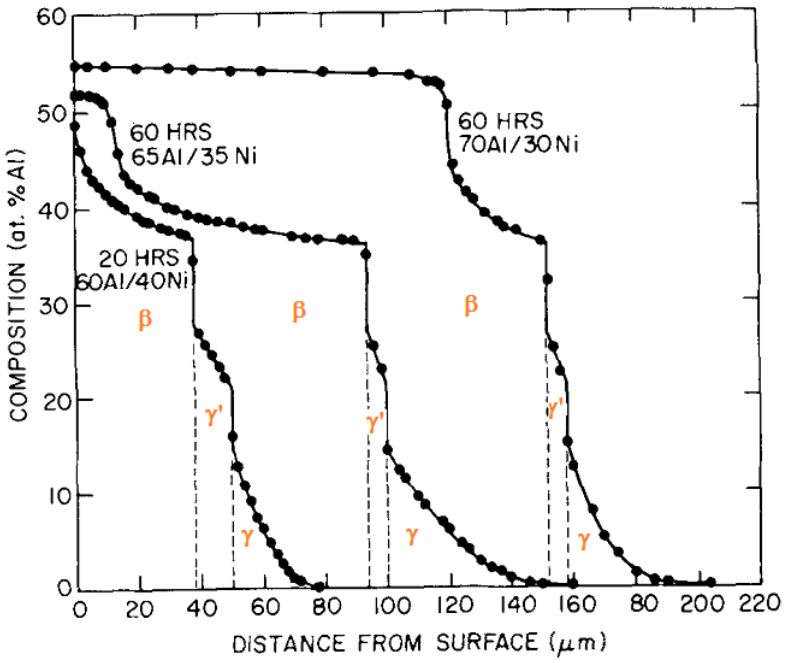

Figure 1-25: *Concentration profiles in pure nickel specimens aluminized at 1000°C to give different surface compositions.*

The interdiffusion coefficient variant with the composition in β-NiAl at 1050°C is shown in Fig. 1-26. It illustrated that the interdiffusion coefficient in the β-NiAl phase of the Al-Ni system varies strongly with composition. The minimum value of interdiffusion coefficient is not at the stoichiometric composition, but displaced to the low-Al side by 1 to 2 at% (that is 48 at% to 49 at% of Al). Ni diffuses predominantly in low-Al β-NiAl.

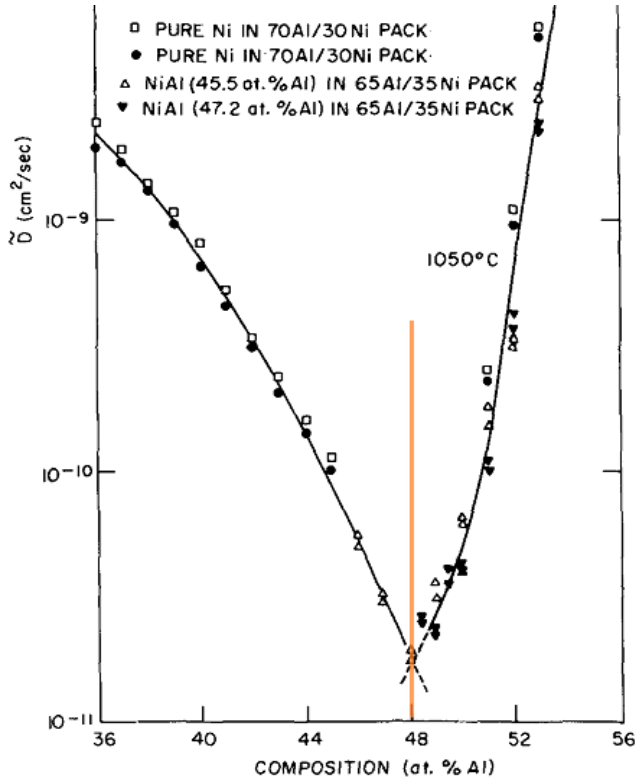

Figure 1-26: *Variation of interdiffusion coefficient Ď with composition in β-NiAl at 1050°C.*

This rapid nickel diffusion to the surface, coupled with the low aluminum activity at the surface, effectively holds the surface aluminum content close to 50 at%. Hence, HTLA coatings are near stoichiometric at the surface and Ni-rich within the substrate β-NiAl phase. This structure ensures outward of Ni transport and the outward growth of the coating microstructure. Another important result is that slowly diffusing elements Ta, W, Re, Mo from substrate are unable to diffuse to form significant concentration levels in the outwardly growing β-NiAl. The outer zone of this coating therefore appears much 'cleaner' and is free from such precipitates as observed in the LTHA coatings [46]. The limited solubility of Cr as well as Ta, Mo, W in the β-NiAl phase produces precipitates of topologically-close packed (TCP) phases forming a interdiffusion zone (IDZ) under the 'clean' β-NiAl phase layer [51]. Thus, the IDZ includes the complicated TCPs and β-NiAl phases. This coating composition and structure are less dependent on the alloy composition. The further diffusion processes between such aluminide coatings and Ni-base alloys are determined by the aluminium activity in the β-NiAl phase. As long as this is lower than the equilibrium

activity among β, IDZ and γ+γ' matrix, Ni will diffuse out of the base alloy into the β phase. The coating grows further outwards.

One example of nickel aluminide diffusion coating produced by HTLA pack cementation process is illustrate in Fig. 1-27. The coating consisted of a well defined top 'clean' layer with NiAl as its major phase and a large diffusion zone underneath.

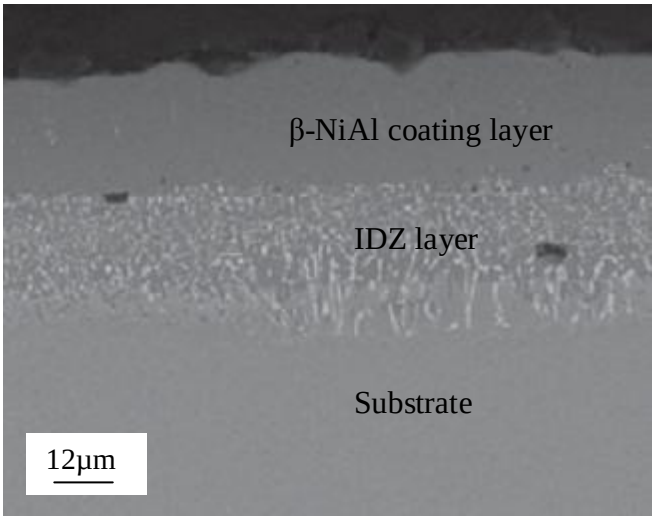

Figure 1-27: *A nickel aluminide diffusion coating produced using HTLA pack cementaion process.*

Sun et al [50] has also studied the kinetics of the formation of aluminide coating on pure Ni by HTLA. Fig. 1-28 illustrates this mechanism. Respect to the THLA theory interpreted above, if the activity of Al is low, Ni preferentially diffuses out through the coating and combines with Al to form NiAl. The coating grows outward. In this case Ni diffuses faster than inward diffusion of Al. Pack particles are entrapped in the coating. These particles are assumed to be dragged out by the diffusion of Ni.

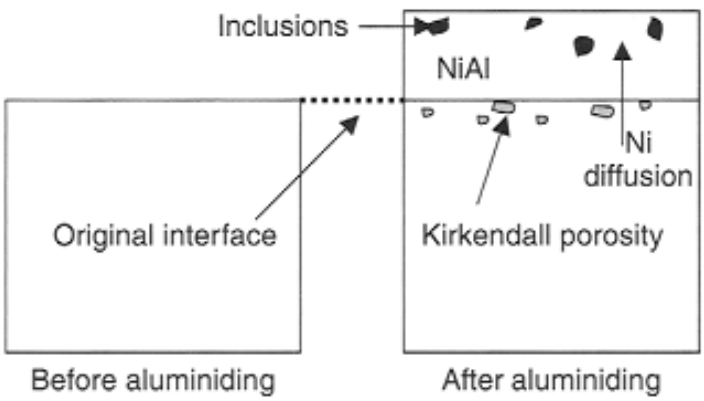

Figure 1-28: *Diffusion aluminide formation on pure Ni.*

Further, moving to the Ni-base alloy (Fig. 1-29), Ni diffuses outward and combines with Al to form the external NiAl zone. The middle layer, the so-called IDZ, loses Ni. The loss of Ni from the substrate alloy (γ+γ'), forms the β-NiAl phase (γ+γ'-Ni=Ni+Ni_3Al-Ni=NiAl+3Ni). The formed β-NiAl in the IDZ layer has very low solubility for many of the alloying refractory elements of the alloy. These refractory elements, therefore, precipitate out to from TCPs. It is notable that the outer β-NiAl phase layer is clean containing a lesser amount of the slowly diffusing substrate elements in the coating.

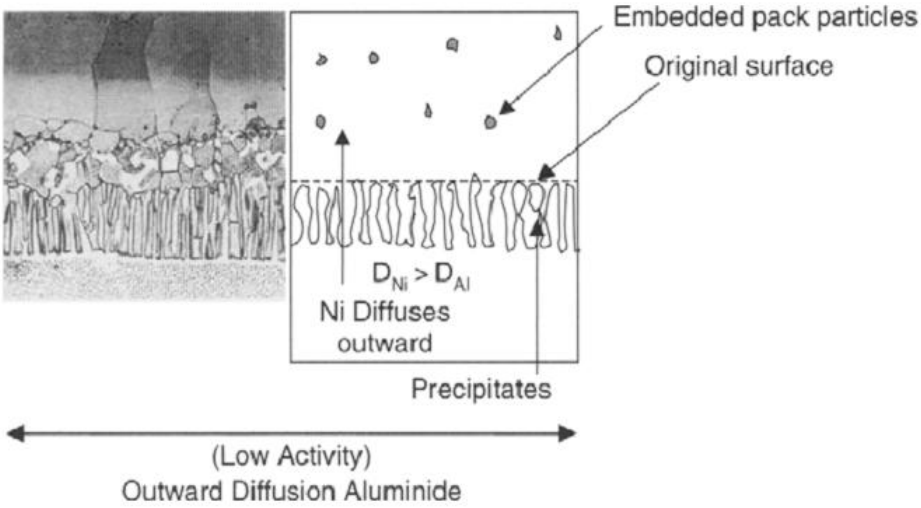

Figure 1-29: *Microstructure and schematic diagram for HTLA aluminide coatings [39].*

Low Temperature High Activity coating (LTHA)

As previously mentioned, LTHA coatings are processed at lower temperature (700-950°C) as the first step, with a higher aluminum content (1.7-2.7 wt% of Al). The substrate material (γ-Ni + γ'-Ni_3Al) reacts with the depositing aluminum forming a surface layer of δ-Ni_2Al_3 [52, 53] over the layer of β-NiAl. The diffusivity of Al through δ-Ni_2Al_3 is very high, and substantial amounts of Al can thus be forced deeper and deeper into the material. In δ-Ni_2Al_3 phase layer, the diffusivity of Ni is near zero, while Al diffuses rapidly [46], thus the formation of surface layer of δ-Ni_2Al_3 results from the inward diffusion of aluminum. Substrate allowing elements such as W, Mo, Ta and Re are selectively duffusing at the coating/susbtrate interface. Once the solubilities of alloying elements of W, Mo, Ta, Re and Cr are saturated, many precipitates rich in these elements will occur for their limited solubility to β-NiAl phase and distribute in the entire coating strucuture. After a second step of heat treatment at higher temperature (950°C - 1100°C), Ni is able to diffuse outward to transform the brittle δ-Ni_2Al_3 phases into an Al-rich β-NiAl. This step is also usually combined with the heat treatment required to recover substrate properties.

An example of SEM-BSE (back scatter electron) image of LTHA coating on Ni-based superaloy CMSX4 is shown in Fig. 1-30. This coating was deposited using an aluminizing pack containing 2 wt% Al at 900°C, and was heat treated for 2 h at 1120°C and then for 24 h at 845°C. The β-NiAl phase layer is uniform in thickness, and many precipitates (white small particles) distributed dispersively in the entire β-NiAl phase layer. Squillace [49] has also analysed clearly the coating structure after the first step of LTHA. Three layers are visible, the inner layer has a striated appearance, the outer layer is equiaxed with many inclusions, the middle layer is featureless. The coating layer has deposited very high amount of Al. In the book entitled 'High Temperature Coatings', edited by S. Bose et al.[9], it was presumed that higher inward diffusion of Al with lower outward Ni diffusion has avoided the formation of Kirkendall porosity and also eliminated the embedded pack particles.

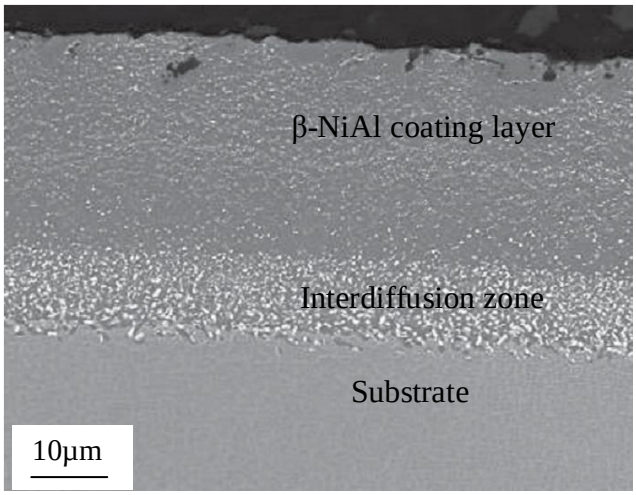

Figure 1-30: *A nickel aluminide diffusion coating produced using LTHA pack cementation process on CMSX4 [53].*

Now we have preliminary concepts of the HTLA and LTHA. According to the basic knowledge we can preliminarily establish whether the coating belongs to HTLA or LTHA. However, in the actual experiments or manufacturing, there are all kinds of operations by adding different amount of Al and at different temperatures. Therefore, the resulted coating could be significantly different and have very complex structures. D.K. Das et al. has studied the single step 'high activity' aluminizing process on CM-247 Ni-base alloy. They conclud that the coating growth takes place primarily by inward Al diffusion initially, followed by an intermediate stage when the growth involves both inward and outward Ni diffusion. Finally, the outward diffusion of Ni dominates the coating formation process [53]. Based on this one step high activity aluminizing method, H. Wei et al. has estimated and calculated the interdiffusion coefficients of the multicomponent β-NiAl phase [54]. H.Rafiee et al [55] has studied the effect of temperature and amount of Al by low activity aluminizing. They showed that by increasing temperature from 850°C to 1050°C, the coating mechanism is changed. The content of Al also affects the movement of coating front layer.

Coating-superalloy interdiffusion is principally responsible for the phase transformations, oxidation behavior and degradation of the mechanical properties of the coating [56]. Moreover, the diffusion hehavior in the multicomponent coating layers is very complicated due to the interactions among the components. Thus, diffusion is an important factor to be considered when designing β-NiAl coatings.

Unfortunately, although the multicomponent coating is a critical system for high temperature coatings, there is few reported diffusion data on it. Through the work of this thesis, some new data will be added to the databank of the complicated multicomponent diffusion.

1.5.2.6 Modified Aluminide Coatings

A large number of simple aluminide coatings have been studied and produced for their successful protection of turbine blades and vanes. G.W.Goward has reviewed the progress in diffusion coatings for gas turbines [33]. At working temperature above 1050°C, especially under cyclic conditions, or under severe hot corrosion, these plain aluminide coatings offer limited protection. Thus modified aluminide coatings have been developed for demanding applications. The modified coatings can be fabricated using the following techniques:

a. Codeposition of elements from the same pack
b. Codeposition from two separate vapor sources (in out-of-pack or CVD processes)
c. Pretreatment of the superalloy before aluminizing process
d. Deposition of a metallic layer, using electroplating or PVD (physical vapor deposition) techniques, prior to aluminizing, for example, a Pt-modified aluminide coating.

Alloy additions may include precious metals Pt, Pd, the rare-elements Y and other Cr, Si, Ta, Hf, Zr elements.

Platnium-Aluminide Coatings

β-NiAl coatings tend to suffer strongly from interdiffusion with the substrate, which results in the formation of γ' at the expense of β-NiAl.

The idea of introducing a diffusion barrier to obstacle the outward diffusion of Ni and other elements led to the invention of the Pt-modified aluminide coatings. Even if year's layer, it was observed that Pt doesn't act as a diffusion barrier [57], it was also observed that Pt can eliminat Cr-rich precipitates from the outer coating layer, preventing refractory elements such as Mo, W from diffusing into the outer coating layer, thus, Pt has improved the protective nature of the coating [58].

Pt-modified aluminide coatings are produced by electroplating a thin layer of Pt onto the surface of the superalloy. The manner by which the coatings are formed involves

an initial deposition of the layer of Pt (typically 6µm thick) either by electrodeposition or ion plating. A post coating annealing process is then required to diffusion bond the Pt to the substrate. If this pre-aluminising heat treatment is carried out such that significant amont of Pt diffuse into the surface layers of the substrate, the aluminide will lead to form a single phase (Ni, Pt)Al. If the pre-aluminising annealing leads to reduced Pt diffusion to the substrate, then a two phase $PtAl_2$-(Ni-Pt-Al) will form during the following aluminizing process. In this case, the external $PtAl_2$ phase is behaviored as Al-resource (shown in Fig. 1-31).

It is proved that the single phase Pt modified coating has higher oxidation resistance than the two phase modified coatings.

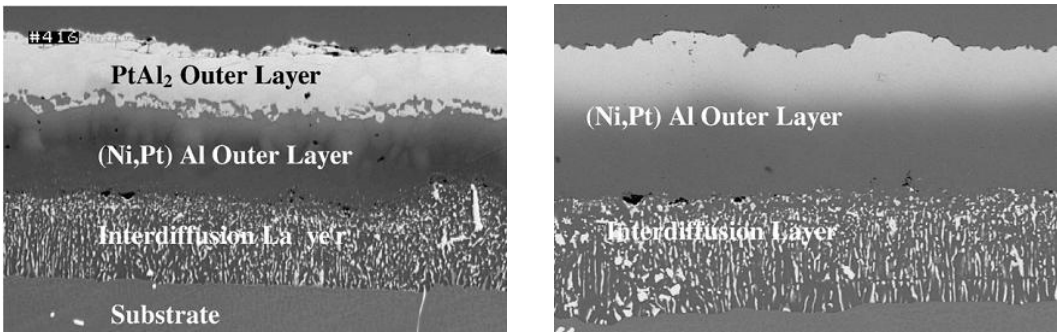

Figure 1-31: *Backscattered cross-section micrographs of Pt-modified aluminide coatings, a) Two phase outer coating layer, b) One phase outer coating layer [37].*

When applied on the 2nd generation superalloy CMSX4, Pt formed TCP phases with some elements of the substrate (Re, W, Mo, Cr) [14]. Y. Zhang et al. [59] have analyzed the effects of Pt on the isothermal oxidation behavior of CVD aluminide coatings, they observed that Pt can inhibite void growth at the scale-metal interface, thus increasing the adherence of the coating. It has also been proposed that Pt acts in a similar way as Y in MCrAlY coatings. In these coatings, Pt combines with S. This greatly increase the coating life, as S is otherwise detrimental to the adherence of the oxide layer and it is one of the main causes of hot corrosion phenomenon in Ni-base superalloys [59]. S.J. Hong et al. [60] has compared the cyclic oxidation behavior of Pt-, Pd, and Pt/Pd-modifed aluminide coatings on Inconel 738LC. Pt/Pd-modified aluminide coating has the best cyclic oxidation resistance.

Reactive Element-Modified Aluminide Coatings

It has been well-known for more than 70 years that the addition of small amount of reactive elements (RE), such as Hf, Zr, Y, Si, etc., has beneficial effects on oxidation behavior [33]. This modification can improve the adherence of Al_2O_3 and Cr_2O_3 scales and significantly reduce susceptibility to spallation during thermal cyclicing. Z.D. Xiang and P.K. Datta [61] have confirmed that the codeposition of Al and Si on Ni-based superalloys can be achieved in the temperatrure range 1000°C-1100°C using pack powder mixtures activated by $CrCl_3 \cdot 6H_2O$. Some research papers have considered the incorporation of RE as part of the CVD process. Published work by B.M. Warns [62] co-deposited Hf, Zr, Si during the CVD process. This modified diffusion coatings have four times greater oxidation resistance than traditional two-phase type Pt-modified aluminide coatings. Recently, Y. Wang [41] has also successfully obtained the low content Hf-modified aluminide coatings with or without Pt additions via a vapor phase process on Ni-base alloys. Hf-rich precipitated particles were located on the coating surface, along grain boundaries. V.K. Tolpygo et al. [63] have compared the surface instability of Pt-modified aluminide coatings deposited with Hf, Y on CMSX4. The surface instability is sensitive to Hf, while not so sensitive to Y addition. The improved spalling resistance observed during cyclic oxidation dur to the dopted of Zr was presented [40] that the Zr inhibits the formation of cavities at the coating/oxide interface, hence explained the improved spalling resistance observed during cyclic oxidations.

Further, small amounts of impurities such as S, P, B, C can also affect the oxidation resistance of the coatings. These elements can be introduced into the coating by diffusing from the superalloy substrate, by Pt plating process and by aluminizing process. B.A. Pint et.al [64] observed that for Ni-base superalloys, the oxide scale spallation from the coating surface was minimized when Hf and Y were added to a casting and the [Y]/[S] content ratio is about 1. The effect of impurity of S on the adherence of protective alumina scales was also published in earlier work in [65]. V.K. Tolpygon [63], has observed an increase of C content in the superalloy has the opposition effect due to the formation of Ta-rich mixed carbides, which tie up Hf, thereby decreasing the oxide growth.

1.5.2.7 Diffusion-Bond Coat in Thermal Barrier Coatings

Diffusion aluminide coatings are also used as bond coat in thermal barrier coatings (TBCs). Fig. 1-32 shows an example of TBC deposited over an aluminized coating used as bond coat. The top ceramic layer consists of vertical column ceramic ZrO_2 (with the addition of stabilized Yttrium) deposited by electron beam-physical vapor deposition process. Under it, is the CVD diffusion alumide layer with IDZ serving as the 'bond coat' to enhance the oxidation resistant of the whole layered structure [66].
By virtue of its low thermal conductivity, TBC provides thermal insulation and thus lowers the temperature of the metallic substrate up to a few hundred degrees. While, the mismatch in thermal expansion coefficients of superalloy substrate and ceramic top coat causes the formation of thermal stresses during thermal cycling, that can easily lead to the eventual failure of the TBCs during operation by spallation.
An intermetallic layer with unchangeable thermal expansion is beneficial to improve the adherence with the substrate. This is the one of the main target of bond coat layers, in addition to improve the oxidation resistance.

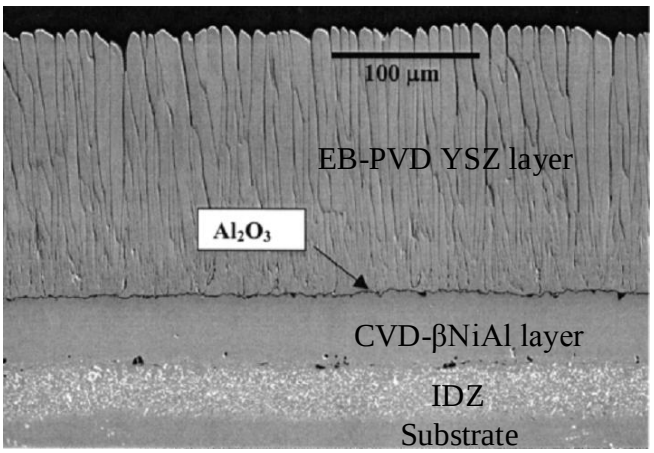

Figure 1-32: *SEM images of a cross-section of an as deposited TBC with a CVD NiAl bond coat. The Al2O3 alumina scale is the thin dark-contrast layer along the TSZ-NiAl interface [66].*

Even with a bond coat in place, spallation of the ceramic layer will eventually occur, after a more prolonged period of time. Promoting TBC life and the design of procedures to estimate it are currently among the biggest challenges faced by materials scientists and engineers working in the gas turbine filed. The columnar

structure of the EBPVD TBC facilitates a certain degree of strain tolerance and is used for rotating parts, such as turbine blades, nozzle guide vanes and combustor section.

The dominant failure mode observed in the TBC coating is progressive fracture along the interface between the bond coat and the thermally grown oxide (i.e. the Al_2O_3) scale during normal engine operation. The adhesion of the oxygen diffusing between the ceramic TBC and the aluminizing bond coat below TBC is a critic problem. From this perspective, the development of bond coats with improved Al_2O_3 scale adhesion is a critical issue in the design of more reliable TBC systems [67]. It is demonstrated that reducing the S content of NiAl coatings fabricated by CVD significantly improved Al_2O_3 scale adhesion during cyclic oxidationf at 1150°C.

1.6 Interdiffusion Degradation of the Coatings and the Formation, Adherence of Al_2O_3

During the service of the superalloy with the coatings, degradation occurs by two mechanisms. One is the interdiffusion between the coating and substrate, driven by the difference in chemical potential, the another is loss of Al by diffusion towards the surface of the coatings to form Al_2O_3 which spalls during thermal cycling. It is to be noted that these two degradation mechanisms can operate simultaneously on different parts of the same blade. Several studies have shown that the former mechanism may contribute more to the overall Al depletion than the latter one does, although repeated spallation of Al_2O_3 scale may accelerate the loss of Al due to oxidation. It is thus important to understand and control the interdiffusion fluxes occurring between coating and substrate in order to optimize the lifetime of the coating, or ideally the performance of the component [68].

1.6.1 Interdiffusion Degration of Diffusion Coatings

Coatings have a totally different composition from the alloys to which they are applied. For example, a stoichiometric NiAl coating contains 31.5 wt% Al and 68.5wt%Ni. In contrast, as it is illustrated from Fig. 1-7, the typical Al contents of Ni-based superalloys are lower than 6 wt% and Ni contents range between 60-75wt%. Because of the concentration differences between them, also the coating is not in thermodynamic equilibrium with the alloy, and hence on long exposure,

aluminum in the coating diffuses into the substrate. Accordingly, Ni is expected to diffuse from the substrate into the coating.

J.Angenete with his coworkers [69] studied the effect of such interdiffusion effects on microstructure and observed the degradation of the single phase β-NiAl layer progressively transforming into β+γ'(Ni_3Al). In addition, the interdiffusion effects caused microstructural changes in the substrates. They observed that the oxide spallation was not consistent with the formation of γ'(Ni_3Al). Co strongly partited into γ'(Ni_3Al) and Cr to β. Pt in the coatings substitutes for Ni and Co. It was suggested that Pt acts as an 'inert filler', which suppressed the amount of Ni and Co and allowed a sufficiently high amount of Al at the surface. In particular, in [70], the W, Mo, Re, Ta, Ti displayed significant movement during this interdiffusion. Because of the fast outward moving of Ni, Kirkendall porosities occurred. Angenete concluded that Pt diffusion into the substrate resulted in the precipitation of TCP phases. These phases are known to be deleterious to the mechanical behavior of Ni-based superalloys and much work has done to predict compositional and temperature ranges over which they form, such that these compositional and temperature ranges can be avoided. Ta is soluble in γ'(Ni_3Al) but not in β-NiAl. When the original Pt modified β-NiAl has transformed to a mixed β+γ'. The Ta-rich γ'(Ni_3Al) grains are prone to catastrophic oxidation and thus if the alumina scale forms then pitting oxidation may arise. Fig. 1-33 shows the transformation of β-NiAl to γ'-Ni_3Al in the coating layer by the interdiffusion of Al and Ni.

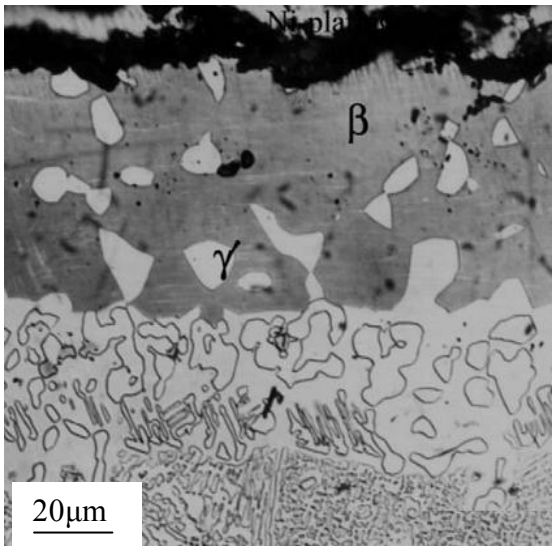

Figure 1-33: *The transformation of β-NiAl to γ'-Ni_3Al in the coating layer [71].*

1.6.2 The Formation and Adherence of Al_2O_3

During thermal cycling, Al_2O_3 is formed by the loss of Al diffusing towards the surface of the coatings. This is followed by a transient period during which all possible oxides, namely NiO, Cr_2O_3, Al_2O_3 form on the surface. A layer of Cr_2O_3 then forms under these oxides, below which a continous layer of Al_2O_3 develops. This process is repeated until outward flux of aluminium is insufficient to form a continuous scale [38].

As mentioned in 1.5.2.6, the reactive elements (RE), are added or codeposition with the coating with the aim of increasing the adherence and durability of Al_2O_3scale on the surface of the coating. For example, the coating contains small controlled percentage of Hf [72]. Hf have a greater affinity for oxygen than aluminum and it is believed that the oxygen which diffuses into the coating forms internal hafnium oxide particles extending from the surface oxide layer into the coating material. These hafnium oxide particles are believed to anchor or peg the alumina layer to the coating material thus reducing spallation of the alumina layer during cyclic thermal exposures.

1.6.2.1 Cyclic Oxidation Behavior

The Cyclic oxidation behavior of the coating is a very important factor which determines the ultimate life-time of diffusion aluminide coatings. The β-NiAl in coating layer oxidises, resulting in the protective scale alumina-Al_2O_3. It is necessary to understand the stability of the interface between the Al_2O_3 scale and superalloy. The Al_2O_3 scales must remain adherent to the substrate metal if they are to remain effective under thermal cycling conditions. Generally, the thermal-expansion mismatch between the oxide and metals is large enough to result in residual compressive stresses in the scale on the order of 5 GPa after cooldown. This puts a buckling and interfacial shear on the scale that may result in decohesion at the scale-metal interface. These stresses remain high whether there are appreciable growth stresses in the scale or they have relaxed due to creep.

The oxidation behavior of the coating is evaluated by measuring the change in weight of the samples. Two processes occur and cause the weight change: formation of an oxide layer leads to an increase, while spallation of the oxide leads to a decrease. The process of formation and spallation are competitive in the sense that the actual

change in weight reflects the combined effects of the two processes. The Al_2O_3 film can detach at its interface with the superalloy when thermal shock occurs. As a result, Al is depleted and the coating becomes unstable and degraded rapidly under thermal cycling condition by cracking and spalling of the oxide scale Al_2O_3 [73]. The oxidation performance of β-NiAl is not strongly sensitive to changes in stoichiometric induced by differing Al/Ni ratios. Fig. 1-34 shows the total mass gain against the concentration of Al during oxidation. The black bar is the weight of spalled oxide, while the grey bar is the corresponding total mass gain. It is clear that at the Al concentration of about 40 at%, the total mass gain is equal to the spalled oxide. After the Al concentration is lower than 40 at%, the weight of spalled oxide is much higher than total mass gain, which means that the catastrophic spallation occurred, leading to the failure of the components.

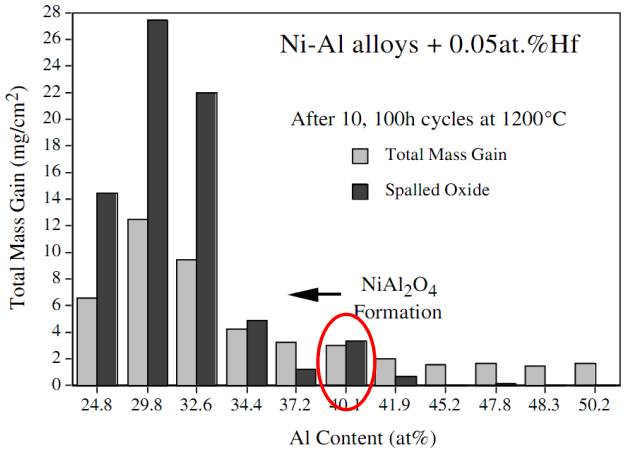

Figure 1-34: *Total mass gain (Specimen+spallation) and specific spalled oxide for various Ni-Al alloys after ten 100h cycles at 1200°C [1,74].*

Hence, the cyclic oxidation behavior is a critical factor to evaluate the quality of aluminide diffusion coatings. Cyclic oxidation behavior can be perfromed in the lab condition. Hence, many authors and researchers have been engaged in this study. According to the literatures, one cycle of test is usually performed in air at 1000°C-1150°C, oxidizing the components for about 30min~2h, then taking samples out and cooling them in air for about 10~30minuts [75-78].

The most desirable situation is the formation of a thin adherent oxide layer which then increase at a rate inversely proportional to its thickness. Thus for evaluating

oxidation data in the form of weight change curves, the desirable curve would show an initial small increase followed by a steady state portion with only a minimal weight change. Thus, the number of cycles at which the weight grow return on the value zero can be used as a measure of the cycled oxidation resistance.

Fig. 1-35 shows the typical cyclic oxidation curve of an aluminized alloy and uncoated alloy at 1100°C. The oxidation resistance of the alloy is improved by the aluminized coating.

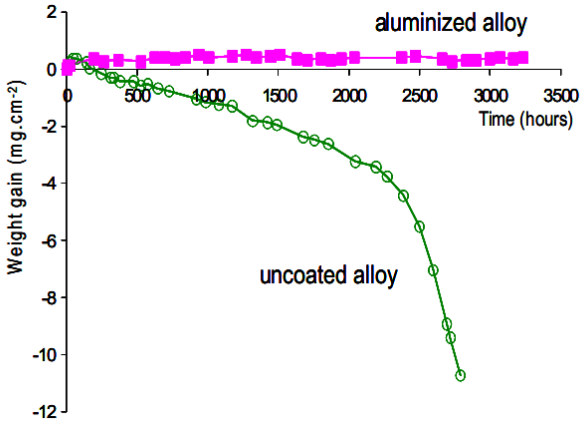

Figure 1-35: *Cyclic oxidation examination at 1000°C of the aluminized alloy and the uncoated alloy [79].*

Fig-1-36 shows the BSE images of the aluminide coating and Zr-modified aluminide coating after 200 cycles of oxidation [73]. During oxidation, Al at the surface of β-NiAl phase changes to Al_2O_3. Ni diffuse outward to transform β-NiAl into γ'-Ni3Al and finally γ-Ni phase occurred during long term cyclic oxidation. Transformation to the γ'Ni_3Al phase from β-NiAl is caused by depletion of Al. During the transformation, thermal-expansion mismatch between the oxide and metals causes spallation. After 200 cycles of oxidation, the surface of the aluminide coating is more rougher than the Zr-modified aluminide coating. Thus, Zr-modifed aluminide coating has incrased the cyclic oxidation resistance.

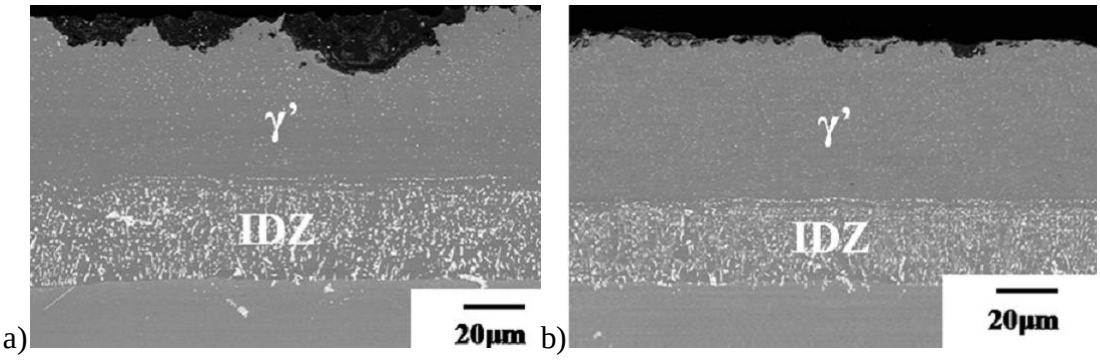

Figure 1-36: *BSE images of (a) Aluminide coating, (b) Zr-modified aluminide coating after cyclic oxidation for 200 cycles (1 h cycling).*

Overall, the chapter 1 has reviewed the state of the art of Ni-base superalloys and their oxidation/corrosion resistant coatings. Next chapters will discuss in detail this thesis work around this topic, including the base materials studied, vapor phase aluminizing process application, the experiment results, especially the microstrucuture analyses and discussion on the coating layers.

CHAPTER 2

Base Material, Experimental Procedures

This chapter is focused on the investigation of the substrate material CMSX4 alloy and of the aluminizing procedure on which the experimental activities were carried out. In order to compare and better understand the aluminizing mechanism in CMSX4 alloy, the pure Ni (Ni201 grade) has been aluminized simultaneously using the same aluminizing method as the CMSX4 alloy. The first part is concentrated on the experimental investigation of the features of the base materials CMSX4 and the issues related to the vapor phase aluminizing. The surface preparation for aluminizing, the aluminizing process and the experimental metallographic analyses are then given. The second part introduces the experimental methods. The specimens have been analyzed by several techniques in order to characterize the features of the aluminizing coating layers.

2.1 Experimental Material CMSX4 Bar and Ni201 in the As-supplied Condition

CMSX4 alloy is a typical 2nd generation Ni-base Single Crystal (SC) superalloy characterized by the replacement of most of the Ti with Ta, by relatively high Co and low Mo content. The nominal chemical composition of the alloy is presented in Tab. 2-1. Further, the low Cr, high W and the 3wt% of Re are the typical features of 2nd generation SC alloys. A cylindrical CMSX4 bar, shown in Fig. 2-1, typically 185 mm in length and 24.5 mm in diameter was produced by investment casting, with [001] direction of the γ/γ' crystal oriented parallel to the cylinder axis. This CMSX4 bar was solution and aging heat treated. This bar was marked with a reference line parallel to the cylinder axis.

Table 2-1: *Nominal chemical composition of CMSX4 [80].*

Element	Ni	Cr	Al	Co	W	Ti	Ta	Re	Mo
Wt %	61.8	6.5	5.6	9.0	6.0	1.0	6.5	3.0	0.6
At %	63.8	7.6	12.6	9.2	2.0	1.3	2.2	1.0	0.4

Figure 2-1: *As-supplied CMSX4 SC cylinder bar.*

One disc with the thickness of 10 mm was transversally sliced from the CMSX4 bar. Conventional metallographic polishing was carried out on one of the parallel flat (100) surface to obtain a homogeneous and low roughness surface (shown in Fig. 2-2). After the polishing, the disc was metallographic prepared by etching it using Marble reagent (10g $CuSO_4$, 50ml HCl, 50ml H_2O) for 15 seconds. This etchant is a γ' etching that selectively dissolves the γ' in the microstructure.

Figure 2-2: *The sliced CMSX4 specimen disc, being 10 mm thick and 25 mm in diameter.*

Light optical microscopy (LOM) and scanning electron microscopy (SEM) were used to observe of (100) surface microstructure of the as-supplied CMSX4 material. The low and high magnifications of the microstructures are shown in Fig. 2-3a and 2-3b.

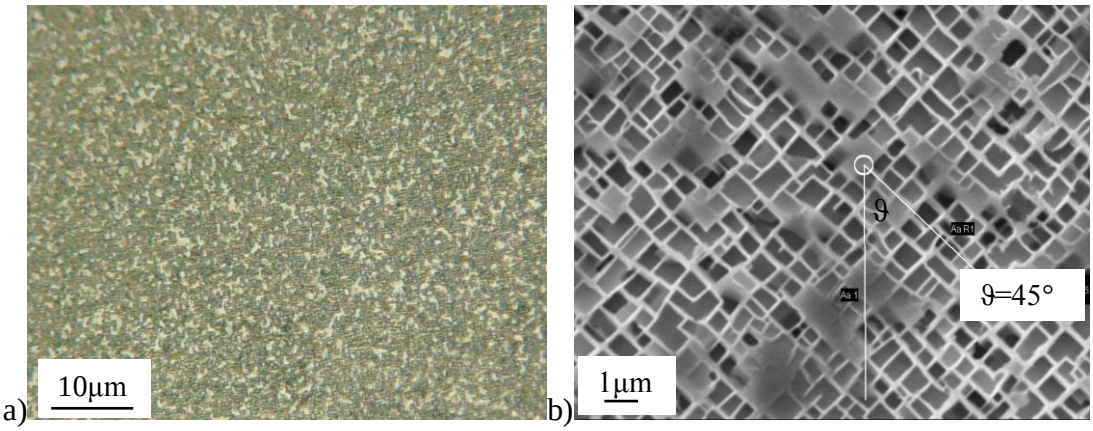

Figure 2-3: *Low magnification microstructure under LOM, b) High magnification microstructure under SEM.*

Fig. 2-3a shows that on the whole material, the CMSX4 bar has a homogeneous microstructure. There isn't any TCP phases formed. On high magnification in Fig. 2-3b, two-phase γ + γ' microstructure of the as-supplied CMSX4 bar is clearly shown. The fine γ' precipitates have an average edge of 0.5μm size and homogeneously embedded throughout the γ matrix. This morphology reflects the typical crystallographic coherent of γ' and γ phases as determined in literature [81] by high

resolution of energy dispersive X-ray (EDS) analysis inside a transmission electron microscope (TEM).

The γ + γ' phases exhibited in a special orientation, which oriented at about 45° with the vertical direction. This vertical direction line is normal to the reference line. Thus the vertical direction corresponding to crystallographic orientation along $[110]_{\gamma'}$ and the line at 45° corresponding along $[100]_{\gamma'}$.

This orientation relationship was recorded which has been used for later preparation of the specimen for aluminizing. Compared with the survey of solution and aging heat treatment on CMSX4 in section 1.3.4, in the full heat treated CMSX4, the γ and γ' have similar lattice parameters, and the volume fraction of γ' is about 65%. The CMSX4 bar used in this thesis was considered to have been correctly treated.

The chemical composition of low carbon commercially pure Ni (Ni201 grade) is shown in Table 2-2. The Ni content is more than more than 99 wt%. Since the substrate phase of Ni201 is only γ phase, the vapor phase aluminizing on Ni201 is simpler than that of the CMSX4 alloy, and the phase equilibrium evolution is presumed to develop according to the Ni-Al binary diagram. A set of 30X10X4.5 mm^3 rectangular samples were cut and their surfaces were metallographically polished for further aluminizing. The aluminizing results on Ni201 could offer important information to evaluate and analyze the aluminizing mechanism occurred on CMSX4.

Table 2-2: *Chemical composition of Ni201 [82]*

Element	Ni	Fe	Cu	C	Mn	S	Si
Wt.%	99min	0.4max	0.25max	0.02max	0.35max	0.01max	0.35 max

2.2 Preparation of the Surface for Aluminizing

The CMSX4 bar was sliced into a series of discs with 24.5 mm diameter and 4 mm thickness for aluminizing. On each disc, a hole with 1 mm in diameter at the position of the reference line was drilled with the double aim of marking the direction corresponding to [110] crystallographic direction and of obtaining a passage for a wire to sustain the disc in a suitable position in the aluminizing chamber in order to obtain homogeneous coating on the surface of the disc. Each of the disc was polished

according to conventional metallographic techniques on the parallel plane surfaces. Then all of the discs were sent back for aluminizing by means of low-activity high temperature process.

2.3 Aluminizing Process

All of the discs were vapor phase aluminized in industrial plants by means of low-activity high temperature process. The industrial plants were set up for other industrial products, so these discs were aluminized jointly with other products in the industrial plants. Normally, aluminizing is performed at the temperatures of 1050°C or 1080°C. Two groups of discs were planned to be aluminized on the base of the two different temperatures at different holding times. Thus, the effects of temperatures and hold time on the aluminizing layers could be compared. The actual heating and cooling curves are strictly dependent on the industrial procedures and they can not be presented in this thesis for confidential reasons. For the description of the vapor phase low-activity aluminizing procedure reference should be made to section 1.5.2. Finally, the discs aluminized for 3 h, 6 h and 12 h at 1050°C and the ones aluminized for 0 h and 1.5 h at 1080°C were obtained.

The set of Ni201 specimens were also vapor phase aluminized simultaneously with CMSX4 discs for 3 h, 6 h and 12 h at 1050°C.

2.4 Metallographic Analyses

A metallic grey coating was formed by aluminizing on the surface of the specimen, as shown in Fig. 2-4a. The orientation directions of the disc are also illustrated in Fig. 2-4a, with the surface corresponding to the flat (100) surfaces of disc oriented normally to [001] direction. In order to investigate the aluminizing temperature and holding time effects, as well as the base material orientation effect on the coating layers, the discs were radially cut along planes at 45° and 90° with respect to the small reference hole as shown in Fig. 2-4b. The surfaces intercepted on the cylinder

surface by these planes (referred as 45° and 90° planes), were normal to [100] and [110] direction, respectively. The aluminized coatings on these two intercepted surfaces, are also shown in Fig. 2-4 (the surfaces highlight by blue arrows). The [100] and [110] orientations are referred to the crystal orientation of base substrate γ + γ' phase. Since γ and γ' phases are oriented in the same direction and have the similar lattice parameters, in later EBSD analyses, only the γ' phase has been considered. The observed surfaces were mounted in resin and conventionally polished for SEM analysis.

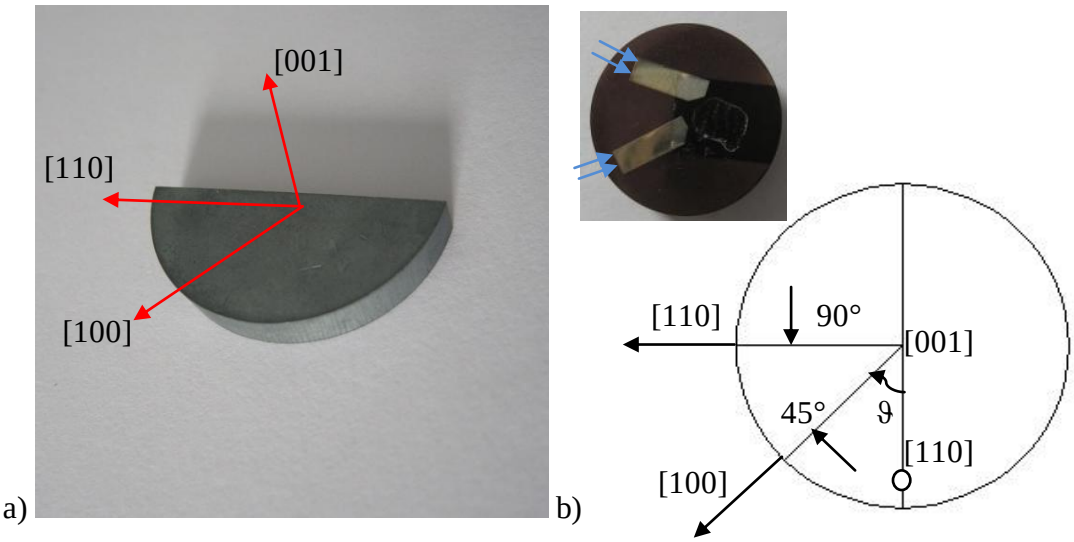

Figure 2-4: *a)The aluminized disc was cut in half and the specimen coordinate is marked, b) Scheme of the metallographic section planes of aluminized disc-shaped samples.*

Metallographic features were investigated on the surfaces oriented at [100] and [110] direction of different aluminized discs by means of SEM (scanning electronic microscopic) observations, combined with EDS (Energy Disperse X-Ray Spectroscopy) microanalysis and EBSD (Electron Backscatter Diffraction) mapping. GDOES (Glow Discharge Optical Emission Spectroscopy) is also used to supply qualitative chemical profiles along [001] direction of the substrate.

SEM experimental analyses in BSE (Back Scattered Electron) are aimed to checking the presence and thickness of the sequence layers at the surface of the aluminized discs.

SEM-EDS analyses are carried out to check the chemical composition and to obtain the chemical profiles of the aluminized layers. In this case, punctual quantitative

microanalyses have been performed along the [001] direction of each sample. These analyses involved a material volume of some μm^3 and resulted in a relatively wide scatter in the non-homogeneous and fine structures. Nevertheless, the EDS chemical profiles showed the clear enrichment of some alloying elements in the depth range corresponding to the different aluminizing layers.

SEM-EBSD analyses are used to check the orientation relationship between the coating layers and the substrate.

GDOES analyses are also utilized to obtain the chemical profiles. Because, the light elements such as oxygen and sulphur are obtained which are not seen in the SEM-EDS analyses. The other element profiles detected by GDOES can be compared with the EDS profiles, thus, the diffusing mechanism of the main elements could be understood.

Since EBSD and GDOES are not widely be used, they will be introduced shortly here.

EBSD Method Introdution

EBSD is used to identify the orientation features of the coating and the effects of the substrate alloys. This can help us to understand the growth mechanism of the low-activity vapour aluminide coating made at different temperatures and times. In EBSD, the accelerated electrons in the primary beam of a SEM can be diffracted by atomic layers in crystalline materials. Electron backscatter patterns are generated, which are projections of the geometry of the lattice planes in the crystal, and they can give direct information about the crystalline structure and crystallographic orientations of the grains from which they originate. In crystal orientation mapping, the electron beam is scanned over the sample on a grid of points and at each point a diffraction pattern obtained and the crystal orientation measured according to a colour allocated reference. When applying EBSD, the polished samples is placed in the SEM and inclined approximately by 70° relative to normal incidence of the electron beam. The EBSD scheme and one example of orientation map are shown in Fig. 2-5. The CCD camera is equipped with a phosphor screen integrated with a digital frame grabber. Then the CCD camera is used to collect the Kikuchi lines through the phosphor screen. The pattern of Kikuchi lines on the phosphor screen is electronically digitized and processed to recognize the individual Kikuchi lines. These data are transmitted to

a computer to identify the phase, to index the pattern, and to determine the orientation of the crystal from the pattern that was generated [83].

EBSD analysis needs strictly preparation of the specimen surface. The specimens of aluminized CMSX4 in this thesis are prepared firstly by the same procedure of SEM preparation, after that the specimens were polished in silica for 25 minutes to obtain a much finer surface roughness.

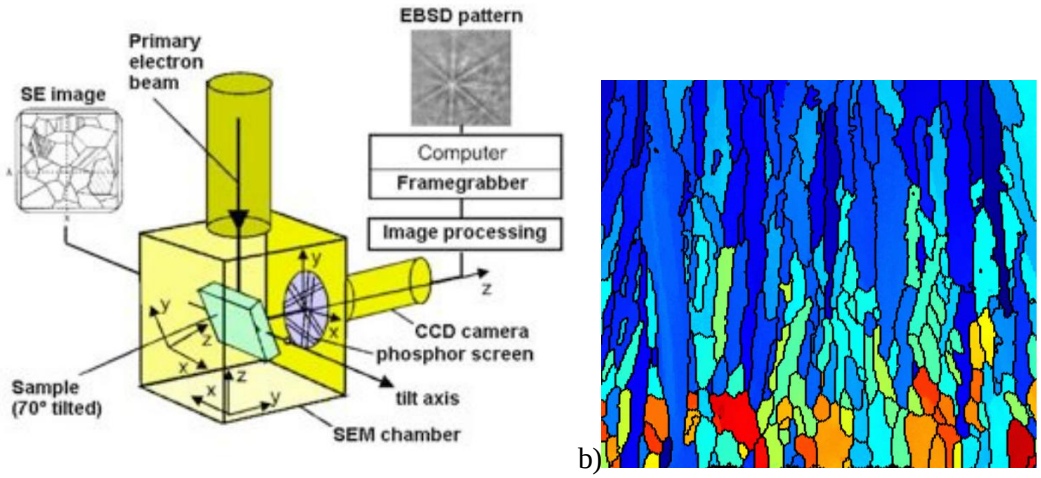

Figure 2-5: *EBSD scheme, b) One example of orientation map of the grains, different color corresponding to different orientations.*

GDOES Method Introduction

GDOES, which is an optical emission spectrometry technique using glow discharge plasma, gives the quantitative depth distribution of elements in a thin surface on a metallic material. The only requirement is the use of primary vacuum calibration of the GDOES instrument with samples of known chemical analyses and a matrix composition similar to that of the samples to be analysed. Glow discharge has been used to study atomic structures for many years. Recently it has also been applied in the quantitative depth profiling of metallic and non-metallic coating area [84-86].

Here in this thesis, the chemical composition profiles of aluminized coating layer on the Ni-base superalloy substrate at different temperature and hold times aluminizing are also analyzed by GDOES technique. The depth profiles are obtained by measuring emission intensities for constituent elements as a function of sputtering time. The quantitative relationship between the composition and depth are also estimated according to a normalization procedure. The element content is normalized

by the ratio between the local amounts of the specific element to its average content in the substrate. The x-axis depth is roughly obtained assuming a constant material removal rate.

CHAPTER 3

Results

3.1 SEM Analyses of Coating Morphology - Coating Layers, Coating Thickness, Identified Phases

3.1.1 SEM Analyses of Ni201 High Temperature Vapor Phase Aluminized Specimen

The results of aluminized coating formed on pure Ni201 are presented for first so as to have reference information for the main analyses of the CMSX4 aluminized alloy. The surface morphology of the coating at 1050°C for 12 h on Ni201 is shown in Fig. 3-1. The coating consists of large grains (~ 30 - 100 μm) outlined with a distinct network of prominent grain boundary ridges on the coating surface.

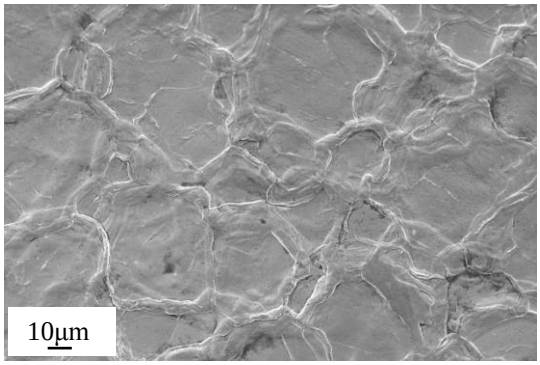

Figure 3-1: *The morphology of the coating surface of Ni201 aluminized for 12 h at 1050°C.*

The SEM micrographs of a metallographic cross section of this coating on Ni201 are shown in Fig. 3-2a. The external coating phase layer is about 30 µm thickness. It is a 'clean' coating layer without any precipitate or particle. Below it, some voids and the presence of a thin single-phase γ'-Ni_3Al layer are clearly appeared. The cuboidal morphology of γ'-Ni_3Al phase in high magnification is shown in Fig. 3-2b, with the thickness of about 2 µm.

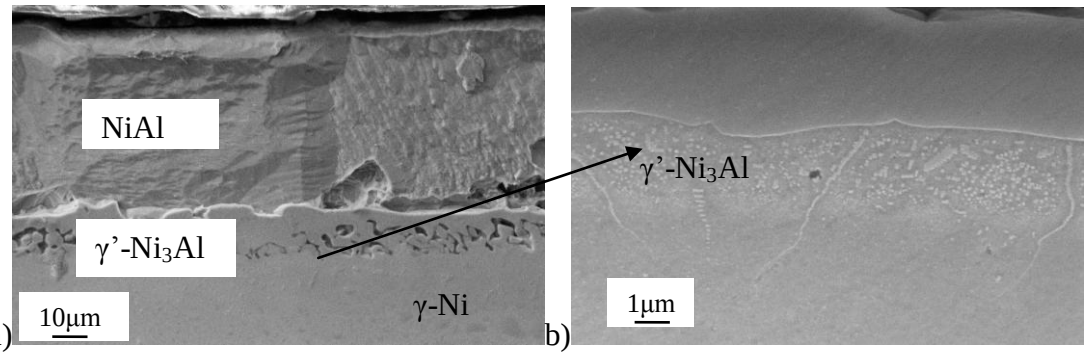

a) b)

Figure 3-2: *SEM microstructure of Ni201 aluminized at 1050°C for 12 h, b) Under the external single phase layer, a very thin layer about 2 µm thick of γ'-Ni3Al phase is observed at high magnification.*

The specimens Ni201 aluminized for 3 h and 6 h using the same aluminizing condition have the same features of the coating layers as for 12 h aluminizing, except that the thickness of the external coating single phase layers increased by extending the aluminizing time.

The chemical composition profile versus depth from the surface is obtained by SEM-EDS analysis shown in Fig. 3-3. The compositional gradients of Al and Ni are clearly shown. Taking the specimen aluminized for 12 h (black lines) for example, the Al composition curve can be divided into three parts (shown in Fig. 3-3) according to the concentration of Al in Al-Ni binary diagram at 1050°C. The thickness of I zone is about 60 µm. The II zone is roughly 10 µm. In zone I, a peak of Al corresponding to a valley of Ni (shown in the red circle) has been observed. At the surface of the coating, the Al content is about 40 at%, and this content hasn't decreased much for a large thickness. The composition curves of specimens aluminized for 3 h and 6 h have the same behaviour.

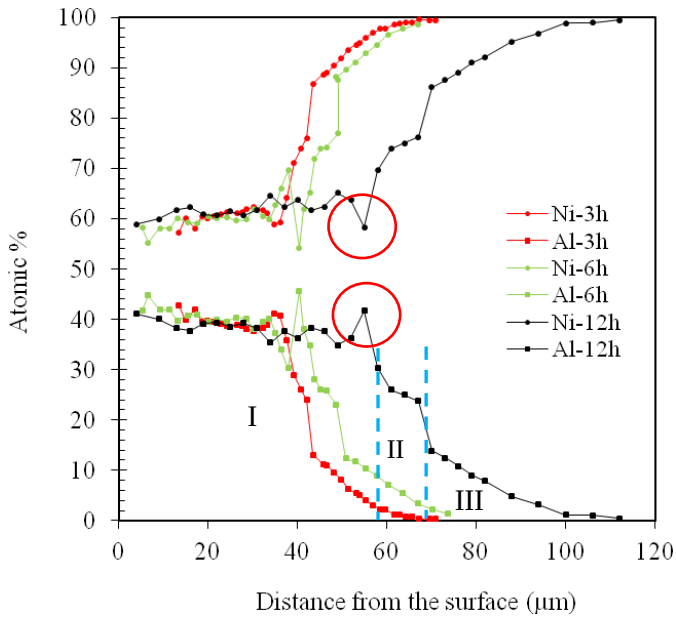

Figure 3-3: *EDS chemical profiles for Ni201 specimens aluminized at 1050°C for 3 h, 6 h and 12 h.*

3.1.2 SEM Analyses of CMSX4 High Temperature Vapor Phase Aluminized Specimens

3.1.2.1 SEM Analyses of Specimen CMSX4 Aluminized at 1050°C

The SEM micrographs obtained by BSE probe of the sample aluminized at 1050°C for 3 h are displayed in Fig. 3-4. The coatings in the two images in Fig. 3-4 are based on the different orientation of substrate material. Fig. 3-4a is the coating on the [100] direction of substrate, while Fig. 3-4b corresponding to [110] direction of

substrate. Nevertheless, the crystallographic orientations of substrate in this case haven't been clearly illustrated. Three layers can be distinguished close to the external surface (top side of the image). In the external layer, it is a 'clean' coating layer, no precipitates or particles were present, with a thickness of about 15 µm. Below it, much white spherical or acicular shaped particles can be observed, with the thickness of about 12 µm. In addition to these, under the IDZ, another layer rich of some particles together with the substrate phases (γ + γ' phase) is occurred. Here this layer is defined as mixed zone (MZ). The additional third layer was differently considered in literature: sometimes it was omitted, including it into IDZ or into the substrate layer [19, 52, 85]. Sometimes it was widened to include the whole Al-enriched substrate layer [85] and in other cases it was considered as a secondary reaction zone [20]. The etched cross sectional view of the coating in Fig 3-4b clearly shows that some large grain boundaries extended thorough all the layer.

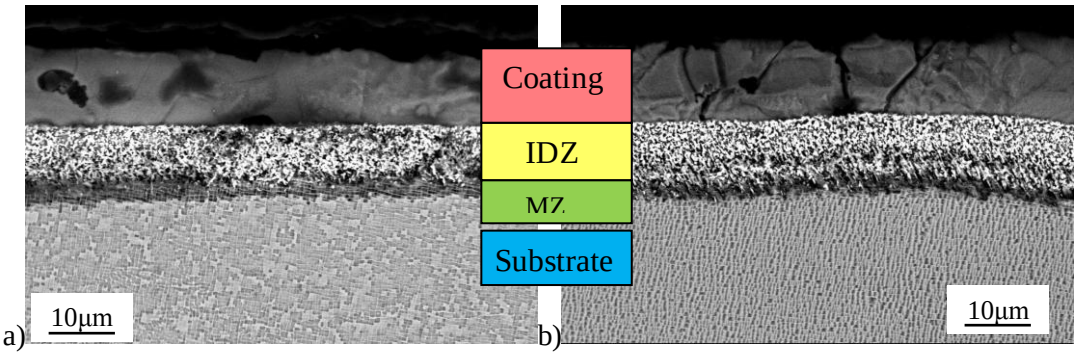

a) b)

Figure 3-4: *SEM (BSE) micrographs of the surface layers of the specimens aluminized for 3 h at 1050°C along: a)[100]$_{\gamma'}$, b) [110]$_{\gamma'}$ directions.*

The typical morphology of the specimens aluminized at 1050°C for 6 h is shown in Fig. 3-5. Coatings on those two directions of substrate mentioned above are illustrated. The crystallographic orientations of substrate are clearly detected here, with Fig. 3-5a in [100]$_{\gamma'}$ direction and Fig. 3-5b in [110]$_{\gamma'}$ direction. High magnification images clearly show that the alloy substrate, characterized by the typical γ' cuboidal particles aligned within the γ matrix. The coated layers include the same three observed layers in the previously examined aluminized CMSX4 sample: external a β-NiAl phase layer (coating), beneath it the interdiffusion zone (IDZ) and close to the substrate a mixed zone (MZ). The differentiation between IDZ and MZ

was not always clear, depending on the substrate orientation. Within the MZ, the particles were still of globular or acicular shape and they were disposed along parallel lines in Fig. 3-5b, separating 'intrusions' of the γ + γ' structure form the substrate. At the MZ/substrate these particles tended to be thinner and elongated within the γ matrix channels. The thicknesses of both external coating layer and IDZ have increased apparently.

a)

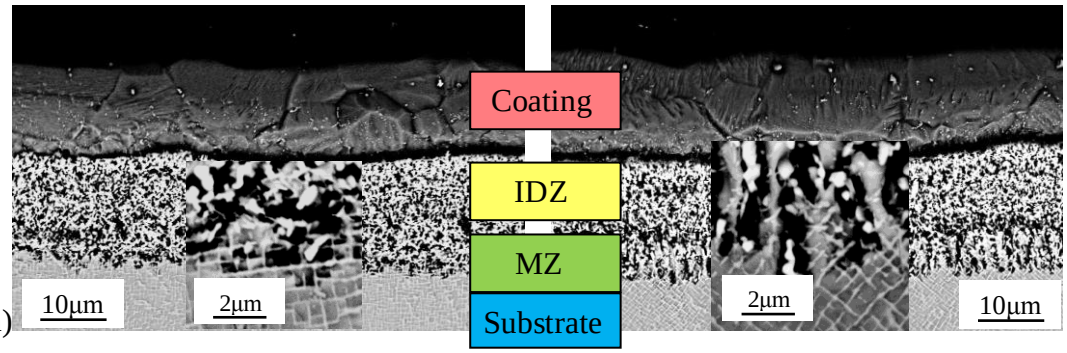

Figure 3-5: *SEM (BSE) micrographs of the surface layers of the specimen aluminized for 6 h at 1050°C along: a)[100]$_{\gamma'}$, b) [110]$_{\gamma'}$.*

The SEM micrographs obtained by BSE probe and the corresponding EBSD image of β-NiAl orientation on the samples aluminized at 1050°C for 12 h is displayed in Fig. 3-6 a and b, respectively. The same three layered structures are again presented. The thickness of both external coating layer and IDZ are continually increased, with the external coating layer about 28 μm and IDZ about 20 μm. Focusing the attention on the external layer, it consists of large grains and the grain boundaries are observed clearly in BSE images, but clearer in EBSD maps (here an EBSD analysis is taken as example for comparison, while the full series of EBSD analyses are shown layer in section 3.2). Grains are finer close to the coating/IDZ interface. A series of black particles in BSE (Fig. 3-6a) corresponding to the series of white particles (Fig. 3-6b) are also revealed. In the EBSD analysis, the specimen should be placed at a tilt angle of 70°, for this reason, the thickness of the coating layers observed in EBSD are not exactly the real condition, however, the white particles in EBSD are located in the same position with the black particles in BSE image. In the higher magnification of MZ (Fig. 3-6a), the spherical shaped particles are located in some channels, seemed oriented in some directions.

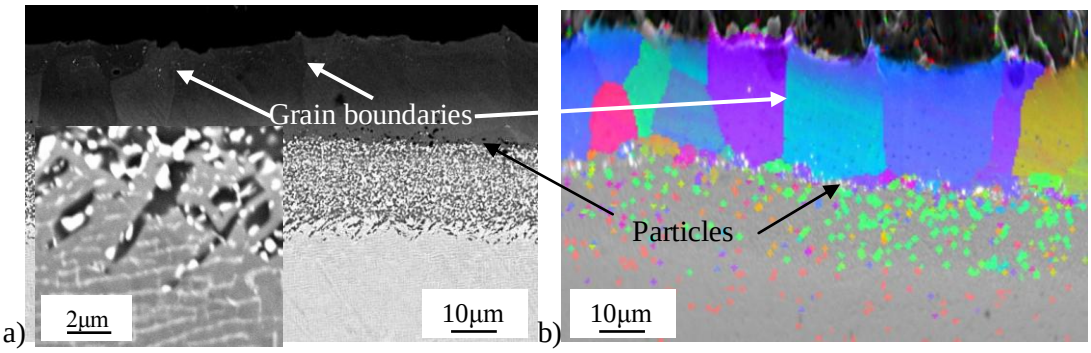

Figure 3-6: *Metallographic section [100]γ' of the specimen aluminized for 12 h at 1050°C. a) SEM (BSE) micrographs at different magnifications, b) Overlapped SEM-SE micrograph and EBSD map of the β-NiAl phase orientation.*

Considering the above observations (Fig.3-4, 3-5, 3-6), it was observed that increasing the holding time, the microstructures of the aluminized specimen are similar, all of them containing three layered structure. The general characters are the 'clean' external coating layer, IDZ consisting by the complex particles and MZ containing complex particles with some relationships with substrate. However, some differences or changes in the thicknesses and the morphologies of these layers are clearly observed.

3.1.2.2 SEM Analyses of Specimen CMSX4 Aluminized at 1080°C

The microstructure features of the specimen nominally aluminized for 0 h, are presented in Fig. 3-7. The coating structures have already been established during the thermal cycle, with thin external coating layer and IDZ consisted complex particles. This revealed that the time spent in the aluminizing atmosphere at relatively high temperature was sufficient to start the formation of the coating. The thickness of external coating layer is about 7 µm and IDZ of about 6 µm. The morphology of coating and IDZ is somewhat different from that of other aluminized specimens. Their interface is wavy, with structures that can be referred as 'extrusions' of the IDZ into the coating, often located at its grain boundaries. These features are more frequent where the specimen surface was normal to $[100]_{\gamma'}$.

Nevertheless, the morphology of the MZ is quite different from that observed in other specimens. The layer is not homogeneous in thickness. As for the IDZ, its

morphology appears to be related to the substrate orientation, since 'intrusions' of MZ into the substrate are more frequent where the $[100]_{\gamma'}$ is normal to the specimen surface (Fig. 3-7a), while they seldom appear where surface is normal to $[110]_{\gamma'}$ (Fig. 3-7b). The extension of the intrusions is of the order of 5 µm, slightly higher in $[100]_{\gamma'}$.

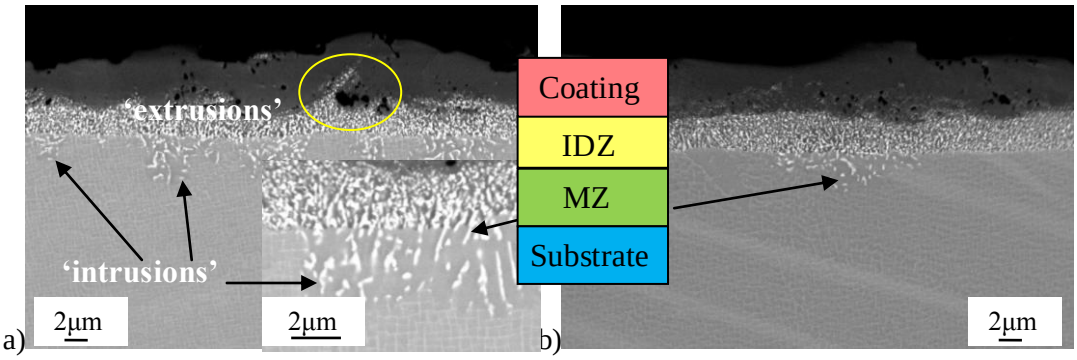

Figure 3-7: *SEM micrographs of the specimens aluminized for 0 h. (a) Coating morphologies in $[100]_{\gamma'}$ and the 'intrusions' in high magnification, (b) Coating morphologies in $[110]_{\gamma'}$.*

The microstructure features of the specimen aluminized at 1080°C for 1.5 h are shown in Fig. 3-8. The interface between coating layer and IDZ is not as straight and distinct as that obtained from process carried out at lower temperatures. Additionally the white particles within IDZ and MZ seem finer and in lower amount. More frequent pores are visible on the external part of the coating. The average thickness of coating, IDZ and MZ are about 23 µm, 14 µm and 3 µm, respectively. The first two values are close to the corresponding thickness of the specimen aluminized at 1050°C for 6 h, but the MZ is thinner in the specimen aluminized at the higher temperature. Small pores can be found in the coating layer.

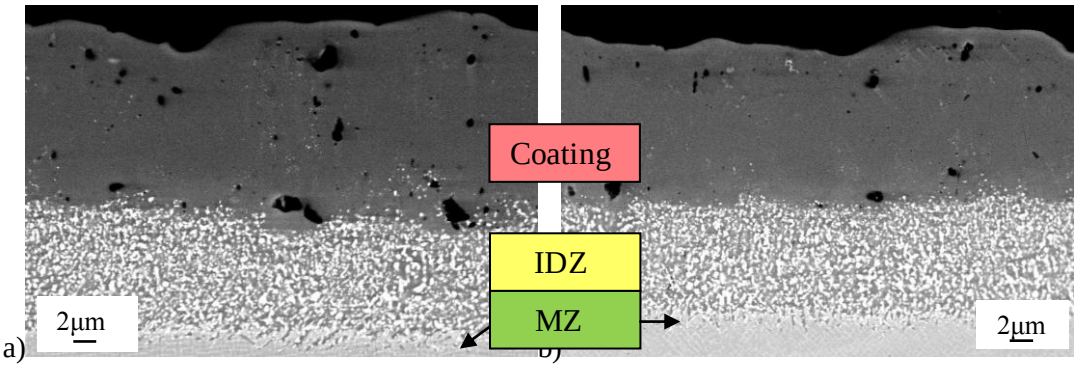

Figure 3-8: *SEM BSE micrographs of the metallographic section of the specimen aluminized for 1.5 h at 1080°C. a) Coating morphology in $[100]_{\gamma'}$ direction, b) Coating morphology in $[110]_{\gamma'}$ direction.*

3.1.2.3 Anisotropy of Coating Layers

The orientation-dependence of the coating morphology was investigated taking into account the easiest measurable microstructural parameter, i.e., the thickness of the layers, measured in section planes parallel to the flat surface of the disc-shaped specimen. Fig. 3-9 shows the results for the specimens aluminized at two different temperatures, i.e., those aluminized at 1080°C for 1.5 h and that aluminized at 1050°C for 6 h. Thickness values are presented as a function of the angular position of the coating where measurements were performed. The substrate orientations are marked by the red vertical line, where at 45°, the crystallographic orientation substrate is [100], while at 90° (or equivalent at 0°) corresponding to $[110]_{\gamma'}$. Considering the two graphs, the total thickness of the layered structure and the external coating layer are almost the same. There is no anisotropy effect on the thickness of layered structure for the specimen aluminized at the higher temperature, while slight orientation effects can be observed in the specimen aluminized at the lower temperature for the MZ and IDZ, being IDZ thicker in the $[100]_{\gamma'}$ direction, MZ thinner in this direction.

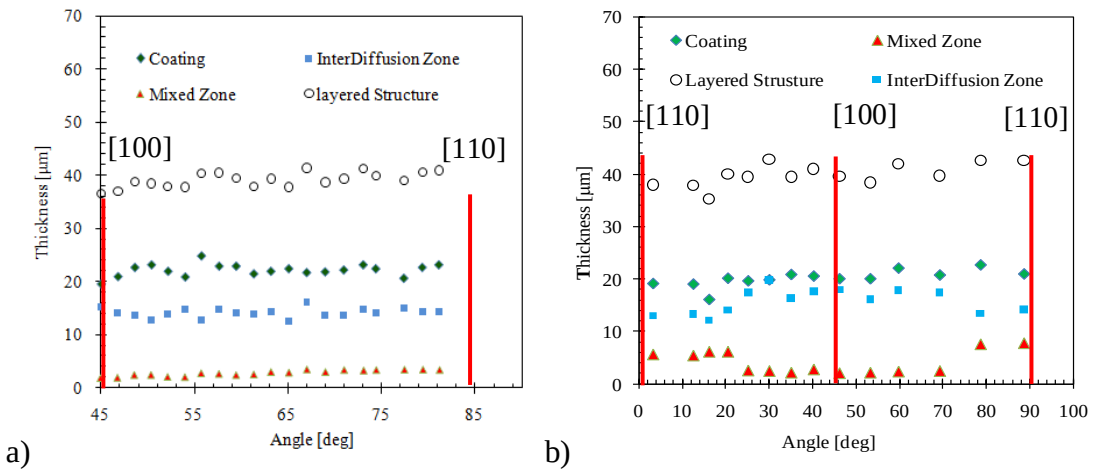

Figure 3-9: *Thickness of different layers as function of their position on the external cylindrical surface. The position is identified by ϑ angle corresponding to Fig.2-4b. a) Specimen aluminized at 1080°C for 1.5 h, b) Specimen aluminized at 1050°C for 6 h.*

The time evolution of the thickness of the different layers, measured normally on surface of (100) of the specimens, is presented in Fig. 3-10 for the two aluminizing temperatures. At 1050°C all the three layers progressively thicken, but their parabolic growth, can not be clearly stated.

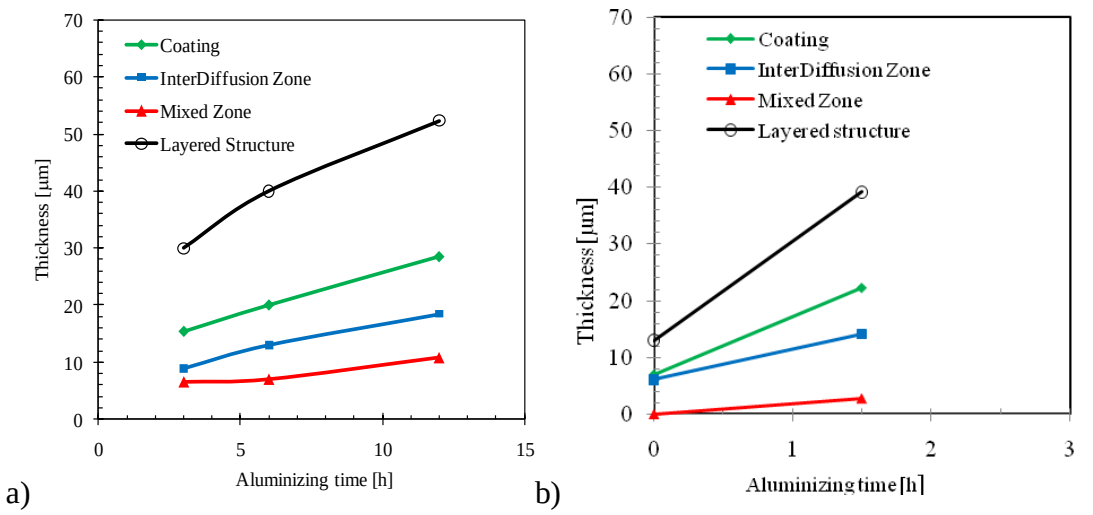

Figure 3-10: *Evolution of the layer thickness with aluminizing time measured along $[100]_{\gamma'}$ in specimens aluminized at 1050°C(a) and 1080°C (b).*

3.2 EBSD Analyses of the Orientation Relationship between the Coating and Substrate

As mentioned previously in Chapter 2, the CMSX4 alloy contains only γ and γ' phase. The orientation relationship between the γ' and the γ-matrix are such that the interfaces correspond to these close-packed planes. They have similar lattice parameters and have the same orientations, therefore, the analysis considers only γ' phase simply. The γ'-Ni_3Al phase is a $L1_2$ type. The parameters used in EBSD analysis are shown in Tab. 3-1.

Table 3-1: *Crystallographic characteristics of the principal phases used for EBSD analysis (data taken from [2, 19]).*

Phases	Strucuture	α(°)	Space Group Number	Space Group	Atomic per unit cell	Lattice parameter
γ'-Ni_3Al	Ordered FCC	90	221	Pm3m	14	a=0.358 b=0.358 c=0.358
β-NiAl	BCC	90	221	Pm3m	9	a=0.288 b=0.288 c=0.288

The phases and orientation relationship between diffusion coating layer and substrate can be analyzed by EBSD.

Taking the specimen aluminized at 1080° for 0 h for example, shown in Fig. 3-11a, the phases of different layers are clearly illustrated. The external coating layer is consisted by the β-NiAl grains. The orientation can be decided according to the triangle collar allocated reference (Fig. 3-11b). These β-NiAl grains have different colours and distributed randomly, hence, these β-NiAl grains oriented randomly. In the IDZ + MZ zone, it contains still the coloured grains of β-NiAl. Therefore, the IDZ consist not only the complex particles observed by SEM analysis, but also the β-NiAl phase.

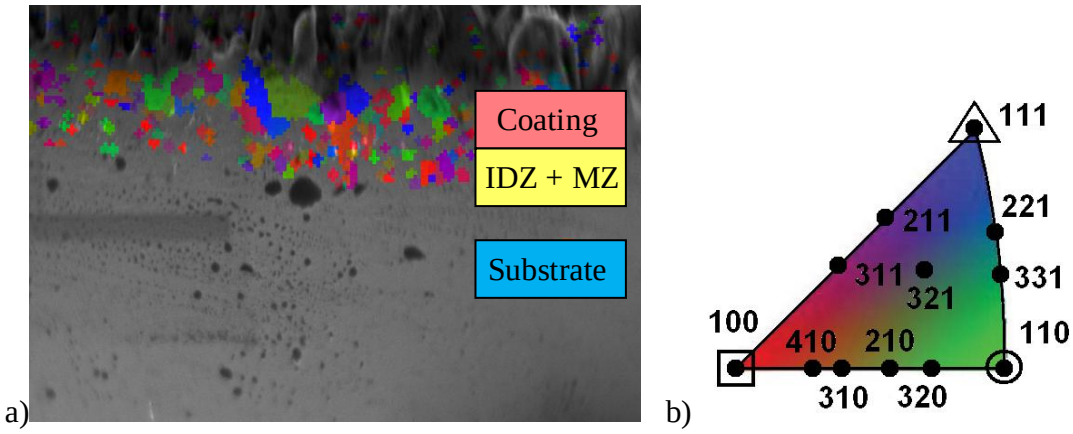

Figure 3-11: *a) EBSD analysis on the coating surface of the specimen aluminized at 1080°C hold 0 h time, b) The colar allocated orientation reference triangle (Ref. [100]).*

The time-evolution of the coating layer in the two reference substrate orientations ($[100]_{\gamma'}$ and $[110]_{\gamma'}$) taken into account into the present experimental study can be observed in Fig. 3-12 in terms of the presence and orientation of β-NiAl grains. Within the external homogeneous layer (coating), the grains of β-NiAl phase, are almost equiaxed and randomly oriented in the specimen nominally aluminized for 0 h. For longer aluminizing times, they tend to become elongated toward the external surface. Smaller grains can be found in any case close to the interface between the coating layer and IDZ. From these grains and within the IDZ, the orientation of β-NiAl phase differs from the homogeneous external layer. In the case of the $[100]_{\gamma'}$, the analysis of β-NiAl phase orientation on the whole area investigated in Fig. 3-12 shows a relative peak close to [110] direction, and this preferred orientation can be observed roughly in the same colour allocated reference. On the other hand, in the case of $[110]_{\gamma'}$, β-NiAl showed two main orientations within in the IDZ, close to [111] and [211] directions.

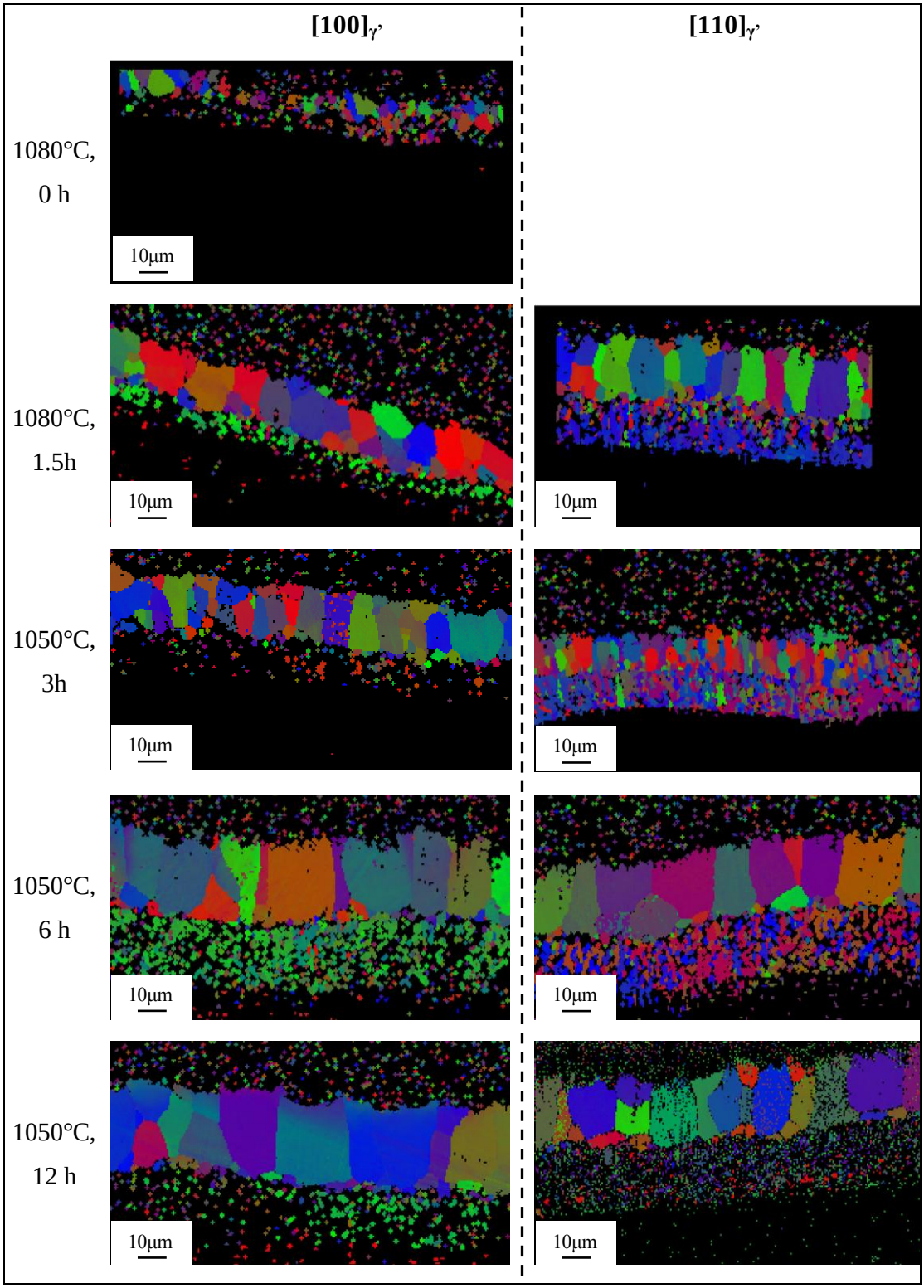

Figure 3-12: *Orientations of β-NiAl phase of all the specimens respected to the orientation of the substrate, taking into the account of Fig. 3-11.*

3.3 Chemical Profiles

3.3.1 EDS Chemical Composition Profiles

The EDS chemical profile of the layered structures obtained by different aluminizing temperatures and holding times are presented in Fig. 3-13 and Fig. 3-14. Punctual quantitative EDS microanalyses are performed along the [001] direction of the samples. Overall, based on the substrate, all of these five profiles have displayed the 3 distinct layers. The layers position can be detected simply on the basis of SEM and EBSD analyses mentioned in section 3.1 and 3.2. The coloured bars marked in each profiles identify the position of the different layers of each specimen. The coating is typically reported to consist in an external Al-rich layer and in an internal low-Al zone. In the present case the composition of the external surface of the specimen aluminized slightly modified with aluminizing time, up to holding times of 12 h (Fig. 3-13c). The Al content was close to 48 at%, in addition to about 2.3 at% Co and 1.3 at% Cr. The internal zone of the coating is characterized by low-Al β phase, where substantially only Co and Cr were found among other alloying elements. The compositional profiles of Co and Cr suggested that the incorporation of these elements in the coating matrix was significant. The profiles of W, Re, Ta also suggested that even some of these heavy elements diffused into the aluminide coating, but at levels below 0.5 at%. Comparing with the back scattered electron images observed above (Fig. 3-8, 3-9, 3-10), grain boundaries in the coating microstructure appeared much lighter than the adjacent grains, implying that the heavy alloying elements were most likely segregated to the grain boundaries due to their low solubility in the β-NiAl phase. Close to the interface with IDZ, small Ta-rich particles were detected. In the IDZ, different phases without evident interfaces can be observed. A detailed analysis of such phases was out of the scope of the present observation, but punctual analysis of such small-sized particles helped to understand the rather complex chemical profiles of these aluminizing samples. Ta-enrichment (up to 10 times that in the alloy composition) and far less W, Re and Ti enrichments characterized many of the particles in the external of the IDZ. Several particles mainly containing W, Re, Ta and Cr, roughly corresponding to chemistry of phases were identified at the internal side of the IDZ.

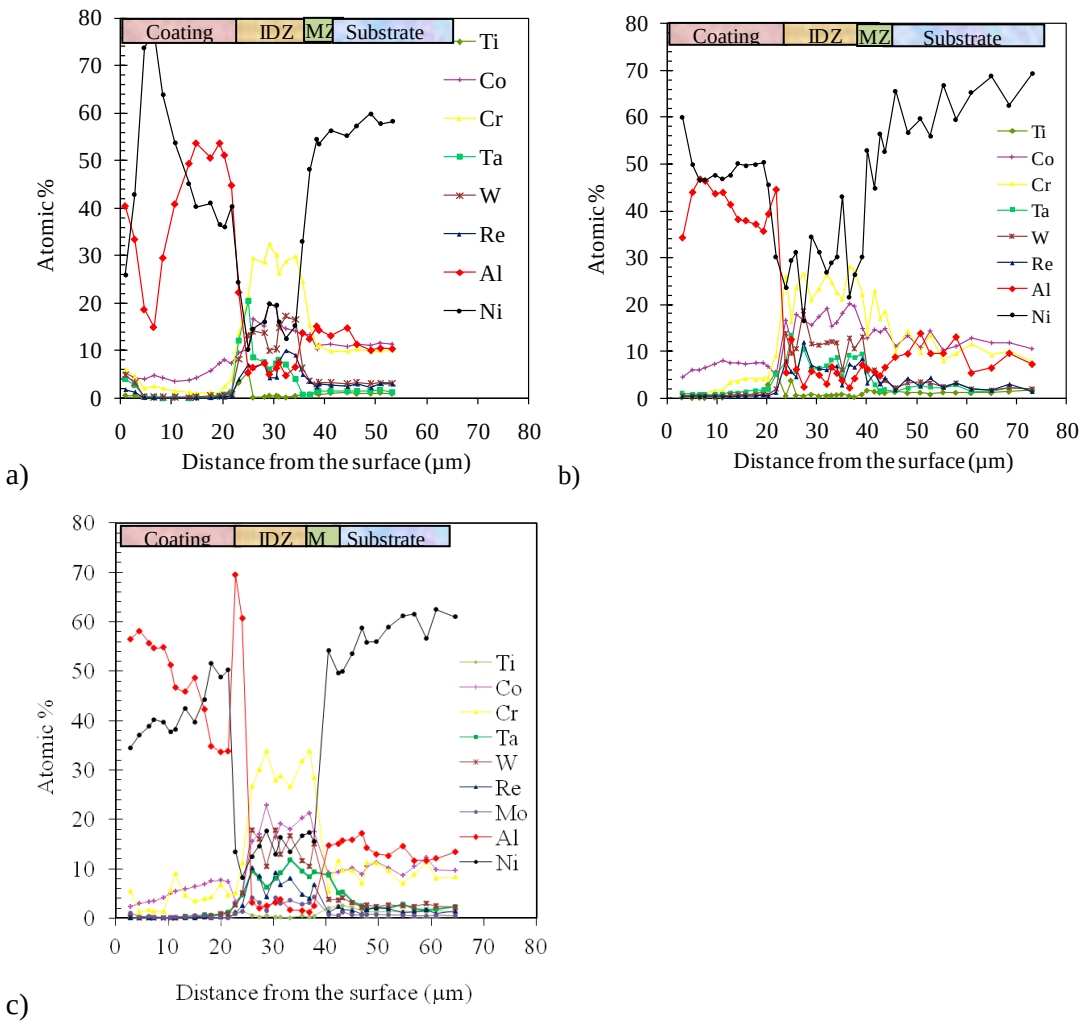

Figure 3-13: *EDS chemical profiles along [001] direction of samples aluminized at 1050°C for 3 h (a), 6 h (b) and 12 h (c).*

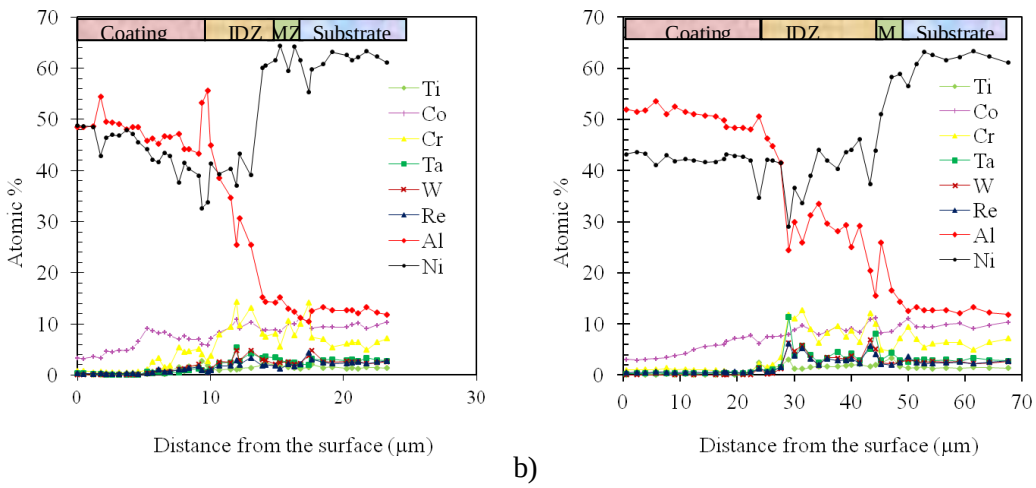

Figure 3-14: *EDS chemical profiles along [001] direction of samples aluminized at 1080°C for 0 h (a) and 1.5 h (b).*

Moreover, moving inward from the external surface to the substrate (from left side to right side), in general, Al deceases gradually, Ni first decreased to a lower level and then increases to the higher substrate level. In both cases (aluminizing at 1050°C and 1080°C), in the coating layer, the average concentration of Al on the specimen surface is roughly 50 at%, and the coating also contains a certain amount of Co. This coating layer mainly contains β-NiAl phase, but, the profiles show that the Al/Ni ratio is not strictly stoichiometric. It is proved in previously chapter (Section 1.6.2.1) that the oxidation performance of β-NiAl is not strongly sensitive to changes in stoichiometric induced by different Al/Ni ratio. However, once the Al concentration drops below ~37.5 at% such that a substantial amount of γ'-Ni_3Al is present, then spallation occurs more rapidly during service. Under the coating layer, the IDZ layer characterized by rich-containing refractory elements is present. A small zone with notable peaks of Al and corresponding valley of Ni are displayed in all of these profiles. Checking from the SEM microscopy, all of these points are located at the interface of coating layer and IDZ. Thus, this zone is also a mark of layers entering into IDZ zone.

For the MZ layer, the chemical composition of Al and Ni has nearly the level of the substrate. This zone serves as the transition from IDZ to substrate. Within the MZ, Al continues to evolute to a stable value. Thus it is supposed that the IDZ layer originated from substrate. The Cr and other refractory elements begin to accumulate toward the MZ/IDZ interface. The content of all these 'heavy' elements is then relatively high within the IDZ, particularly in the case of specimens aluminized at 1050°C. The effect of process temperature affects also the chemical profile of the β-β-NiAl coating, more homogeneous and with monotonic trend of Ni and Al for the specimen aluminized at 1080°C is presented in Fig 3-14. The Al and Ni concentrations are about 42 at% and 50 at% in average, respectively, with fluctuations by the segregation of the heavy elements. Eventually, the Al concentration decreased to ~10 at% after the IDZ region, while the Ni content was measured at ~61 at%. The coating features of specimen in 1080°C aluminized for 1.5 h has already reached the thickness level of β-NiAl coating, the thickness of IDZ is even thicker than that of samples aluminized for 12 h at 1050°C.

It is noticed that in the IDZ, refractory elements Re, W, Mo, Ta are enriched. They precipitate together to form the complex TCPs. For example, σ phase has a tetragonal unit cell, every cell has 30 atoms, containing high Re and Cr. μ phase is a typically formed in CMSX4 ally, rich in W, Mo, Re etc. These refractory elements precipitate are in TCP phases in specific ratios: for example, the W/Re ratio was reported (see Chapter 1) to be roughly 1 or 2 in σ phase. Here we analyse the composition relationship of W and Re content in punctual microanalyses within the in the IDZ for specimen aluminized 1050°C (6 h) and 1080°C (1.5 h), (Fig 3-15), since these two specimens have similar coating morphologies

The W/Re ratio of IDZ particles in the IDZ of specimen aluminized at 1080°C is the same for all of them, close to 1, thus suggesting σ phase as the phase for these particles. The W/Re ratio of small particles in the IDZ of the specimen aluminized at lower temperature includes suggests the presence of two particle populations: σ phase in different W/Re ratios.

a 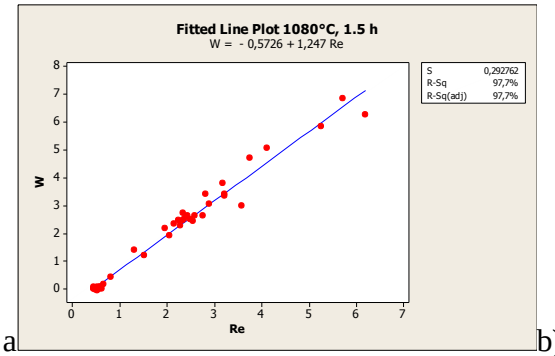

b) 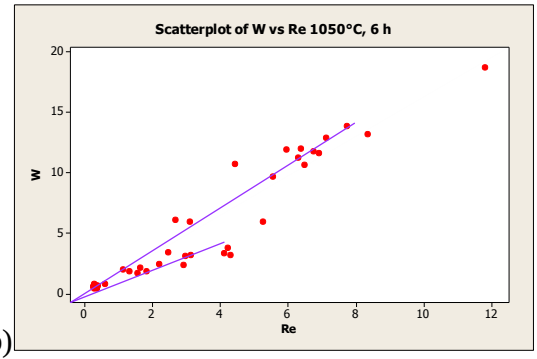

Figure 3-15: *The linear relationship of W and Re in: a) Specimen aluminized at 1080°C for 1.5 h, b) Specimen aluminized at 1050°C for 6 h.*

3.3.2 GDOES Chemical Composition Profiles

GDOES analysis is accomplished with the aim of adding information on light elements to the chemical profiles which can not be obtained by SEM-EDS profiles. In this analyses presented, the element content is normalized, i.e. the content is presented at the ratio between the local amount of the specific element to its average content in the substrate. The depth from the coating surface in x-axis of the same figures was roughly obtained assuming a constant material removal rate. The depth

profiles of the specimen generated by GDOES aluminized at 1050°C for 6 h are presented in Fig. 3-16. Although in the real condition, the sputtering rate can be affected by the different phases encountered in the different layers, the different coating layers could also be distinguished roughly in Fig. 3-16a.

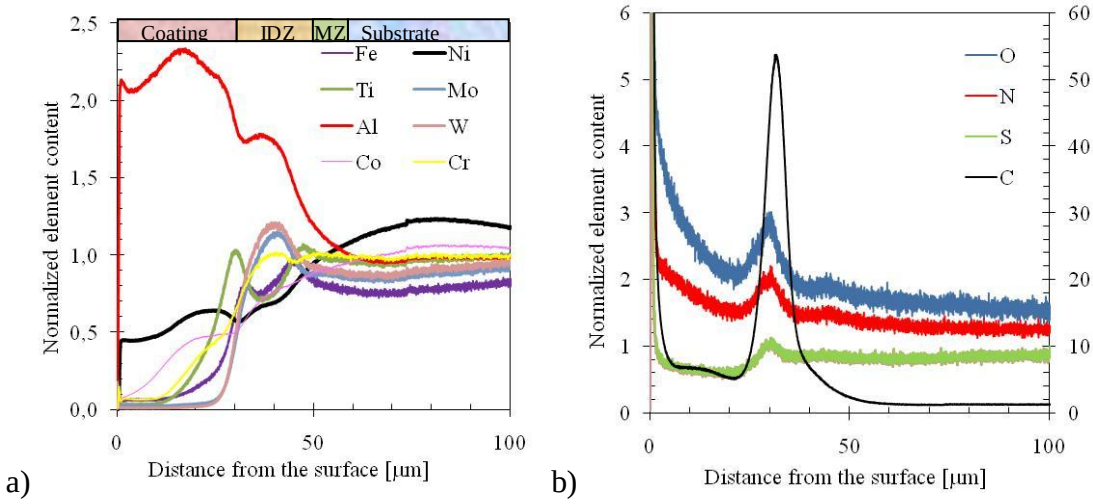

Figure 3-16: *GDOES normalized composition profiles normal to the flat surface of the disc aluminizied for 6 h for different elements ([001] direction of the substrate lattice).*

One of the main features that can be obtained in Fig. 3-16a is that the average composition of the system doesn't show sudden changes of composition between the IDZ and the substrate. Within the coating, a maximum peak of Al below the surface can be found. A wide region with slight Ni enrichment can be observed (Fig. 3-16a) corresponding to a slight increasing of refractory elements with respect to their content in the bulk superalloy. The normalized content of C and O are high within 0-30 µm and a dramatic local enrichment in carbon can be seen (Fig. 3-16b).

Since that the GDOES chemical profiles in Fig. 3-16 are very complex, the diffusion of individual elements can not be distinct clearly. Hence, the separated GDOES chemical profiles for individual elements are considered (shown Fig. 3-17). The individual elements profiles of the specimen aluminized at 1080°C for 0 h and 1.5 h is illustrated and also the GDOES profiles (in Fig. 3-16) are re-analysed. Here, the emission intensities (given as Relative Intensities-RI) for constituent elements versus as a function of sputtering time are considered.

The column a and b show profiles of the specimens aluminized at higher temperature for 0 h and 1.5 h, while, column c reports the profiles of the specimens aluminized at lower temperature for 6 h. The x-axis is started at the coating surface for all the profiles.

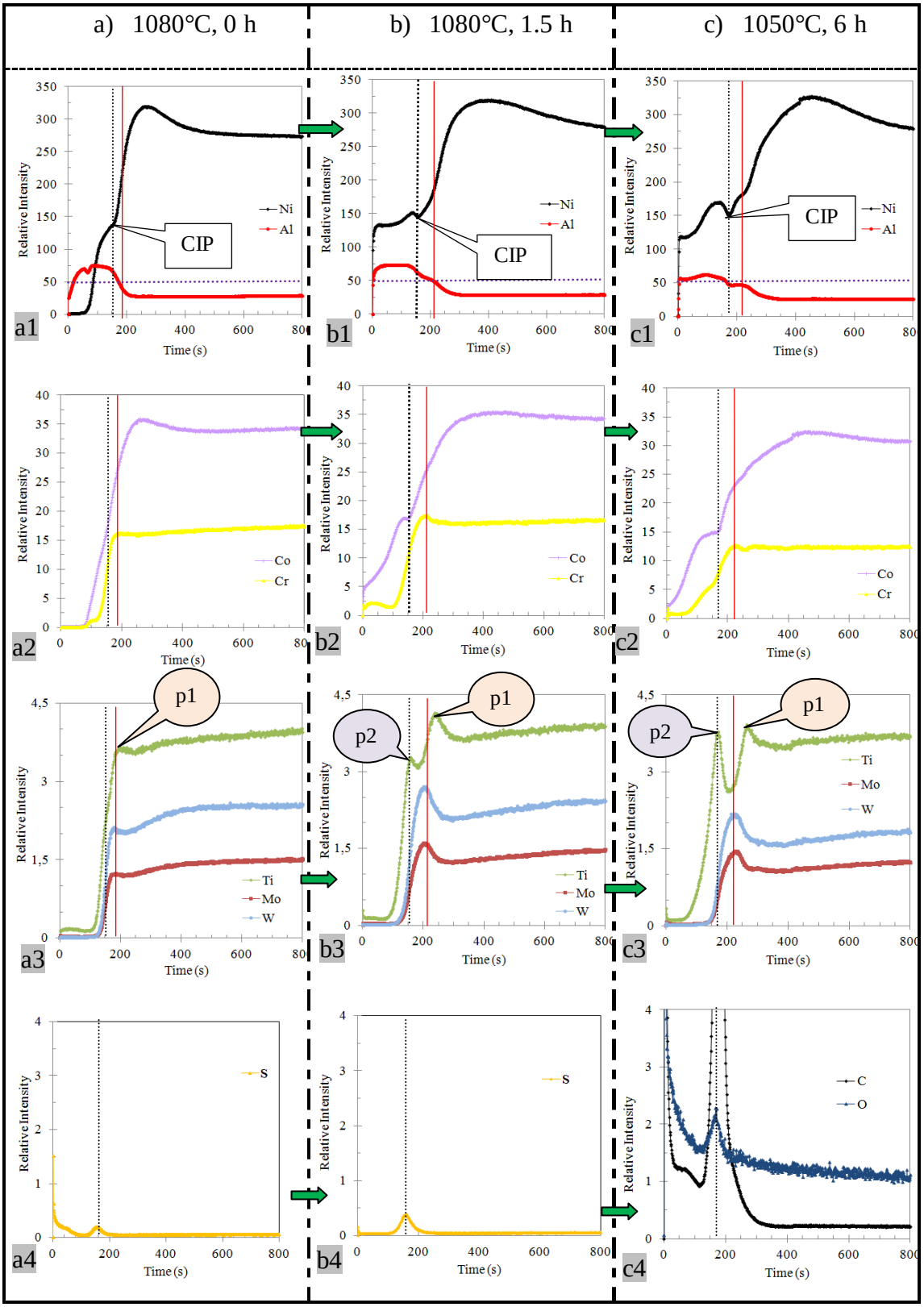

Figure 3-17: *GDOES chemical composition profiles along [001] direction of samples aluminized at 1080°C for 0 h (column a), 1.5 h (column b) and at 1050°C for 6 h (column c). The straight vertical red line in each profile indicates the position of the diffusion peaks of Cr, Mo and W.*

Al-Ni Quantitative Depth Profiling

Firstly, the quantitative depth profiling of Al and Ni is focused in Fig.3-17-profiles a1, b1 and c1. As we move along the distance from the top surface of the coating to the substrate, a general continous decreasing in Al concentration profile along with the corresponding increasing in the Ni concentration, followed by the uniform distributions after a certain distance is observed in the three profiles. The disturbances of Al concentration near the coating top surface presented in profiles a1 and b1 is explained by the roughness of the specimen surface. In profile a1, the Al signal presents a higher concentration lasting 150 s, followed by a decrease of the signal. Then after 200 s, the signal stabilizes to a plateau until the end of measurement. Increasing the aluminizing time, the stabilizing points extends to 300 s (profile b1) and 350 s (profile c1).

The region where all the elements concentration show uniform distribution, indicates the region of substrate matrix. Among the profiles of a1, b1 and c1, Ni signal has shown the same peak in large range in profiles of a1 and b1, and the outward movement of Ni is illustrated. Moreover, in profile c1 the decreasing of Ni locates in a wide domain with its peak tending to disappear. The curve inflection point (CIP) is also observed apparently. Neglecting the disturbances and variation of Al at the initial part of the distance, Al shows concentration higher than 50 RI in profiles of a1 and b1. The concentration of Al decreasing gradually with the trend inward is displayed. By increasing the diffusion time (profile c1), Al tends to keep a uniform RI value of 50, decreasing its concentration gradually, then following the same decreased curve as in profiles a1 and b1.

Cr-Co Quantitative Depth Profiling

Secondly, the Cr and Co quantitative depth profiling are described in Fig. 3-17 profiles a2, b2 and c2. Co has nearly exactly the same evolution curve of Ni, for example, having the same smooth peak point in profiles a2 and b2, the same wide decreasing domain in profile c3 and the same CIP at the same sputtering time. Comparing with Co, the Cr signal shows a delay diffusion from deep matrix to top coating surface (profile a2). With increasing time to 1.5 h (profile b2), a small peak of Cr becomes evident. With increasing time to 6h (profile c2), the shape of Cr peak doesn’t change so much, but with its RI value decreases. Near the top surface, its

concentration is grearly increased gradually. The profile of Co reveals again that Co tends to partition to γ'-Ni3Al by sustituting Ni.

Mo-W-Ti-Quantitative Depth Profiling

Finally, the Mo, W, Ti quantitative depth profiles are presented in Fig. 3-17 profiles c3, b3 and c3. The curves of Mo and W show the same signal evolution trends, with small peaks located at the same time-axis. When increasing the aluminizing time (profile b3), the Mo and W show sharp peaks and higher concentration than at 0 h aluminizing. In profile c3, the curve of Mo and W has kept the sharp peaks but the concentration of Mo is decreased. The evolution of Ti signal is more interesting, because two peaks of Ti are present in profile b3 and c3. We define the peaks of Ti as p1 and p2. The p1 peak exists in the three profiles and the concentration are increased in profile b3 and c3. The newly appeared p2 peak has increased its concentration from b3 to c3.

S-C-O Quantitative Depth Profiling

The concentration of C and O signal are very weak in profiles a4 and b4, while the S signal has shown a small peak at the same position of x-axis. In profile of c4, the high concentration of C and O are detected. The signal of S is neglected for its weak signal. It is noteworthy that, the p2 peak of Ti has located in the same position with the light elements C, O, S in these three conditions.

Now comparing the profiles of the different elements for the same conditions (along vertical columns in Fig. 3-17), Co shows the same evolution trends as Ni, as mentioned above. Mo, W and Cr have the same peaks position, with the peaks located at the time interval from the top surface, indicated by the straight vertical red line respectively. The vertical dashed black lines are indicated also in each profiles respectively. Coincidently, the Ti peak p2 together with the peaks of C and O are also located on this black line. The distance from the top surface layer and the dashed black line is increased. The region with slight Ni enrichment, corresponding to a slight depletion of refractory elements Mo, W Ti with respect to their content in substrate is clearly illustrated.

3.4 Oxidation Test of CMSX4 with a Simulated Crack

A preliminary test to check the effect of oxidation on the superalloy with a cut was prepared by a disc-shaped specimen of SC CMSX4. This cut is considered as the hole or defect of the superalloy. A semicircular notch was performed on it by means of wire EDM process. The diameter of the wire was 0.3 mm. The specimen was then oxidised in air for 24 h at 1124°C. The oxidised specimen is shown in Fig. 3-18. On the external surface, part of the oxide layer was observed (shown in Fig. 3-18a). The microstucture of the oxide is shown in Fig. 3-18b. The spallation of oxides is occurred.

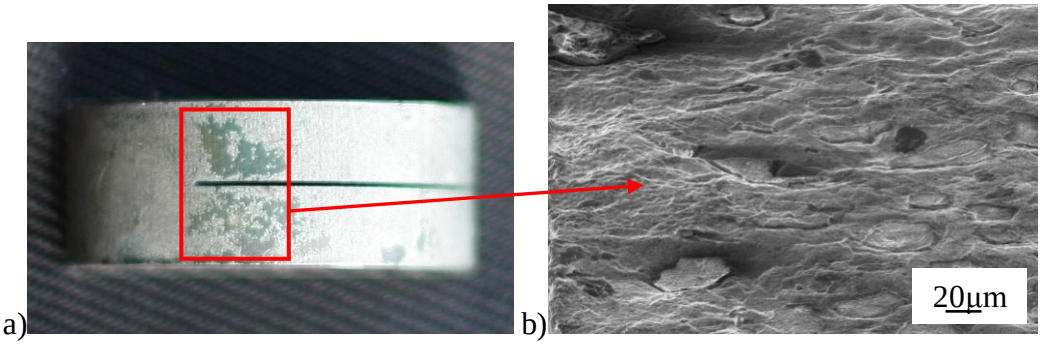

Figure 3-18: *The oxidized CMSX4 specimen with a simulated notch, b) SEM microstructure of the external surface showing the morphology of spallations.*

The SEM microstructure of the flat surface (100) is shown in Fig. 3-19. The channels of γ are thicker than CMSX4 alloy without oxidizing. Many γ' phases become raft elongated along the direction of [100]. The cuboidal γ' has changed the morphology from the sharp corners to spherical corners. This phenomenon is related to the lattice misfit introduced in Section 1.3.3. The lattice misfit is increased by the high temperature oxidizing.

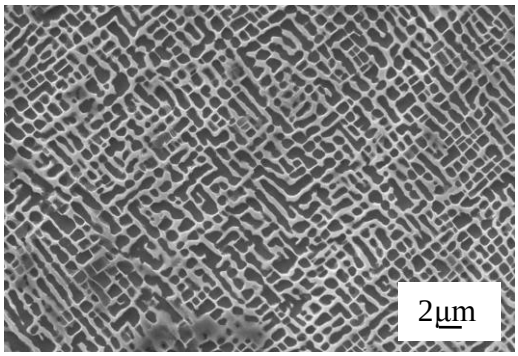

Figure 3-19: *The comparison of the specimen after oxidized.*

The notched disc-shaped specimen was sectioned perpendicular to the notch root line (Fig. 3-20a). Since the notch was machined without reference to any crystallographic orientation, the metallographic section displayed the notch surface has not specific crystallographic orientation apart from [100] direction normal to the disc surface (i.e. horizontal in the Fig. 3-20b).

a) 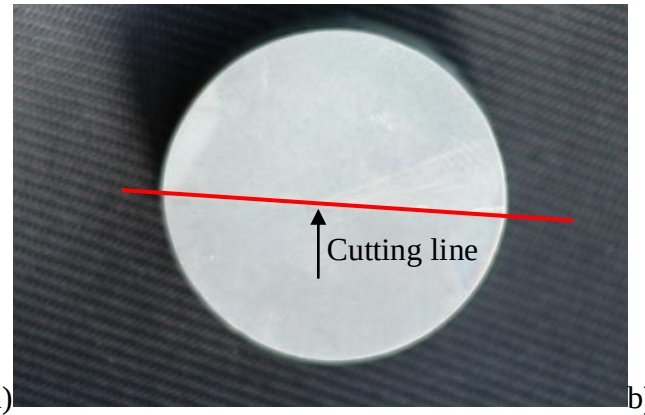

b) 

Figure 3-20: *The specimen was cut in half along the cutting line, b) obtained surface with the simulated crack.*

The oxide scale was observed near the tip of the crack. It is composed of an outer layer (in the form of mushrooms), following a thin black layer and a irregular layer with protrusions and craters (shown in Fig. 3-21). Fedorova and co-workers [87] has made the chemical analysis of these layers. They confirmed that the outer layer is NiO and inner black layer is α-Al_2O_3 layer, and the irregular layer is the substrate on which part of oxides have spallationed so the surface of the substrate becomes coarsened.

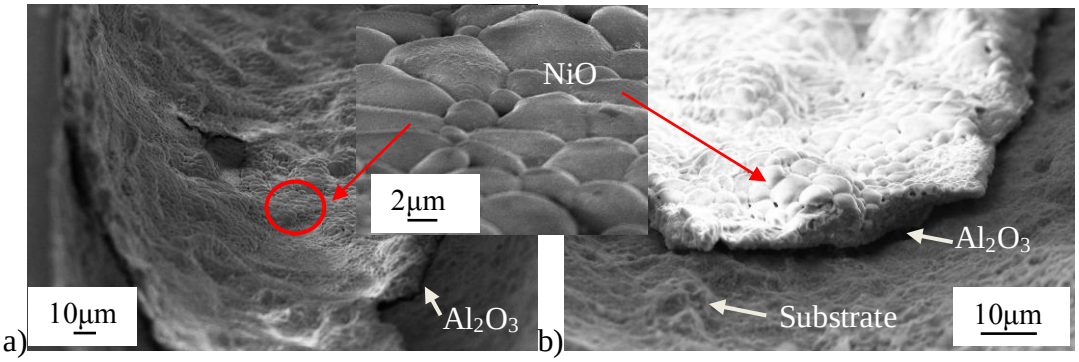

Figure 3-21: *The oxide scale at the tip of the notch, b) The oxide scale in higher magnification, partially detached as scale from the substrate. The substrate appears irregular and contains protrusions and craters.*

For other part of oxidized surface along the crack, no apparent oxide scale was observed. The typical SE and BSE microstructure of the oxide layers are shown in Fig. 3-22. An adherent precipitate-free layer is visible, which is often called γ' denuded layer and it is supposed to be γ phase.

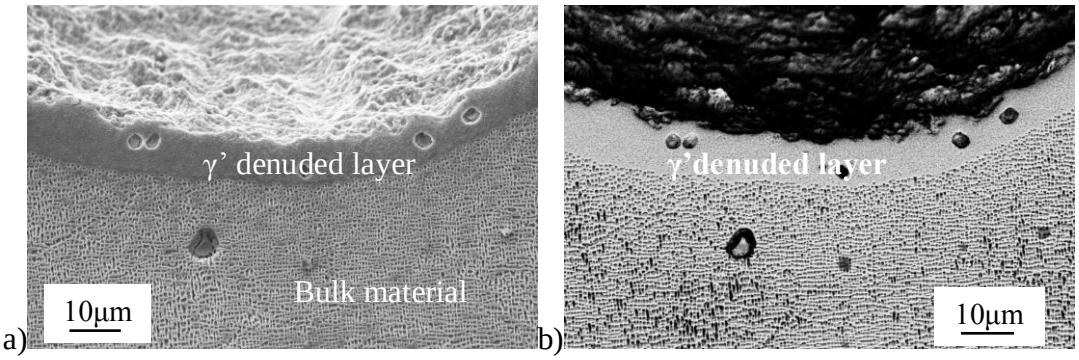

Figure 3-22: *Microstructure of the oxide surface: a) SE image, b) BSE image.*

EDS microanalysis on the γ' denuded layer and bulk material is shown in Fig. 3-23. Compared to bulk material, the concentration of Al and Re has reduced half. Co and Cr are decreased slightly. Ta and W have no much variants.

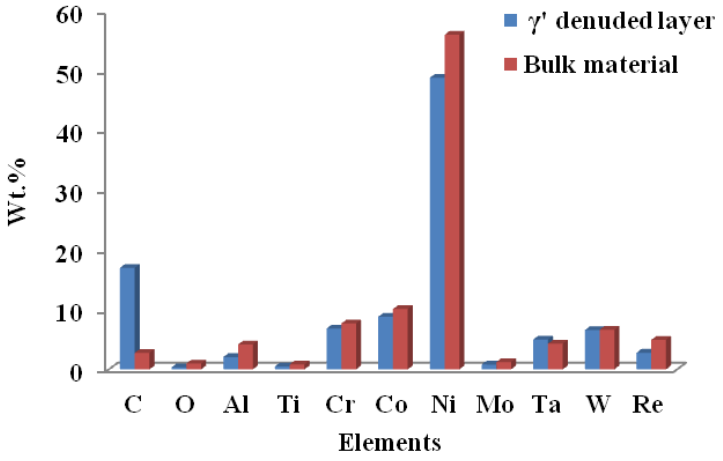

Figure 3-23: *Histogram of chemical composition of γ' denuded layer and the bulk material.*

CHAPTER 4

Discussion

4.1 Discussion on the Aluminide Coatings on Ni201

The chemical composition profile of vapor phase low-activity aluminized pure Ni201, shows that the concentration of Al does not change with increasing the aluminizing time. Nevertheless, the thickness of the external coating layer is increased with extending time. It is supposed that the concentration of gas phase of aluminium halide doesn't change during processing because the Al composition at the external coating layer doesn't change. Kohlscheen and Stock [88] have found that a 'pack' atmosphere made of little HCl and an excess of H_2 is sufficient for releasing a considerable amount of AlCl which serves as precursor for the deposition of aluminium and the subsequent formation of NiAl. Increasing the HCl content doesn't change the surface Al content and thus, it doesn't affect the coating growth rate. Thus, it is deduced that the coating increases its thickness in an equilibrium condition.

Ni diffuses outward to react with the aluminum halides front to form NiAl. When the β-NiAl phase is formed, it is supposed to be in a state of kinetic equilibrium condition, thus the Ni atoms in the β-NiAl phase can be substituted by the incoming Ni atoms (from the substrate), leading to the β-NiAl coating layer front growth outward. The Ni-Al phase diagram shows that β-NiAl phase exists in a wide range of composition. The concentration of Al varies from a minimum of 35 at% to a maximum of 70 at%. In this case, the formed single-phase layer, and its compositional range is easily validated by this Ni-Al binary diagram. Some of the models of aluminizing have taken into account the composition-dependence of the diffusion coefficient for β-NiAl phase. Shankar and Seigle [50] have measured and validated the intrinsic diffusion coefficient at 1100°C as function of composition in the β-NiAl phase of the Al-Ni system. In low-Al condition, Ni diffusion predominates. The characteristic surface morphology of the coating, with a distinct network of grain boundary ridges is typical of outward growing aluminide coatings. The ridges correspond to the grain boundary of β-NiAl phase. This phenomenon has been observed and confirmed by many researchers [41, 63, 89]. Some of them also observed that the β-NiAl phase coatings are columnar grained, with each grain boundary extending across the entire thickness, which seems to be the same as in the previously examined aluminized samples, even if more detailed analyses would be required to confirm this.

Hickl and Heckel [90] have described the progressive movement outward of the external surface. Their model also suggested a faster inward movement of the β-NiAl/γ'-Ni_3Al interface with respect to the γ'-Ni_3Al/γ-Ni interface, also related to the outward diffusion of Ni. The presence of voids close to γ'-Ni_3Al/γ-Ni interface can be explained by the faster outward diffusion of Ni than the inward diffusion of Al. Recently, this model was implemented taking into account diffusivity changes efficiently simulating the evolution of this vapour phase aluminide coatings on pure Ni201 [91].

Rafted structure formation is often observed in creep tested SC superalloys and is believed to be related to stress-driven diffusion. However, the rafted morphology observed below IDZ for aluminized René108 is observed. It is impossible that sufficiently large stresses build up below the IDZ to cause the material to creep.

However, the interdiffusion with the substrate may well in itself be responsible for the raft formation. The outward diffusion of Ni naturally depletes Ni in the region below IDZ, which causes parts of the γ-Ni phase to transform to γ'. The majority of the Ni atoms diffusing outwards originating from the γ regions is located laterally between the γ' cuboids. Moreover, the fastest diffusion path should be along the γ/γ' phase boundaries. The result is that the predominant γ' growth will occur in the lateral direction, resulting in the rafted microstructure. A model has also been established by J. Angenete et al. to explain the γ' coarsening directionally in the substrate [69].

4.2 Microstructure of the Aluminide Coating on CMSX4

The results of the microstructure investigations carried out on CMSX4 alloy will now be discussed in order to get information on the diffusion mechanism and for this superalloy, which chemical composition is far more complex with respect to that of pure Ni. The same results will be here discussed also in order to define possible effects of substrate crystallographic orientation with respect to the surface plane in aluminized layered structure.

4.2.1 Diffusion Mechanism

The aluminizing process led to the presence of three layers in all the investigated specimens of CMSX4 alloy. Externally, there is a layer of β-NiAl phase, substantially homogeneous and relatively thick with respect to the others. Beneath it, an intermediate IDZ layer appears, consisting of β-NiAl and of particles rich in refractory elements. These latter reasonably consists of TCP phases such as the Re-rich σ phase, often referred in literature for superalloy, or the μ phase, previously observed for the same CMSX4 alloy [92-94]. In the third layer, facing the substrate and here referred as mixed zone (MZ), γ' and γ-matrix coexist with TCP particles and β-NiAl, the MZ appears in the form of small linear and oriented protrusions from the IDZ. Beneath the layered structure, within a few micrometers, the substrate progressively decreases its Al content from the solubility limit down to its initial alloy content.

After the external coating layer formation, the β-NiAl phase thickens moving into two directions. Its external surface moves outward and grains coarsen and elongate normally to the surface with the classic competitive growth mechanism. The outward movement of the external surface in low-activity aluminizing processes has often been related to the Ni-diffusion prevailing over Al-diffusion [2, 55]. During the moving of external surface, the Al-content remains almost constant, roughly at the stoichiometric β-NiAl composition. On the other hand the amount of Ni/Al ratio within the phase progressively decreases with time and distance to the outer surface, the chemical profile being related to the strong composition dependence of diffusivity within the β-NiAl phase [94].

The interdiffusion of Ni and Al within the β-NiAl phase also causes the inward movement of its original interface into the single crystal superalloy where γ-matrix and γ' phases are equally oriented. It has been suggested by Wőllner et al. [19] that the atoms of the γ'-Ni_3Al phase, which has reached its maximum solubility of Al, rearrange at the β/γ' interface originating β-NiAl crystals of three well-defined orientation relationships with the former crystal, all having the $\{111\}_{\gamma'}$ planes parallel to the $\{110\}_{\beta}$ planes. Such kind of transformation of γ' into β was stated to have beneficial effect for coated components, since it induces compressive stresses within the IDZ. Wei et al. [54] has also observed the initial inward diffusion of Al during low activity aluminizing, for that the concentration of Al in the pack powder is very high (60 at%). At the initial stage of the aluminizing, the diffusivity of Al and Ni is high enough at the aluminizing temperature to obtain the equilibrium β-NiAl phase.

The outward and inward movements of the β-NiAl interfaces can occur simultaneously, even at different rates, during the early stages of the process. The slow diffusing refractory elements characterizing the superalloy composition, most of which preferentially partitioning in the matrix [95, 96], accumulate in the narrow region of the substrate close to the inward moving β-NiAl front. This fact, joined to the concurrent progressive reduction of Ni, outwardly moving, causes the nucleation of TCPs, as the solubility limits of the refractory elements in the matrix phase are reached at a certain time and at a certain distance from the β-NiAl front. TCPs then grow inward correspondingly to the inward movement of the Ni-depleted region. In

the same region, the γ+γ' structure of the superalloy transforms into the only Al-richer γ' phase. The total result of the loss of Ni and concurrent Al enrichment of the substrate is its progressive transformation of the original γ/γ' structure into the MZ, the extension of which is relatively stable with time. Externally to it, the inward moving β-NiAl grains, after a small growth as a homogeneous phase, meet the TCP phases and embed them originating the IDZ structure. Thus, the position at which TCP phases first appeared during the process corresponds to the external position of the IDZ observed in the aluminized specimens, even if these phases formed at the MZ/substrate interface and coarsened into the MZ [97].

In the region of the coating close to the interface with IDZ, the presence of carbides rich in Ti and Ta, typically presents in γ' but far less soluble in β, as well as of occasional substrate carbides, suggests that they formed later than TCP phases. Their origin can date back to the beginning of the aluminizing process, when these metallic elements accumulated at the inward advancing β-NiAl phase and reacted with non-metallic elements easily diffusing from the external surface.

The exact mechanism of formation of different layers is known in any case to vary also for the same alloy on the basis of process conditions (surface roughness, Al content, temperatures etc.) and the mechanisms explained above differ from other ones proposed in literature.

The W-, Re-, Mo- and Ta- rich TCP phases were for example observed to segregate along the NiAl grains boundaries by I.G. Wright et al. [99]. The segregation of refratory elements to grain boundaries could contribute to accelerated spallation by degrading the oxide-metal bond strength or by forming rapid-growing secondary oxides, such as Ta oxides. The transport of Ta from the alloy into the alumina scale has been found to initiate scale failure and partially counterbalance the benefical effects of reactive element additions.

In the present case the change of aluminizing temperature did not substantially alter the mechanism of formation of IDZ and MZ, but nevertheless it affects the layered structure morphology due to temperature effects both on the element diffusivities and on the solubility of elements within phases. Comparing the morphology (figures in section 3.1) and chemical profiles (profiles in section 3.3.1) of coatings at the two temperatures, approximately of the same thickness is obtained. However, at 1080°C

the amount of refractory elements within the IDZ and MZ is lower than in the same regions of the specimen aluminized at 1050°C. Further, the external (coating) layer obtained at 1080°C displays larger grains and has a more homogeneous composition, with a relatively high Al content and slightly decreasing Al/Ni, suggesting that a slightly Al-enriched NiAl phase was here present. A drastic reduction of Al/Ni ratio roughly occurring at the coating/IDZ interface suggests that, at the aluminizing time taken into account, the β phase here present was of the Ni-rich composition. A coating aluminized at 1080°C is also characterized also by a thinner MZ and by a rapid decrease of the Al content to the alloy initial composition. On the contrary, the coating layer of the specimen processed at 1050°C is externally almost free from porosities and the distribution of Al and Ni within it, is characterized by one or more plateau and by a non monotonic trend for the Al/Ni content (in particular with a peak of Al/Ni in the homogeneous coating close to its interface with IDZ), making a complete understanding of its evolution with time rather difficult.

A rafted morphology of γ + γ' is observed below MZ for samples aluminized for 12 h at 1050°C. The rafted structure formation was already observed in literature on creep tested SC superalloys and it is believed to be related to stress-driven diffusion, even with stress acting locally on a microstructure level. In the present case, no external load was applied as in creep specimen. However, the interdiffusion with the substrate could in itself be responsible for the raft formation. Angenete et al. explained the possibility of the γ' coarsens directionally in the substrate [69]. The outward diffusion of Ni depletes in the region below MZ, which causes parts of the γ-Ni phase to transform into γ'. Moreover, the fastest diffusion path should be along the γ/γ' phase boundaries. The result is that the predominant γ' growth will occur in the lateral direction, resulting in the rafted microstructure. A model has also been established.

4.2.2 Anisotropy of Layer Thickness

The anisotropy effects are only observed at lower temperature for IDZ and MZ, this latter being thicker along [110] direction. Nevertheless, the thickness of this zone was hardly identified for certain microstructure directions, where two sets of parallel structures of particles and γ + γ' crossed each other. In addition, moving toward the IDZ and within it, such particles coarsen and the possibility to identify their

orientation on SEM micrograph was lost. When aluminized at higher temperature, no anisotropy effect was found. Therefore, increasing aluminizing temperature could avoid or eliminate the anisotropy effect.

The microstructure features of diffusion layered coatings in SC are potentially affected by substrate lattice orientation with respect to the external surface. As a matter of fact, solid state diffusion is related to crystallographic orientation of the phases within which it occurs and orientation relationship between lattices in a layered structure exists. The effect of substrate orientation on the overall coating thickness of CM 247 LC alloy was investigated by F.H. Yuan and co-workers [98]. They found slight differences in the as-aluminized layer thickness due to significant anisotropy effects of the structure. They also observed anisotropy effects once the coated surface was exposed to high-temperature in oxidizing environment. The slower oxidation phenomenon on $(110)_{\gamma'}$ orientation has also been observed. Murakami et al. [20] have demonstrated on as-aluminized TMS-75 alloy, that during aluminizing, the anisotropy of TCPs below the IDZ occurred.

4.2.3 Orientation Relationship

Further, the microstructure features of the β-NiAl phases of each specimen vary along the thickness of the layered structure. In most of the coating thickness, the β-NiAl phase does not show a well-defined crystallographic orientation and displays the typical features of a competitive growth from the small crystals not far from the interface to the dual-phase IDZ. Within the IDZ, the same β-NiAl phase shows clear orientation features. In the $[100]_{\gamma'}$ specimens, the β-NiAl crystals grains grew in such a way that their <101> directions are parallel to <100> of the FCC substrate matrix. For [110]γ' specimens, β-NiAl grains in IDZ are oriented so that typically $<211>_{\beta}//<110>_{\gamma'}$ or $<111>_{\beta}//<110>_{\gamma'}$. These relationships are among the possible ones for epitaxial growth of a BCC phase from an FCC one [101]. They were previously observed on aluminized samples of Ni-base superalloys [19].

In the work of S. Wöllmer et al. [19], the relationship of $(111)_{\gamma'}//(110)_{\beta}$ are met by three specific β grains orientations with respect to the substrate lattice. Zhang and co-workers [65] have also observed the higher intensity peaks at the [111] and [211] directions of β-NiAl phases by XRD. They supposed that the crystallographic

orientation of aluminides may have some effects on scale adhesions, the long-term scale spallation behaviour on β-NiAl could also be affected by coating orientation.

4.3 Chemical Composition of the aluminized layers

The EDS and GDOES chemical profiles (in Fig. 3-13, 3-14 and Fig. 3-15), can be examined jointly. Within the coating, a maximum peak of Al below the surface can be found in both chemical profiles. The EDS profiles (Fig. 3-13 and 3-14) showed that in the external coating layer, the content of Cr drastically increases toward the value of IDZ. This features could be related to the fact that, notwithstanding a similar trend for Co and Cr to partition in β rather in than in γ and γ' [89], Co diffuses in β more rapidly than Cr [54], and this latter is also involved in the formation of particles in the IDZ. Ta was revealed by EDS profiles to be accumulated in the same IDZ layer, but closer to its external interface in specimens aluminized for short times, which is assumed to be a phase similar to σ but contains high Re and Ta. A corresponding trend was observed for Ti. Their enrichment extends to the whole IDZ. The depth profiles show that the measured thickness of the coating layers is in agreement with the real thickness with a little deviation. Because the real speed of emission on different coating layers or phases is not uniform. However, this speed difference is negligible.

When analysed the individual elements in GDOES profiles (Fig. 3-17), some hints or doubts can be discussed deeper to explain the diffusion progress within the complicated multi-element alloys. At the beginning of aluminizing, Al was rapidly deposited on the surface of substrate and some Ni has already diffused outward to react with Al to form the β-NiAl phase, which has been observed in SEM microstrucure and EBSD analyses. In high-temperature low-activity vapor phase aluminide coating, due to the higher content of gasous AlCl or $AlCl_2$, diffusion inward occues in a very short time. At such a high temperature (more than 1000℃) the diffusion rate of Ni is high enough to diffuse outwardly to form β-NiAl with Al. During 1.5 h aluminizing, the coating on CMSX4 growth outward with the β-NiAl layer increased. Furthur, increasing aluminizing time, the β-NiAl layer thickess increased. Once the aluminizing started, the gasous ambient of out-of-pack doesn't change, so Al at surface remains substantially constant, while continues to diffuse

inwardly decreasing its content gradually. Ni diffuses outwardly more rapidly than Al inward, forming a wide range of β-NiAl phase.

Now, the attention will be focused on the multi-elements diffusion, making reference to the chemcial profiles presented in Fig. 3-16 for different combinations of aluminizing time and temperature. This red line indicates the diffusion peaks of Cr, Mo, and W at this layer. It can be assumed that at the position of the red lines, the diffusion dynamic has reached the 'saturated condition'. This suggests, that some precipitates enriched in these refractory elements. The increased Al concentration and inward Ni diffusion decreases the solubility of W in the γ' phase. This increases the driving force for formation of W-rich precipitates μ-phase [17], with the formula $(Ni, Co)_7(Cr, W, Mo, Re)_6$. The same author suggests that μ-phase nucleated from the metastable σ phase leading to a weak orientation relationship with the matrix and thus a high surface energy. The high Co content promotes the coarser μ-phase [91, 28]. Ta and Re are not analysed by GDOES, but reasonably they are assumed to have the same peaks as Mo and W, for this reason, the TCPs always contain these elements together.

Under and close the original interface, the appearance of peaks of Ni, Co, Cr, Mo, W, Ti at the initial stage of aluminizing, is explained by the differential potential energy of Al. Al by its high content in the coating would 'drive' or 'pull' Ni, Co, Cr, Mo, and W to diffude outward. Accordingly, the two peaks of Ti could also be understood, the peak p1 has shown the same trend with Mo and W, which is 'drived' out by the diffusing. The peak p2 is located at the rigion rich in O and C, thus Ti-enrichment of oxides, carbides or sulfides formed.

The effect of significant amount of S near the original superalloy interface has also been analyzed by J.A. Haynes [101], they found that NiAl coatings at 1150°C was sensitive to substrate S impurities. Reductions in S impurities resulted in dramatic improvements in scale adherence. In the cyclic oxidation test, the number of voids on the coating surface increased significantly as substrate S increased. The voids is said to be the reason to induce the rumpling of the coating scale. In [102], cyclic oxidation behavior obseved for the coating with impurity of S, the results suggested that there was a source of S in the reactor environment, and this S acted to degrade scale adhesion. As described by Warns and Punola [62], impurity elements, such as S, P, C, O can be introduced into diffusion coatings by the air ambients, not very clean

surface before aluminizing, the aluminizing process. They could also be introduced by Pt plating process or the substrate alloy, in the cases this anticipated aluminizing process. They concluded that the gas-solid reactions are the primary mechanisms of impurities transfer in the process considered.

The distance where the peaks of C and S located proved again the original interface (which passing the curve inflection point of the signal curve). The effect of significant amount of S near the original superalloy interface has also been analyzed by Haynes [101]. They found that β-NiAl coatings at 1150°C were sensitive to substrate S impurities. Reductions in S impurities resulted in dramatic improvements in scale adherence. In the cyclic oxidation test, the number of voids on the coating surface increased significantly as the substrate S increased. The voids are said to be the reason for rumpling of the coating scale. In [101], cyclic oxidation behavior was investigated for the coating with impurity of S, finding that there was a source of S in the reactor environment, and this S acted to degrade scale adhesion.

Engström et al. [68] have recently simulated the interdiffusion occuring between NiAl coating and Ni-base superalloy subsrate. The so-called homogenization approch implemented successfully into the DICTRA software was used. This approch is based on the assumptions that: a) local equilibrium is established in each volume element at each time-step in the calculation, b) that diffusion occurs exclusively in a continous matrix phase, and c) that diffusion taking place in the β- and γ'- phase. Fig. 4-1 is the simulated and calculated elemental composition profiles from the right substrate to the left coating surface.

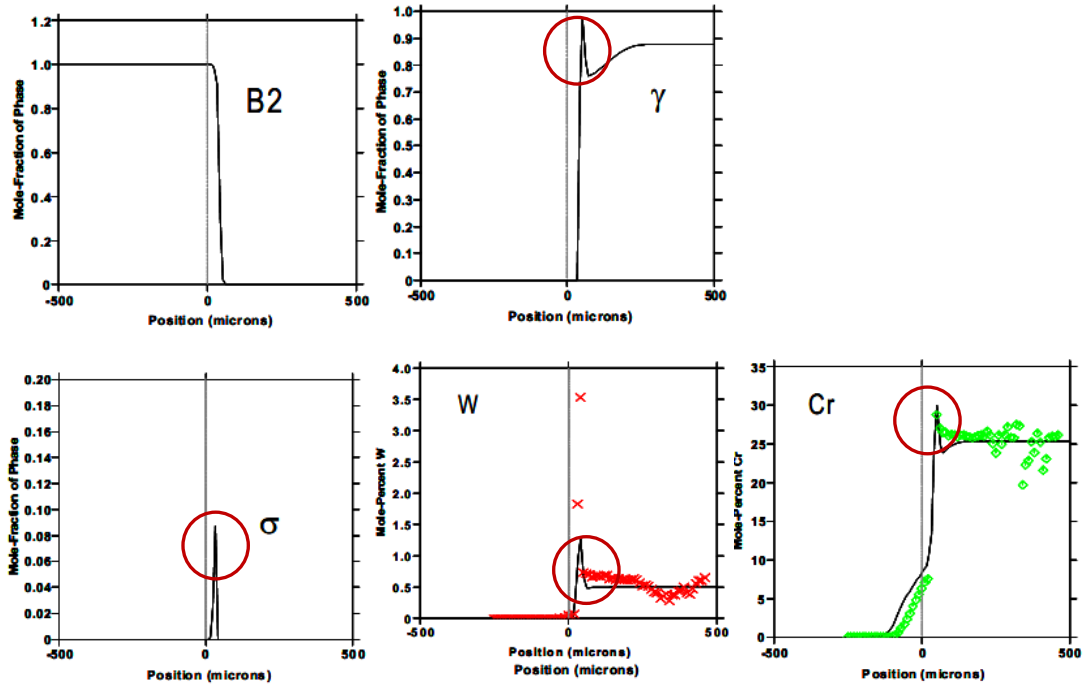

Figure 4-1: *Concentration profiles for β-, γ-, σ-, W, and Cr in a β-NiAl/IN939 diffusion couple. Solid vertical line indicates the position of the initial interface.*

It is shown that the single β-NiAl grew inward respect to the original surface of the substrate alloy, whereas the γ+γ' phase region has receded back toward the susbtrate. γ' phase is observed close to the region of mixed zone (MZ) and within it. The W and Cr peaks together with that of the presence of σ phase indicate the formation of TCPs under MZ. Their results can also be compared to the present GDOES results, where that the peaks of Co, Cr, Ti, W are peak p1 could suggest the presence of the same phase.

CHAPTER 5

Conclusion

This chapter illustrates the main conclusions drawn from the study and investigations carried out.

This thesis was introduced by an extensive state of the art on evolution and application of Ni-base superalloys in 60 years development. Thermodynamic considerations have always led gas turbine manufactures to seek the maximum turbine inlet temperature compatible with existing blade technologies. In Ni-base superalloys, the precipitation of γ' phases provides the first and important mechanism for strengthening, which has increased greatly the creep resistance. The excellent creep properties in modern generation of superalloys have been reached by means of combined composition and process improvements. The chemical compositional changes were also related to the fact that protective oxidation and corrosion resistance of the superalloy was guaranteed by the use of coatings. Among them, the role played by overlay and diffusion coatings containing high amount of aluminum is essential, since Al has best resistance to oxidation and corrosion. The diffusion of

aluminum into the Ni-base superalloy surface substantially allows the formation of layers of very stable nickel aluminide compounds. A thin, effective and uniform Al coating is always the objective for the researchers and manufactures.

The methods to obtain diffusion coatings were then reviewed. Diffusion coatings can offer a low-cost solution and a friendly production process for providing environment protection. Within then, diffusion aluminizing processes are well-known techniques industrially adopted to enrich of aluminum the surface layer of Ni-based alloys. Aluminum can also be used in combination with other elements to produce Cr/Al, Si/Al and Pt/Al layers. The diffusion temperature and time are two critical factors affecting the mechanism of the surface layers formation.

After the state of art chapter, the thesis described the experimental work carried out during the PhD years. The purpose of the work was to study the evolution features of the coatings under different aluminizing conditions and to understand the effects of crystallographic orientation of the substrate crystal on the coating layers. The low-activity vapor phase aluminizing process was chosen to prepare diffusion coatings at the temperatures of 1050°C and 1080°C. The substrate takes into account is mainly a CMSX4 single crystal alloy.

Several results have been obtained through this thesis work:

1. The aluminized CMSX4 alloy coating layers is characteristic made of an external layer of β-NiAl, an interdiffusion zone (IDZ) and a mixed zone (MZ), following the substrate. The IDZ is consisted with β-NiAl phase, topological-close packed (TCP) phases. The TCP phases is rich in refractory elements. The mixed zone (MZ) represents a transition region within which refractory elements, rejected by the growing β-NiAl phase, accumulate in the γ phase channels, and form particles when/where their solubility limits are exceeded.

2. The thickness of the diffusion layers increased with aluminizing time in all cases. The total coating thickness obtained at 1050°C for 6 h is equivalent to the coating obtained at 1080°C for 1.5 h. The anisotropy of the layer structure was substantially observed only for the layer of MZ at lower aluminizing temperature, slightly thicker when growing along [110] direction. While, at higher temperature

(1080°C), there is no anisotropy effects observed. From the economic point of view, increasing temperature from 1050°C to 1080°C, can reduce greatly the aluminizing time, thus can reduce the cost of aluminizing. It also limits the interdiffusion of refractory elements evolution from substrate to coating surface, thus increases the coating performance.

3. The layer of homogeneous β-NiAl phase doesn't show a well-defined crystallographic orientation. Additionally, β-NiAl grains display features of a competitive growth from the small crystals not far from the interface with interdiffusion zone (IDZ). The effect of high aluminizing temperature was to give rise to larger grains for corresponding thickness. Also, different content of elements in the phase of layered structure were observed for different process temperatures. Within the IDZ, the same β-NiAl phase shows clear orientation features. In specimen, where the coating grows in [100] direction of the substrate, the β-NiAl grains grow in such a way that their <101> directions are parallel to <100> of the substrate matrix. For coating growth along $[110]_{\gamma'}$ direction, β-NiAl grains in IDZ are oriented such that typically $<211>_{\beta}$ // $<110>_{\gamma'}$ or $<111>_{\beta}$ // $<110>_{\gamma'}$.

4. The chemical profiles and the morphological texture features of the coating layers suggest that the vapor phase aluminizing mechanism led important information of β-NiAl phase forming. The β-NiAl phase thickens moving towards two directions. The external surface moves outward and grains coarsen and elongate normally to the surface with the classic competitive growth mechanism. The internal interface moves inward. The β/IDZ interface gives rise to the crystallographic orientation relationship presented above.

The above conclusions of the experimental work offer a new view on the process-related microstructure features of aluminized coatings and to the effects of substrate grain orientation on the morphological and physical/mechanical service-related properties of the coatings.

The experimental data and the suggested growth mechanism can be used to improve the aluminide diffusion coating process.

List of Figures

List of Tables

References

[1] R.C.Reed: The superalloys: fundamentals and applications. Cambridge Univ.Press. (2006).

[2] M. Durand-Charre: The microstructure of superalloys. Overseas Publishers Association (1997).

[3] T.Sourmail:Http://www.msm.cam.ac.uk/phase-trans/2003/Superalloys/index.html.

[4] S. Neumeier, J.Ang, R.A. Hobbs, C.M.F.Rae, H.J.Stone: Adv. Mater. Resear. Vol. 278 (2011).,p.60-65. S. Neumerier in conference EuroSuperalloys 2010. Organized by Deutsche Gesellschaft- DGM, in Germany. 25-28th May, 2010.

[5] P. Caron, T.Khan: Aerosp. Sci. Techn., Vol. 3 (1999).,p. 513-523.

[6] M.J. Pomeroy: Mater. Design., Vol. 26 (2005).,p. 223-231.

[7] Y. Koizumi, T. Kobayashi, T. Yokokawa: Superalloy 2004. Edited by K.A.Green, T.M. Pollock, H.Harada, T.E.Howson, R.C. Reed, J.J.Schirra and S.Walston. TMS (The Min. Metal. Mater. Soci), 2004, p.35-43.

[8] H.T.Pang, R.A. Hobbs, H.J.Stone, C.M.F.Rae: Adv.Mater. Resear., Vol. 278 (2011).,p.54-59.

[9] S. Bose, et al.: High temperarture Coatings 2007, Chapter 2., Rensselaer Polytecnic Hartford, CT.

[10] M.P. Simonetti, P. Donnadieu, P. Caron: Scripta Met. Mater.,Vol. 30 (1994).,p.1553-1558.

[11] Matthew.J. Donachie, Stephen.J. Donachie: Superalloys-A tecnical guide, 2nd Edition. Copyright by the Materials Information Society. 2002. IBAN:0-8170-749-7.,SAN: 204-7586.

[12] J.Y. Guedou: Materials Evolution in Hot parts of aero-turbo-engines, in: ICAS 2010, 27th International congress of the aeronautical sciences. 19-24th, Sep 2010, Nice-France.

[13] G.A. Kool: J. Therm. Spray. Techn.,Vol. 5 (1996).,p.31-34.

[14] Y.H. Zhang, D.M. Konwles, P.J. Withers: Surf. Coat. Techn., Vol.107 (1998).,76-83.

[15] C.M.F. Rae, R.C. Reed: Acta. Mater. Vol. 49 (2001)., p.4113-4125.

[16] C.M.F. Rae, M.S. Hook, R.C: Reed: Mater. Sci. Eng. A.,Vol. 396 (2005).,p.231-239.

[17] M. Reid, M.J. Pomeroy, J.S. Robinson: J. Mater. Process. Techn.,Vol.153-154(2004).,p.660-665.

[18] J. Angenete, K. Stiller: Mater. Sci. Eng. A.,Vol. 316 (2001).,p.182-194.

[19] S. Wöllmer, S. Zaefferer, M.Göken, T.Mack, U.Glatzel: Surf. Coat. Techn., Vol. 167 (2003)., p. 83-96.

[20] F. Pyczak, S. Neumeier, M. Goeken: Mater. Sci. Eng. A., (2009).,Doi: 10.1016/j.msea.2008.08.052.

[21] V. Sass, U. Glatzel, M.F. Kniepmeier., Acta Mater.,Vol.44 (1996).,p.1967-1977.

[22] H. Murakami, T. Sakai: Scripta. Mater., Vol. 59 (2008).,p. 428-431.

[23] Http://cmsx4.8m.com/custom2.html.

[24] B.C. Wilson, J.A. Hichman, G.E: Fuchs: J. Min. Metal. Mater., Vol.55.,p.(35-40).

[25] Http://cmsx4.8m.com/custom.html.

[26] G.E. Fucks: Mater. Sci. Eng.A., Vol.300 (2001).,p.52-60.

[27] T.Hammerschmidt, B. Seiser, R. Drautz, D.G. Pettifor: Superalloys 2008, edited by R.C. Reed et al. TMS (The Min. Met. Mater. Soci).,p.847-853.

[28] C.M.F. Rae, M.S. Hook, R.S. Reed: Mater. Sci. Eng.A., Vol.396 (2005).,p231-239.

[29] S. Bose, et al.: High temperarture Coatings 2007, Chapter 5., Rensselaer Polytecnic Hartford, CT.

[30] K. Kawagishi, H. Harada, A. Sato, T. Kobayashi: J. Min. Met. Mater. Soci. Vol. 58 (2006).,p.43-46.

[31] R. Streiff: J. De Physique IV.,Vol.3 (1993).,17-41.

[32] R. Sivakumar, B.L. Mordike: Surf. Coat. Techn., Vol. 37 (1989).,p.139-160.

[33] G.W. Goward: Surf. Coat. Techn.,Vol. 108-109 (1998)., p. 73-79.

[34] J.T. Demasi-Marcin, D.K. Cupta: Surf. Coat. Techn., Vol. 68-69 (1994).,p.1-9.

[35] S.M. Jiang, C.Z. Xu, H.Q.Li, S.C. Liu, J. Gong, C. Sun: Corr. Sci., Vol. 52 (2010).,p. 435-440.

[36] M.A. Bestor, J.P. Alfeno, M.L. Weaver: Intermatallics., Vol. 19 (2011).,p. 1673-1704.

[37] Y.Q. Wang, G. Sayre: Surf. Coat. Techn., Vol. 203 (2009).,p.1264-1272.

[38] D.He, H. Guan, X. Sun, X. Jiang: Thin. Solid Films., Vol. 376 (2000).,p. 144-151.

[39] B.M. Warnes: Surf. Coat. Techn., Vol. 376 (2001).,p.7-12.

[40] S. Hamadi, M.-P. Bacos, M. Poulain, A. Seyeux, V. Maurice, P. Marcus: Surf. Coat. Techn., Vol. 204 (2009).,p.756-760.

[41] Y. Wang, et al. : Surf. Coat. Techn.,2011, Doi:10.1016/j.surfcoat.2011.08.031.

[42] J.T.John, G.B.Kale, S.R. Bharadwaj, R.S. Srinivasa, P.K.De: Thin Solid Films., Vol. 466 (2004).,p331-338.

[43] MF. Singleton, JL. Murray, P.Nash. In: Massalshi TB, editor. Binary alloy phase diagrams. Metals Park, OH: ASM International; 1986.,p.140-143.

[44] S. Bose, et al.: High temperarture Coatings 2007, Chapter 6., Rensselaer Polytecnic Hartford, CT.

[45] F.S. Liao, C.W. Hsu, D. Gan, P. Shen, S.Z. Lia: Mater. Sci. Eng. A., Vol.125 (1990).,p.215-221.

[46] Z.D. Xiang, J.S. Burnell-Gary, P.K. Datta: J. Mater. Sci.,Vol 36 (2001).,p.5673-5682.

[47] P. Shen, M.J. Tsai, D. Gan: Mater. Sci. Eng. A., Vol. 82 (1986).,p.197-202.

[48] J.R. Nicholls, K.A. Long, N.J. Simms: Scheris's Corr., Vol. 4 (2010).,p.2532-2555.

[49] A. Squillace, R.Bonetti, N.J. Archer, J.A. Yeatman: Surf. Coat. Techn., Vol. 120-121 (1999).,p.118-123.

[50] S. Shanker, L.L.Siegle: Met. Trans.A.,Vol.9 (1978).,p.1467-1476.

[51] L. Singheiser, H.W. Grünling, K. Schneider: Surf. Coat. Techn., Vol. 42 (1990).,p.101-117.

[52] W.P. Sun, H.J. Lin, M.H.Hon: Thin Solid Films, Vol. 146 (1987).,p.55-67.

[53] D.K. Das, V. Singh, S.V. Joshi: Metall. Mater. Trans. A.,Vol.29 (1998).,p.2173-2188.

[54] H.Wei, H.Y. Zhang, G.C. Hou, X.F. Sun, M.S. Dargusch, X. Yao, Z.Q. Hu: J. Alloys. Comp.,Vol.481(2009).,p. 326-335.

[55] H. Hafiee, H. Arabi, S. Raetegari: J. Alloys. Comp.,Vol.505 (2010).,p.206-211.

[56] B.Gleeson, N. Mu, S. Hayashi: J. Mater. Sci.,Vol. 44(2009).,p.1704-1740.

[57] J.H. Chen, J.A. Little: Surf. Coat. Techn.,Vol. 92 (1997).,p.69-77.

[58] H.M. Tawancy, N.M. Abbas: Surf. Coat. Techn., Vol. 49 (1991).,p.1-7.

[59] Y. Zhang, J.A. Haynes, W.Y. Lee, I.G.Wright, B.A. Pint, K.M. Cooley, P.K. Liaw: Matall. Mater. Trans. A.,Vol. 32 (2001).,p.1727-1741.

[60]S.J.Hong, G.H.Hwang, W.K.Han, S.G.Kang: Intermetallics, Vol.17 (2009).,p.381-386.

[61] Z.D. Xiang, P.K. Datta: Mater. Sci. Eng. A.,Vol.356 (2003).,p.136-144.

[62] B.M. Warns, D.C. Punola: Surf. Coat. Techn.,Vol. 94-95 (1997).,1-6.

[63] V.K. Tolpygo, P.K. Murphy, D.R. Clarke: Acta. Mater.,Vol.56 (2008).,p.489-499.

[64]B.A.Pint, J.A.Haynes, T.M.Besmann: Surf. Coat. Techn., Vol.204 (2010).,p.3287-3293.

[65] J.G. Smeggil, A.W. Funkenbusch, N.S. Bornstein: Metall. Mater. Trans. A., Vol. 17 (1986).,p.923-932.

[66] J.A. Haynes, M.J. Lance, B.A. Pint, I.G.Wright: Surf. Coat. Techn., Vol.146-147 (2001).,p.140-146.

[67] Y. Zhang, J.A. Haynes, W.Y. Lee, I. G. Wright, B.A. Pint, K.M. Cooley, P.K. Liaw: Metall. Mater. Trans. A., Vol. 30 (1999).,p. 2679-2687.

[68] A. Engström, J. Bratberg, Q. Chen, L. Höglund, P. Mason: Adv. Mater. Resear., Vol. 278 (2011).,p. 198-203.

[69] J. Angenete, K. Stiller, E.Bakchinova: Surf. Coat. Techn., Vol.176 (2004) ., p. 272-283.

[70] A.L. Purvis, B.M. Warns: Surf. Coat. Techn.,Vol.133-134 (2000).,p.23-27.

[71] M.J. Li, X.F. Sun, H.R. Guan, X.X. Jiang, Z.Q. Hu: Surf. Coat. Techn.,Vol. 185(2004).,p.23-27.

[72] Giggins, Jr. et al. : United States Patent, N. 4,086,391.,Apr. 25.,1978.

[73] S.J. Hong, G.H. Hwang, W.K. Han, K.S. Lee, S.G. Kang: Intermetallics.,Vol 18 (2010).,864-870.

[74] B.A. Pint, J.A. Haynes, K.L. More, I.G. Wright: Superalloys 2004, edited by K.A. Green, T.M. Pollock, H. Harada et al. eds Superalloy 2004 (The Min. Metals.Mater. Soci. (TMS), 2004.,p.597-605.

[75] P. Kuppusami, H. Murakami: Surf. Coat. Techn.,Vol.186 (2004).,p.377-388.

[76] V.K. Tolpygo: Surf. Coat. Techn.,Vol. 202 (2007).,p.617-622.

[77] S. Dryepondt, D.R. Clarke: Scri. Mater. Vol.60 (2009).,p.917-920.

[78] A. Raffaitin, D. Monceau, E. Andrieu, F. Crabos: Acta. Mater.,Vol.54 (2006).,p.4473-4487.

[79] X. Ledoux, M. Vilasi, S. Mathieu et al.: Adv. Mater. Resear.,Vol.278 (2011).,491-496.

[80] J. Angenete K. Stiller: Oxi.Metals.,Vol. 60 (2003).,p.47-82.

[81] U. Hemmersmeier, M.F. –Kniepmeier: Mater. Sci. Eng. A., Vol. 248 (1998).,p.87-97.

[82] Http://www.megamex.com/nickel 200 201.html.

[83] Http://serc.carleton.edu/research education/geochemsheets/ebsd.html.

[84] S.D. Baschi, M.Dutta, N. Bandyopadhyay, N. Rajesh: Surf.Coat. Techn.,Vol. 201 (2007).,p.4547-4552.

[85] S. Suzuki, K. Kakita: J. Surf. Analysis, Vol.12 (2005).,p.174-177.

[86] P.L. Coustumer, M.M. Heino, P. Chapon, H. François, S. Cyr, R. Payling: Surf. Interface. Analy., Vol. 35 (2003).,623-629.

[87] E. Fedorova, D. Monceau, D. Oquab: Corro. Sci., Vol.52 (2010).,p.3932-3942.

[88] J. Kohlscheen, H.-R. Stock: Surf. Coat. Techn.,Vol202 (2007).,p.613-616.

[89] Y. Zhang, W.Y.Lee, J.A. Haynes, I.G. Wright, B.A. Pint, K.M. Cooley, P.K. Liaw: Metall. Mater. Trans. A., Vol. 30 (1999).,p.2679-2687.

[90] A.J. Hickl, R.W.Heckel:Metall.Mater. Trans.A.,Vol.6 (1975).,p.431-440.

[91] E. Gariboldi, M. Verani, C. Riva: Adv. Mater. Resear.,Vol.278 (2011).,p.228-233.

[92] Y.H. Zhang, D.M. Knowles, P.J. Withers: Surf. Coat. Techn.,Vol.107 (1998).,p.76-83

[93] E. Gariboldi, X.H. Han, G.A. Longo, G.P.Zanon: Adv. Mater. Resear.,Vol.278 (2011).,p.521-526.

[94] A. Suzuki, C.M.F. Rae, M.S.Hook, R.C. Reed: Mater. Sci. Eng. A.,Vol.396 (2005).,p.231-239.

[95] T. Helander, J. Agren: Acta. Mater., Vol. 47 (1999).,p.1141-1152.

[96] C.C.Jia, K. Ishida, T. Nishizawa: Metall. Mater. Trans. A.,Vol.25 (1994).,p.473-485.

[97] X.H. Han, E. Gariboldi, G.A.Longo, G.P.Zanon: Adv. Mater. Resear., Vol. 418-420(2012).,p.1012-1021.

[98] F.H. Yuan, Y.S. Yoo, C.Y. Jo, B.G.Choi, Z.Q. Hu: Surf. Coat. Techn., Vol. 183 (2004).,p.106-110.

[99] B.A. Pint, I.G. Wright, B.A. Pint, W.Y. Lee, Y.Zhang, K.Prüβner, K.B. Alexander: Mater. Sci. Eng. A.,Vol. 245 (1998).,p.201-211.

[100] O. Engler, V. Randle: Introduction to Texture Analysis CRC Press. 2006.

[101] J.A: Haynes, B.A.Pint, K.L.More, Y. Zhang, I.G. Wright: Oxid. Metal., Vol.58 (2002).,p.513-544.

[102] W.Y. Lee, Y. Zhang, I.G: Wright, B.A. Pint, P.K. Liaw: Metal. Mater. Trans.A.,Vol. 29 (1998).,p.833-841.